Far-Infrared Studies of Some Strongly Correlated Electron Systems

Ton Gerrits

Far-Infrared Studies of Some Strongly Correlated Electron Systems

CIP-GEGEVENS KONINKLIJKE BIBLIOTHEEK, DEN HAAG

Gerrits, Antonius Maria

Far infrared studies of some strongly correlated electron systems / Antonius Maria Gerrits. - [S.l. :s.n.]. - Ill.
Proefschrift Katholieke Universiteit Nijmegen. - Met lit. opg.
ISBN 90-9008284-0
Trefw.: hoge-temperatuursupergeleiders / organische geleiders / infraroodspectroscopie.

Far-Infrared Studies of Some Strongly Correlated Electron Systems

een wetenschappelijke proeve op het gebied van
de Natuurwetenschappen

Proefschrift

ter verkrijging van de graad van doctor aan
de Katholieke Universiteit Nijmegen,
volgens besluit van het College van Decanen
in het openbaar te verdedigen op
vrijdag 16 juni 1995
des namiddags om 12.30 uur precies

door

Antonius Maria Gerrits

geboren op 23 april 1968
te Boxmeer

Promotor:	Prof. Dr. H. van Kempen
Co-promotores:	Dr. P.J.M. van Bentum
	Dr. A. Wittlin

At every corner of Life
a surprise awaits you;

Life is full of corners.

Omdat het aantal auteurs op de voorpagina anders suggereert, wil ik hier benadrukken dat niet één maar vele personen direct of indirect aan de totstandkoming van dit proefschrift hebben bijgedragen. Hen wil ik mijn dank betuigen alhoewel een simpel dankwoord als dit in geen enkele verhouding staat tot de enorme betekenis die vele van die bijdragen voor mij hebben gehad.

Ten eerste wil ik Herman van Kempen bedanken omdat hij mij in de gelegenheid heeft gesteld dit promotie-onderzoek te doen en voor de bereidwilligheid waarmee hij elk verzoek mijnerzijds benaderde.

Jan "Bouw en Constructie" van Bentum ben ik zeer erkentelijk voor zijn stortvloed aan heldere, fysische ideeën, zijn leerzame schrijflessen en het nooit ontmoedigen van eigen initiatief ;-). Olek Wittlin ben ik zeer dankbaar omdat hij mij met groot enthousiasme heeft laten delen in zijn grote kennis en ervaring op FIR- en computergebied. Bedankt dat jullie deur steeds voor mij openstond.

Verder wil ik alle medewerkers van de afdeling Experimentele Vaste Stof Fysica 2 bedanken voor de prettige sfeer en dito samenwerking. Met name wil ik hier noemen, Cees Beers, Jan Hermsen en Jan Gerritsen voor hun veelzijdige hulp vooral toen ik mijn eerste stappen als AIO zette en Jan H. speciaal nog voor veel gedegen polijstwerk. Ook Albert van Etteger hoort in dit rijtje thuis, niet in de laatste plaats voor het slaan met woorden en tennisballen in de kantine respectievelijk op de tennisbaan. Dank ook aan Paul van Loosdrecht van wie ik op meerdere fronten veel geleerd heb; ook het rondje Koningsplein ter gelegenheid van de xx-ste succesvolle afkoeling van de CryoVac, staat nog vers in het geheugen. Riki Gommers bedank ik hartelijk voor haar hulpvaardigheid, positieve uitstraling en betrokkenheid. Furthermore, I am very thankful for many stimulating discussions with Sergei Shafranjuk. Jan-Theodoor Janssen verdient een erevermelding voor alle dagen (en vooral nachten) vol helium plempen, cryostaten uitlijnen, "Bep en Toos"-conversaties en metingen met "onze baby".

Mijn dank gaat zeker ook uit naar alle medewerkers van het magnetenlab (tegenwoordig Experimentele Vaste Stof Fysica 1) waar ik het grootste deel van mijn promotietijd actief ben geweest. Jos Perenboom bedank ik voor zijn grote aandacht voor de menselijke kanten van zijn collega's hetgeen aan de basis staat van de goede sfeer op het lab. Verder gaat mijn dank uit naar Klaas van Hulst ("voor al uw Tesla's") voor de geleverde magneet-

velden, Jos "RVS" Rook voor zijn vakmanschap (speciaal voor het weer tot leven (willen) wekken van de ^{3}He-insert waardoor ik toch nog de metingen kon doen die aan de wieg stonden van hoofdstuk 1), Peter van der Linden voor allerlei hulp en tips, Lijnis Nelemans voor het uitvoeren van vele essentiële klusjes en verder natuurlijk Harry Balster, Hung van Luong en niet te vergeten Elma Burg. Jan Kees Maan bedank ik voor zijn frequente "zeurrondjes" (zijn eigen woorden) die me dikwijls stof tot nadenken opleverden. Speciaal wil ik hier Marc Boonman bedanken voor de bijzonder goede en prettige samenwerking tijdens mijn laatste experimentele loodjes en voor zijn voortreffelijke (maar loodzware) warme rijstepap met rozijnen.

In deze lijst mogen Dick van der Marel, Jae Kim, Johan Feenstra en Herpertap Somal van de Universiteit Groningen zeker niet ontbreken vanwege onze experimentele samenwerking en vele stimulerende discussies.

Hoofdstuk 1 zou nooit tot stand zijn gekomen zonder de fantastische $La_{1.85}Sr_{0.15}CuO_4$ samples van Vincent Duijn en A.A. Menovsky van de Universiteit van Amsterdam. Bedankt daarvoor.

I would also like to thank James Brooks and Alex Perel from Boston University for our fruitful cooperations on the Bechgaard salts.

X. Granados, J.L. Garcia-Muñoz and J. Fontcuberta from the Institut de Ciència de Materials de Barcelona are acknowledged for drawing our attention to and cooperating in the field of rare earth nickelates which has resulted in the fifth chapter of this thesis.

Furthermore, I am grateful to Pawel Kaczor from the Polish Academy of Sciences in Warsaw and N. Joshi from the Technical University of Eindhoven for cooperation on interesting projects not described in this thesis.

Verder wil ik mijn grote waardering uitspreken voor het werk van de dienstverlenende afdelingen van onze faculteit (met name de instrumentmakerijen en de heliumwinkel). Hoewel dit werk vaak op de achtergrond wordt gedaan, zouden wetenschappers bar weinig beginnen zonder.

Urs Wyder is uit mijn promotietijd niet weg te denken. Heel veel dank, Urs, voor de vele diepe gesprekken over het leven en de fysica en bovendien voor het waterfietsen, het "printers kopen" en voor vele meest hartelijke groetjes (!).

Bijna aan het einde van dit dankwoord gekomen wil ik mijn ouders, oma, Theo en Anika en ook Ingrid en Lex ten zeerste bedanken voor de hulp en steun die ik alle jaren van hen heb mogen ontvangen. Verder bedank ik hier ook alle nog niet met name genoemde vrienden en kennissen, speciaal

de leden van het "mensaclubje", voor de nodige ontspanning buiten het lab.

Tot slot, Margrit, enige woorden voor jou. Het geduld en begrip dat jij aan de dag hebt gelegd als ik weer eens moest overwerken of mijn frustraties kwijt moest, is werkelijk bewonderenswaardig te noemen. Zonder jouw Liefde zou de totstandkoming van dit boekje schier onmogelijk zijn geweest. Bedankt!

Contents

Preface

This thesis presents the results of far-infrared optical studies on a number of solids which are presently very popular in the world of solid state physics. The first three chapters deal with the dynamics inside and perpendicular to the CuO_2 layers in some high temperature superconductors. Chapter 4 is dedicated to the magnetic-field-induced spin-density-wave formation in the organic conductor $(TMTSF)_2ClO_4$ and chapter 5 is devoted to an optical study of the metal-insulator transition in ceramic rare earth nickelates.

In optical studies one makes use of the electric interaction of light waves with charges, electric dipoles etc. in the material. A magnetic equivalent of this interaction is also present but is generally much smaller. Quantummechanically described, matter interacts with light by absorbing and emitting photons. Through conservation of energy and momentum these processes create respectively annihilate excitations in the material such as phonons, magnons, and so on. The reason why we used far-infrared light is that its energy is comparable to the energies of the excitations we want to study, such as low-energy collective modes or correlation gaps in the electronic density of states. Examples of these are the pinned spin-density-wave collective mode and the superconductive gap.

An important parameter used in our experiments is the magnitude of the applied magnetic field. The interesting feature about applying a magnetic field is that this does not simply add an extra energy scale in the system such as temperature does but it fundamentally changes the equations of motion of the charges. This leads to interesting new physics such as Landau level formation, the quantum Hall effect and the creation of magnetic vortices in type II superconductors.

The materials that we have investigated share a number of common features which distinguish them from other conductors such as normal metals and highly doped semiconductor systems. These features are the cause

of the importance of electronic correlations in these solids.

First, the number of mobile carriers is rather low, typically a factor of ten smaller than in classical metals. As a result, the total kinetic energy of these carriers, the Fermi energy ϵ_F, is relatively small. Therefore, the potential energy caused by Coulomb interactions and magnetic exchange interactions between the carriers are no longer negligible compared to ϵ_F.

Second, the delocalized states necessary for conductivity are not formed by highly itinerant isotropic s-states but are formed by the smaller overlap (hybridization) of molecular p- or d-orbitals. In the high T_c superconductors and the nickelates the overlap is mainly between the transition metal $3d$ and the oxygen $2p$ states and in $(TMTSF)_2ClO_4$ the overlap is largest between Selenium π-orbitals. These narrow bands imply that the electrons are rather localized which increases the effect of the on-site Coulomb repulsion (the energy cost to have a site doubly occupied). Because the overlap of the molecular orbitals varies strongly in different directions the electronic properties of these materials are highly anisotropic. The anisotropy ranges from quasi three-dimensional to almost two-dimensional for different members of the high T_c family. The electronic structure of $(TMTSF)_2ClO_4$ is almost one-dimensional. Because the reduced dimensionality restricts the movements of the electronic system and because the charge carrier density is low, the screening of the electron-electron interactions is small. This further increases the importance of correlation effects.

Due to the large on-site Coulomb repulsion, these physical systems are theoretically hard to tackle [1]. This is caused by the fact that the on-site repulsion is most naturally represented in real space whereas the electron wave states are most conveniently described in reciprocal space. Furthermore, the description of the energy bands and their hybridization requires two creation/annihilation operators. In contrast, the on-site repulsion involves two density operators and thus four creation/annihilation operators. The mathematical difficulties which arise when these ingredients have to be accounted for are enormous. An overview of the many different approaches to solve these difficulties are given in Ref. 2. Models which are being used to tackle the physics of specifically the high T_c superconductors are given in Ref. 3.

The properties of electron systems including correlation effects have been described very successfully within the Landau theory for Fermi liquids [4]. The observation of clear Shubnikov-de Haas oscillations in closed

orbit organic salts and the understanding of the spin-density-wave properties on the basis of band structure calculations shows that the organic salts can still be described within this framework. A topic presently under intense discussion is whether this also holds for the doped copper oxides.

It goes beyond the scope of this thesis to give an elaborate account of all the sophisticated models which have been developed to describe the unusual properties of the correlated electron systems investigated in this thesis. I have therefore restricted myself to explain very briefly the concepts necessary to be able to follow the lines of thought in this thesis and have given references to guide the interested reader to more extensive and detailed work.

References

1. A clear treatment of electronic correlations (in heavy fermion systems) can be found in: U. Wyder, Ph.D. Thesis, University of Amsterdam (1995).
2. P. Fulde, in *Electron Correlations in Molecules and Solids*, Springer Series in Solid State Sciences, (Springer-Verlag, Berlin 1991).
3. E. Dagotto, Rev. Mod. Phys. **66**, 763 (1994) and references therein.
4. L.D. Landau, Sov. Phys. JETP **3**, 920 (1957); **5**, 101 (1957); **8**, 70 (1959).

Chapter 1

Far-infrared study of the *c*-axis properties of $La_{1.85}Sr_{0.15}CuO_4$

Parts of this chapter have been published in the following papers:

- Physica C **235-240**, 1117 (1994).
- Proceedings of the Fourth International Symposium on Research in High Magnetic Fields, to be published in Physica B (1995).
- Phys. Rev. B, in press (1995).

1.1 Introduction

Shortly after the discovery of the first high temperature superconductor La-Ba-Cu-O [1] many more similar materials with extremely high critical temperatures were found*. The members of this new class of superconductors have a common structural building block, the CuO_2 planes. Soon, the general belief arose that the peculiar physical properties of these cuprates originate from the spin and charge dynamics within the CuO_2 layers. As a result, most theoretical and experimental efforts were directed towards exploring the basic physics inside a single CuO_2 layer. The only importance of the layers separating the superconducting planes was considered to be their ability to act as charge reservoirs which can supply additional carriers to the CuO_2 planes.

Another, more practical reason why the out-of-plane or c-axis properties were initially less intensively studied is that no high quality single crystals of sufficient c-axis dimensions could be grown and thin films grew preferentially with their c-axis perpendicular to the substrate. The development of new growth techniques such as the Traveling Solvent Floating Zone technique [3] with which it is possible to grow high quality single crystals with characteristic dimensions of several millimeters, resolved this problem to a large extent.

Although the initial investigations focused on the dynamics inside the CuO_2 planes, the interest of the interplane coupling must not be underestimated as it determines many of the anisotropic properties of the high temperature superconductors. Even new physical phenomena which are related to the anisotropy, such as 2D-3D dimensional crossover effects, have been observed in these materials. Thus, a thorough understanding of the highly anisotropic properties of the cuprate superconductors requires sound insight in the nature of the interplane coupling.

Even in the normal state, the nature of this coupling is rather puzzling. The interlayer hopping rate, for instance, is much smaller than expected from band structure calculations. Likewise, the actual value of the out-of-plane conductivity is mostly much smaller than the Mott minimum for metallic conductivity ($\sim 100\ \Omega^{-1}\mathrm{cm}^{-1}$), which is very counter-intuitive for materials that can superconduct.

*The cuprate superconductor which, until now, has the highest transition temperature is $HgBa_2Ca_2Cu_4O_{8+\delta}$ (134 K at ambient pressure) [2].

The discussion of interlayer coupling is further hampered by the fact that the cuprates consist of well separated blocks or cells of n closely spaced CuO_2 plane layers. The number $n = 1$ in unilayer systems (*e.g.* $La_{2-x}Sr_xCuO_4$), $n = 2$ in bilayer compounds (*e.g.* $Bi_2Sr_2CaCu_2O_8$) and $n = 3$ in trilayer materials (*e.g.* $Tl_2Ba_2Ca_2Cu_3O_{10}$). Thus, in the $n > 1$ systems, one has to make a distinction between the coupling between the closely spaced CuO_2 planes ('interplane' coupling) and coupling between adjacent cells ('intercell' coupling).

As a consequence, much more effort was put forth in the last few years to explore the mechanism behind the large anisotropy and the interlayer coupling in the high T_c cuprates. A summary of recent development can be found in the review by Cooper and Gray [4].

One of the more interesting topics in this field is that of the low frequency reflectance edge which appears below T_c in far-infrared spectra. This feature was originally observed in ceramic samples [5] and grains embedded in a dielectric host [22] but its origin was not identified before Tamasaku *et al.* [7] measured the c-axis interlayer infrared response of large single crystals of $La_{2-x}Sr_xCuO_4$. They found that, in the normal state, the optical c-axis conductivity is completely phonon dominated with only a marginal contribution of free carrier transport. Below T_c a zero crossing developed in the real part of the dielectric function causing a very weakly damped plasma edge in the reflectance. The appearance of the low frequency plasmon marks the onset of coherent transport perpendicular to the CuO_2 layers.

The energy of the plasmon is found to be *lower* than the superconductive gap[†]. It is often stated that this indicates a violation of the Anderson-Higgs mechanism, which pushes collective modes involving density changes in the electron system to energies above the gap energy due to the Coulomb interaction [9]. However, the theorem only holds for isotropic systems and for collective modes with an acoustic dispersion. Soon after the work of Tamasaku *et al.*, similar observations were done in single crystals of $YBa_2Cu_3O_{6.7}$ [10] and $YBa_2Cu_4O_8$ [11][‡]. Therefore,

[†]The gap energy is the minimum energy needed for a photon to break up a superconducting Cooper pair. In the weak coupling Bardeen-Cooper-Schrieffer (BCS) theory [8], this energy equals $3.52k_BT_c$. In the rest of this chapter we will implicitly assume that the gap in $La_{1.85}Sr_{0.15}CuO_4$ is close to the BCS value (≈ 80 cm^{-1}).

[‡]The low frequency plasmon was not seen in $Bi_2Sr_2CaCu_2O_8$ down to 30 cm^{-1} [12] but it may be found at lower frequencies.

the low frequency plasmon seems to be a universal feature in the very anisotropic layered high T_c superconductors.

To study the nature of the interplane coupling that causes the low frequency plasmon we performed an infrared study on $La_{2-x}Sr_xCuO_4$ as a function a temperature and magnetic field. In section 1.2 we present new measurements on the c-axis reflectivity of $La_{1.85}Sr_{0.15}CuO_4$ and show that the plasma edge can be explained by Josephson interlayer coupling. A subsequent study in high magnetic fields is described in section 1.3. We found that the plasma *edge* changes with increasing magnetic field. In contrast, the plasma *frequency* is field independent up to the highest magnetic fields used which shows that the edge changes cannot be explained by magnetic vortices moving in the sample under the influence of the Lorentz force. The theoretical models that we developed with regard to this plasmon are described in detail in the last part of this chapter.

1.2 Josephson plasma edge

We start this section by introducing the concept of Josephson coupling. When two superconductors A and B are brought in close proximity to each other (but not in direct contact) superconducting electron (or hole) pairs can travel from one superconductor to the other without altogether loosing their phase coherence [13]. This takes place by either tunneling (when the separation region is isolating) or diffusion (when the separation region is conducting). Through this process, the macroscopic phases of the two superconductors are weakly coupled. This coupling is called Josephson coupling and has two main characteristics: 1. a supercurrent can flow between A and B (dc Josephson effect) 2. with an applied dc voltage V between A and B, the structure emits radiation with frequency $\nu = 2eV/h \approx 483$ MHz/μV (ac Josephson effect).

Measurements of the upper critical field of the cuprate superconductors indicate that the superconducting coherence length along the c-axis is of the order of the interplanar distance d. This suggests that one can approximate these highly anisotropic materials as Josephson coupled stacks of two dimensional (2D) superconducting building blocks. In the mixed state

it has for example become necessary to describe vortices perpendicular to the layers as pancake-like Abrikosov vortices weakly coupled by Josephson strings [14]. Direct observation of Josephson-like interplane coupling in several different high T_c compounds with double and triple CuO_2 layers, was reported in the work by Kleiner and Müller [15].

In this section we present reflectivity measurements on single crystals of the unilayer compound $La_{1.85}Sr_{0.15}CuO_4$ and show that the observed reflectance edge in the *c*-axis optical response of this compound can be understood in terms of a simple model based on Josephson coupling which we describe in detail further on (section 1.4.1). In this model the sample is treated as a stack of superconducting sheets, separated by dielectric or very weakly conducting barriers. The bulk superconductivity and coherent *c*-axis transport is then induced by the Josephson coupling between the layers. For such a layered system with characteristic conductance σ_{qp} and capacitance C, the following dielectric function can be derived,

$$\epsilon_J(\omega) = \epsilon_0\epsilon_c\left(1 - \frac{\omega_{ps}^2}{\omega^2} + i\frac{\gamma}{\omega}\right) \tag{1.1}$$

$$\omega_{ps} = \sqrt{\frac{2ej_c}{\hbar C}} \tag{1.2}$$

$$\gamma = \frac{\sigma_{qp}}{C} \tag{1.3}$$

where ω_{ps} is the Josephson plasma frequency, and γ is the plasmon damping. Equation 1.1 shows that for low values of γ no radiation can penetrate the sample at frequencies below ω_{ps}. The plasmon can be characterized as a propagating electromagnetic mode coupled to local oscillations of the phase of the complex superconductive order parameter. From expression 1.2 one can deduce directly the critical current density j_c, which provides an alternative (spectroscopic) method for the determination of j_c. An advantage of this approach is that the electromagnetic field probes the bulk properties of the sample at near equilibrium conditions and at very low effective current densities.

1.2.1 Experimental details

For the measurements we used various single crystals of $La_{2-x}Sr_xCuO_4$ grown by the Traveling Solvent Floating Zone method at the University of

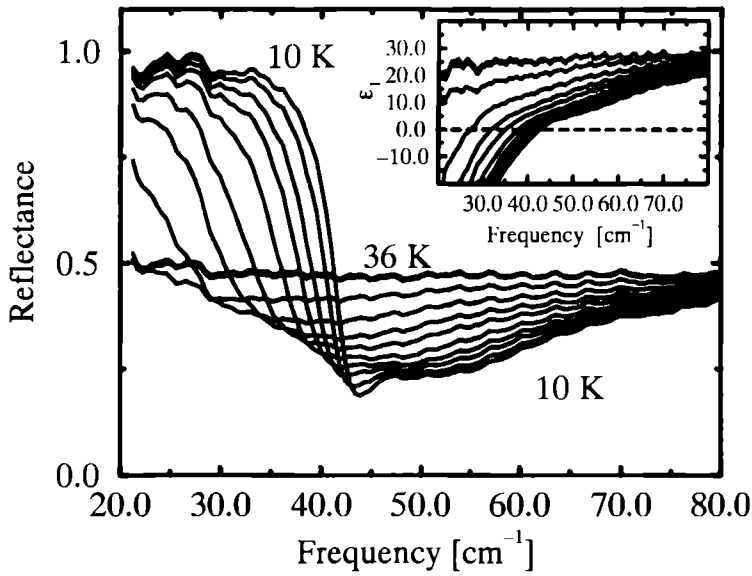

Figure 1.1 *Reflectance of $La_{1.85}Sr_{0.15}CuO_4$ at 10, 13, 16, 18, 21, 23, 25, 27, 29, 32, 35, and 36 K. The small regular wiggles in the spectra are interference fringes and not intrinsic to the material. The inset shows the real part of the dielectric function $\epsilon_1(\omega)$.*

Amsterdam [16]. We concentrate on the samples that are close to optimal doping ($x = 0.15$, T_c as determined by magnetization measurements is 34 K). The size of the *a-c* oriented sample surface was typically 3×5 mm^2. Reflectivity measurements were done with a Bruker IFS113v Fourier Transform spectrometer coupled to a variable temperature cryostat (Oxford CF1104). Reference measurements were performed on a 0.5 μm thick gold mirror evaporated on glass. To polarize the infrared radiation we used a commercial metal grid polarizer and a silicon plate Brewster polarizer made in the group of van der Marel at the University of Groningen.

1.2.2 Results and discussion

Figure 1.1 shows the *c*-axis reflectance $\mathcal{R}$ below 80 cm^{-1} at various temperatures between 10 K and 36 K. The data are very similar to the previous results of Tamasaku *et al.* [7]. Above T_c the spectrum resembles that of an

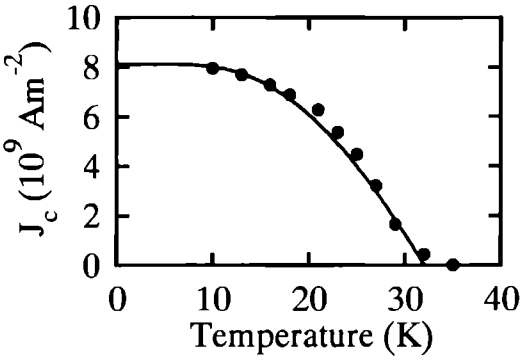

Figure 1.2 *The temperature dependence of the critical current deduced from the measured plasma frequency (circles) along with a BCS based theoretical prediction.*

insulator whereas below T_c a weakly damped plasma edge appears. The frequency of the plasma edge is somewhat lower than reported in Ref. 7. Although the critical temperature of our sample determined by magnetization is 34 K, from the analysis below we find that the T_c which fits the data best is 32 K. When we take this value to be the correct value for T_c we find agreement with results on a 32 K sample investigated by Tamasaku *et al.* which also shows a plasma edge around 42 cm^{-1}. The difference is that Tamasaku's sample has a lower T_c because it is has a lower Sr content whereas in our sample (microprobe analysis revealed the optimal Sr content of 0.15) the reduced T_c is more likely caused by a lower oxygen content. The inset clearly shows the characteristic feature of a plasmon edge related to the zero crossing of the real part of the dielectric function $\epsilon_1(\omega)$. The real part of the conductivity $\sigma_1(\omega)$ decreases substantially at low frequencies when cooling below T_c. This is consistent with the opening of a gap. However, the conductivity does not vanish completely, which explains why the damping of the plasmon is low but not zero.

Figure 1.2 shows the j_c deduced from equation 1.2 versus temperature (circles). The only unknown parameter in the conversion from ω_{ps} to j_c is the capacitance C, which we calculated from the measured dielectric function. The solid line represents the functional dependence of j_c on temperature using the Ambegaokar-Baratoff (AB) expression [17] for a BCS weak coupling gap $\Delta(T)$ with $\Delta(0) = 1.76 k_B T_c$ and $T_c = 32$ K. A better

agreement with the temperature dependence is obtained if we use a slightly larger gap value ($\Delta(0) = 2.5k_BT_c$). The absolute value of the measured j_c agrees well with the AB result and the optically determined normal state conductivity $\sigma_n = 8\ \Omega^{-1}\text{cm}^{-1}$.

The absolute value of j_c at low temperatures is larger than the values found *e.g.* in the magnetization measurements of Ref. 18 by roughly a factor of 10. This is related to the fact that the infrared probes the intrinsic critical current due to Josephson coupling whereas magnetization experiments measure the current at which vortices get depinned. The difference between these currents will be illustrated in the magnetic field data of section 1.3.2.

The feature which appears in $\mathcal{R}$ just above the plasma frequency gives rise to a small peak in the conductivity. This peak, which is also visible in Tamasaku's data, shifts to lower frequencies when the temperature is increased and closely follows the position of the plasma edge. The origin of this feature is most likely related to the fact that just above the plasma frequency the real part of the dielectric function is close to one. Because the absorption is low the sample is effectively transparent and any residual absorption is therefore easily detected around this frequency. This absorption can originate from normal inclusions in the sample such as inhomogeneities or small off-stoichiometric grains. Figure 1.3 shows the data at 10 K together with a fit according to equation 1.1 (dashed line). The solid line represents an effective medium calculation [19] for the same model, but now with a volume fraction of 10 % of non-superconducting spherical inclusions. We *ad hoc* assumed a Drude-like conductivity of the normal inclusions described by the dielectric function

$$\frac{\epsilon_i(\omega)}{\epsilon_0} = \epsilon_i - \frac{\omega_{pi}^2}{\omega(\omega + i\gamma_i)}. \tag{1.4}$$

With $\omega_{pi} = 215\ \text{cm}^{-1}$, $\gamma_i = 4\ \text{cm}^{-1}$ and $\epsilon_i = 8$, the correspondence we find between fit and experimental data is quite good. The 10 % volume fraction of non-superconducting material is much larger than expected from crystallographic data and microprobe analysis of the sample. This indicates that the defects probably have a more extended character.

Furthermore, figure 1.3 shows that part of the non-zero conductivity observed inside the gap can be due to the normal inclusions. On the other

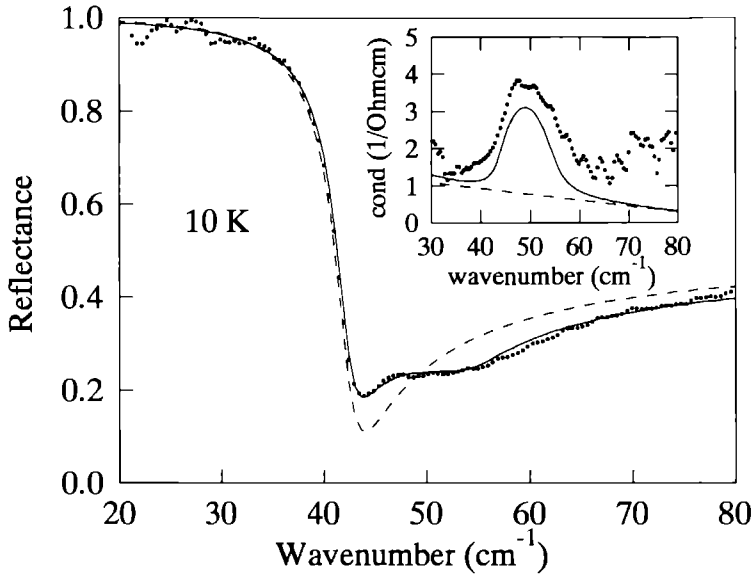

Figure 1.3 *Reflectance at 10 K (small dots) together with a bare plasma fit (dashed line) and a fit (solid line) assuming 10 % normal inclusions in the sample. The inset shows the corresponding conductivity.*

hand, this background conductivity is not incompatible with an order parameter with *d*-wave or anisotropic *s*-wave symmetry. Unfortunately, we cannot determine the (anisotropic) gap in this direction due to the very strong contribution of the phonons at higher frequencies.

1.2.3 Summary

We presented the *c*-axis reflectivity data on $La_{1.85}Sr_{0.15}CuO_4$. Using a simple model based on Josephson coupling we obtain a good quantitative description of the observed plasma edge. Details of the spectrum near the zero crossing of $\epsilon_1(\omega)$ can be explained by taking into account a small fraction of normal inclusions in the sample.

1.3 Magnetic field dependence

It is known that an external magnetic field suppresses superconductivity through the breaking of time-reversal symmetry which is essential for the formation of Cooper pairs. A magnetic field, thus, tends to break up superconducting pairs (the pair breaking effect), which leads to, for instance, a reduced superconducting order parameter Δ and critical temperature T_c [20] (see also chapter 2).

When the applied magnetic field B is sufficiently low, it is completely expelled from the interior of the superconductor (Meissner effect) [21]. For $B > B_{c1}$ (typically 10 mT) the high temperature superconductors are in the vortex state. In this state, part of the magnetic field penetrates in the form of Abrikosov vortices, each carrying one flux quantum. The structure of an isolated vortex is such that the order parameter Δ decreases towards the middle of the vortex on the scale of the coherence length ξ and vanishes at its center. This structure is sometimes approximated by a zero Δ at distances $r < \xi$ (the vortex core) and an undisturbed Δ outside this range. The vortex is surrounded by screening currents which decrease on a characteristic length scale λ, the magnetic penetration depth. The reduction of the order parameter in the vortex center costs energy. Therefore, it is energetically favourable for an Abrikosov vortex to stay at positions where the order parameter is locally reduced due to *e.g.* impurities. This effect is called vortex pinning.

In a pure Josephson *tunnel* structure the order parameter is zero in the isolating region. Vortices which enter this region are only accompanied by screening currents; no local reduction of the order parameter is involved. These so-called Josephson vortices can therefore not be pinned to the underlying lattice.

In this section we investigate the magnetic field dependence of the c-axis reflectance of single crystal $La_{1.85}Sr_{0.15}CuO_4$. Related measurements have been reported before on small particles of $La_{2-x}Sr_xCuO_4$ albeit with a smaller Sr content [22].

The fact that there is a plasma resonance in a frequency region where there is little or no damping allows a detailed study of the electromagnetic interaction with the vortices introduced by the magnetic field. In the geometry we use ($B \parallel ab$ planes) the vortices will enter the sample preferentially

between the superconducting layers. As we will show, this spectroscopic investigation of the vortex dynamics provides specific constraints on the nature of the vortices, the pinning potential and vortex viscosity. This information can, in principle, also be derived from transport measurements. However, a full spectral analysis provides self-consistency checks on model assumptions and is not hampered by extrinsic problems such as local heating, self field effects, edge problems etc.

1.3.1 Experimental Details

We used two complementary techniques to measure the magnetic field dependence of the reflectance of the *ac* oriented surface of the same samples which were studied in the previous section. We coupled the Bruker IFS113v spectrometer to a superconducting magnet system in which a special sample insert with ^{3}He cooled bolometers was placed to measure the wide band reflectivity at 1.2 K in magnetic fields up to 17.5 Tesla. The zero field measurements in this setup were in good agreement with the results obtained in the flow cryostat. This allowed us to deconvolute the unpolarized magnetic field data to obtain the *c*-axis spectra, where we assumed that the flat *a*-axis reflectivity is relatively insensitive to the applied field. This assumption is quite reasonable in view of the in-plane reflectivity data of $YBa_2Cu_3O_7$ films in similar fields (see chapter 2). In principle, the *a* and *c*-axis response will be mixed due to the Hall field. However, from previous measurements on the *ab* response there are no reasons to assume that the magnetic field will induce any features in the *a*-axis reflectivity. The spectral position and shape of the plasma edge will be exclusively determined by the *c*-axis response. Therefore, any Hall field mixing is expected to give a small featureless renormalization of the reflectivity within the experimental noise.

In another setup we measured the temperature dependent microwave and far-infrared reflectivity in a hybrid Bitter/superconductor magnet at fields up to 25 Tesla using both an optically pumped molecular gas FIR laser and a tunable millimeter wave vector network analyzer with heterodyne detection. In this case, the magnetic field dependent reflectance of the sample is measured at various discrete energies as a function of temperature. The magnetic field was in all experiments parallel to the crystal *b*-axis.

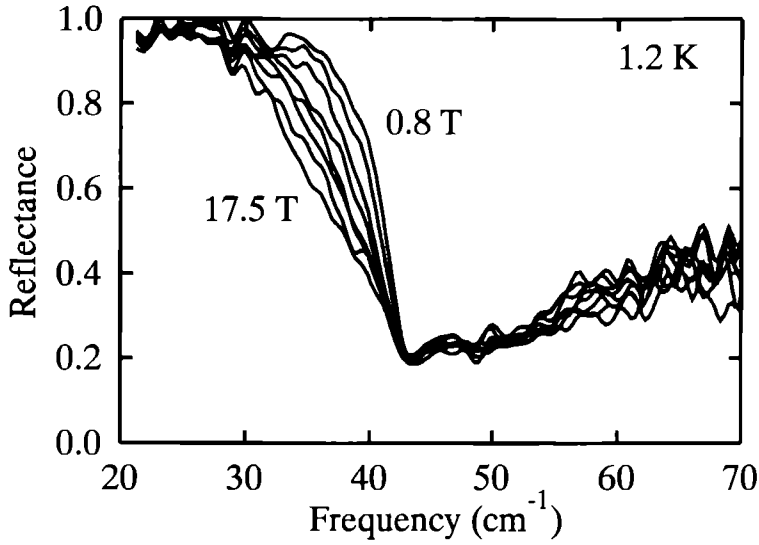

Figure 1.4 *Reflectance spectra at 1.2 K for magnetic fields of 0.8, 2.5, 5, 7.5, 10, 12.5, 15 and 17.5 Tesla.*

1.3.2 Results

Figure 1.4 shows the normal incidence c-axis at 1.2 K at various fields up to 17.5 Tesla. The spectra were taken in three separate runs, always with increasing field and were averaged afterwards. A hysteresis corresponding to a remanent magnetic field of about 2 Tesla is found in the spectra when after each run the applied field is lowered to zero again. We observe a clear renormalization of the reflectance edge which increases with field. In contrast, the position of the reflectance minimum at 43 cm^{-1} does not shift appreciably to lower frequencies and its depth is also rather field insensitive.

From these data a few qualitative observations are obvious: In contrast to theoretical predictions, there is no appreciable field induced shift of the plasma frequency (or zero crossing in the real part of the dielectric function $\epsilon_1(\omega)$). This shows that in this field range and for this geometry ($B \parallel b$) pair breaking effects can be neglected and the interlayer coupling remains largely unaffected. A second qualitative observation is that there is no clear reduction of the reflectivity at low frequencies, as would be expected if the vortices could freely move in the layers separating the CuO_2 planes. This illustrates that the vortices are rather efficiently pinned and cannot be

described in terms of ideal Josephson vortices. Instead, their character is Abrikosov-like.

This is consistent with the observed hysteresis. Using Bean's model [23] and an average sample diameter of 4 mm, we find that the hysteresis corresponds to a critical current of 1.6×10^9 A/m^2. We can compare this value with results obtained from magnetization measurements on similar samples [18] and find a reasonable agreement. It is important to note the difference between this pinning limited transport critical current density and the intrinsic critical current density which is limited by the coupling between the layers. It is this last critical current which we measure in the infrared. (In the simple Josephson model the observed plasma frequency is equivalent to an intrinsic upper limit for j_c of 8×10^9 A/m^2).

Typical curves of the reflectivity versus temperature, taken at 6.5 and 17.5 cm^{-1}, are shown in figure 1.5a and 1.5c, respectively, at four different fields between 0 and 25 Tesla. The pronounced reflectance drop upon heating is caused by the plasma edge shifting below the frequency of the applied radiation. After applying the magnetic field, the reflectance edge shifts only slightly to a lower temperature and the main effect of the field is an increase of the transition width. This again illustrates that even at 25 Tesla there is no appreciable pair breaking reduction of both T_c or ω_{ps}. Although it is known that the low temperature upper critical field B_{c2} for the present orientation is quite high (> 100 Tesla), it is still surprising that the plasma frequency, which is a measure of the interplanar coupling strength, is hardly affected by the magnetic field even at elevated temperatures.

1.3.3 Discussion

We will now give a more quantitative discussion of the results in terms of existing theoretical models.

As described in section 1.2, the zero field reflectance edge can be fitted suitably to a Josephson coupled layer model, where the screened plasma frequency squared ω_{ps}^2 is proportional to the critical current density j_c which in turn is related to the order parameter Δ by the Ambegaokar-Baratoff expression for a Josephson tunnel junction. The electromagnetic interaction of the induced currents with the vortex lattice due to the Lorentz force was treated explicitly in the work of Brandt [24], Coffey and Clem [25] (CC), and more recently by Tachiki, Koyama and Takahashi [26] (TKT). In

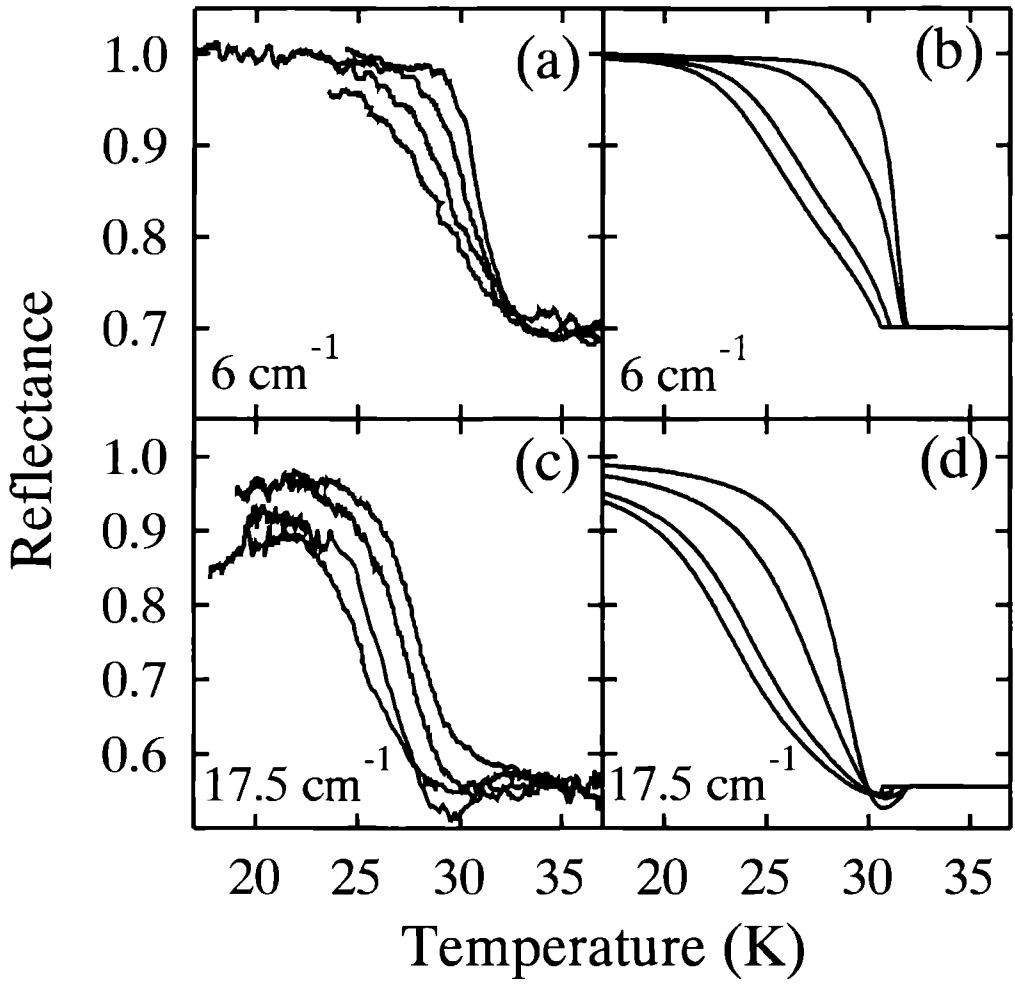

Figure 1.5 *Measured reflectance as a function of temperature for (a) $\omega = 6$ and (c) 17.5 cm^{-1} at (from right to left) $B = 0$, 8, 20 and 25 Tesla. Corresponding calculations based on the model by CC are shown in (b) resp. (d).*

these models, the interaction with the vortices is treated phenomenologically by introducing an effective pinning force constant κ_p, vortex viscosity η and vortex mass M. In the absence of pinning, one expects an enhanced microwave absorption due to dissipation in the cores of moving vortices. In the Bardeen-Stephen approximation [27] one can relate the vortex viscosity to the normal state resistivity multiplied by the density and size of the vortex cores. It is not evident that the mass of the vortices can be neglected at FIR frequencies. Nevertheless, in the analysis presented here we took M=0. Taking a finite value for M only adds an extra fitting parameter and does not change the main conclusions of this analysis.

A drawback of these models is that they are based on the semi-phenomenological London approximation for the ac response of the superconductor with a two-fluid description of the quasiparticle contribution to the complex conductivity. As a result, none of the models is strictly applicable near the plasma edge. This is due to the fact that in the London approximation dielectric displacement currents are neglected. However, the essential cause of the plasma edge is that the inductive current carried by the condensate is balanced by the out of phase dielectric current of the bound charges, manifested by a zero crossing of $\epsilon_1(\omega)$. The unique aspect of the high T_c superconductors is that the low c-axis conductivity leads to a plasma edge below the gap frequency. The fact that there is almost no damping due to dissipative currents (ϵ_2 is small) below the gap leads to the pronounced plasmon effects that are observed. It is important to note that it is the total current that drives the vortex motion by the Lorentz force and not just the free carrier supercurrent. This general argument shows that, at the zero crossing in $\epsilon_1(\omega)$, the electromagnetic coupling to the vortices vanishes (except for the small resistive currents due to excited quasiparticles). Thus, in contrast to some theoretical predictions, we expect basically no reflectance change near the plasma frequency due to the presence of vortices. The experimental observation that the reflectance minimum is independent of the field as shown in figure 1.4 confirms this picture.

A shift of the plasma frequency would, however, be possible due to a pair breaking reduction of the superconductive order parameter. For the present orientation ($B \parallel ab$ planes), the upper critical field is very high (above 100 Tesla). Using standard theory for quasi-2D superconducting layers in a parallel field [20] this would lead to a depression of the plasma frequency of 0.4 cm^{-1} at the maximum field. This is within the experimental

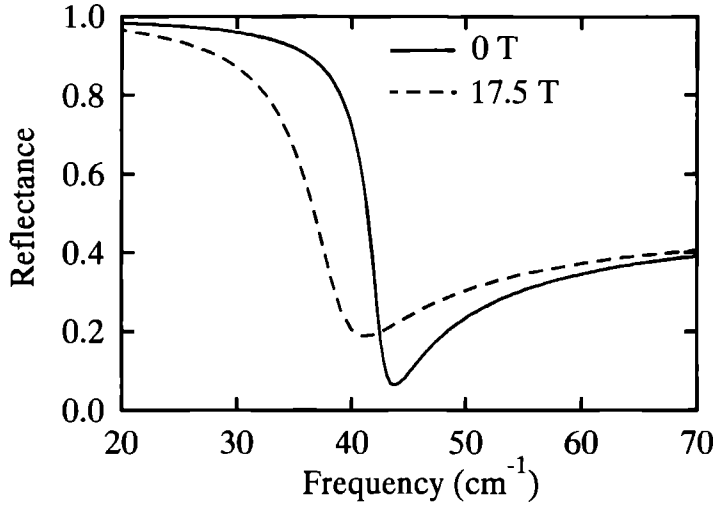

Figure 1.6 *Calculation using the TKT model of the effect of vortex motion on the plasma edge at 17.5 Tesla (dashed line) together with a zero field calculation (solid line).*

accuracy of the data.

For a more quantitative comparison with theoretical predictions we calculated the reflectance using the dielectric function of TKT:

$$\frac{\epsilon_{\mathrm{T}}(\omega)}{\epsilon_0} = \epsilon_c \left(1 - \frac{\omega_{\mathrm{p0}}^2 - \omega_{\mathrm{pn}}^2}{\omega(\omega + i0^+)} - \frac{\omega_{\mathrm{pn}}^2}{\omega(\omega + i\gamma)}\right) \times \left[1 + \frac{\Phi_0}{\mu_0 \lambda^2(0)} \frac{B}{\kappa_{\mathrm{p}} - i\omega\eta - M\omega^2}\right]^{-1} \tag{1.5}$$

The results for zero and 17.5 Tesla are shown in figure 1.6, where we used the following parameters $\kappa_{\mathrm{p}} = 2500$ Pa, $\lambda(0) = 6.8$ μm, $\omega_{\mathrm{p0}} = 42.5$ cm^{-1}, $\omega_{\mathrm{pn}} = 15$ cm^{-1}, $\gamma = 20$ cm^{-1}, and $\epsilon_c = 30$. The vortex viscosity η was calculated from the Bardeen-Stephen relation using $\rho_{\mathrm{n}}(T) = 0.125$ Ωcm. In this parameter set κ_{p} is the basic unknown. All other parameters are either determined directly by the experiment, or taken from independent measurements on similar samples. For the present parameter range the TKT result is

identical to that of the earlier work by CC. Although the general agreement between theory and experiment is not too bad, an essential disagreement is the fact that the experimental plasma frequency is not field dependent as predicted. This is due to the London approximation that is used in these models, as already mentioned. We generalized the theoretical expressions to include displacement currents of the bound charges, and indeed find a much better agreement near the reflectance minimum. However, at present we are not able to reproduce the detailed shape of the observed reflectance edge. In particular, for the same parameters as above we find only a very small deviation from the zero field curve. If we assume a much lower pinning force constant we find a somewhat better agreement near the edge, but a serious discrepancy at low frequencies arises. A full description of the generalized model and details is presented in section 1.4.2. We conclude that the qualitative agreement of the data with flux flow models is somewhat fortuitous and more theoretical work is needed to decide whether the renormalization of the edge can be understood in terms of electromagnetic interaction with flux motion. Also it is not clear whether collective pinning and vortex deformation need to be incorporated. However, it is clear that pinning is substantial and a description in terms of pure Josephson vortices for magnetic fields parallel to the planes is not appropriate.

This brings us to another possible cause for the reflectance changes that occur in a magnetic field: the presence of the vortex cores. In a generalized Abrikosov vortex model it is plausible to assume that the coupling between adjacent planes is no longer uniform and is locally depressed near the vortex cores. Within the assumption of local electrodynamics, this will lead to a local suppression of the plasma frequency and a broadening of the reflectance edge. Despite the small characteristic dimensions of the vortex core this influence can be quite substantial. This is because the large anisotropy in the coherence length implies a large elliptical eccentricity of the vortices and thus a large depolarization factor. Unfortunately, an effective medium model for a continuously varying dielectric function cannot be solved analytically. A preliminary numerical discrete approximation shows that accounting for the local depression of ω_{ps} can indeed have an influence on the reflectivity close to the observed one.

Finally, we turn to the analysis of the data taken at high temperatures. At these elevated temperatures one may expect that vortices become more

mobile and thermally activated (Brownian) motion becomes possible. To account for the thermal effects, we will use the CC approach. The basic expression for the dielectric function $\epsilon_{CC}(\omega)$ which includes both vortex motion and thermally activated creep effects is:

$$\frac{\epsilon_{CC}(\omega)}{\epsilon_0} = \epsilon_c - \frac{c^2}{\omega^2} \frac{1 + 2i\lambda^2(B,T)\delta_{nf}^{-2}(\omega,B,T)}{\lambda^2(B,T) - (i/2)\tilde{\delta}_{vc}^2(\omega,B,T)} \tag{1.6}$$

in which $\delta_{nf}(\omega,B,T)$ and $\tilde{\delta}_{vc}(\omega,B,T)$ are, respectively, the normal fluid skin depth and the complex effective skin depth due to vortex motion and creep. We replaced some of the two fluid expressions used by CC by their analogues in the Josephson picture. The temperature dependent (Josephson) penetration depth $\lambda(T)$ in the absence of pair breaking effects follows from the relation $\lambda = c/\omega_p$,

$$\lambda^2(T) = \lambda^2(0)\frac{\Delta(0)}{\Delta(T)}\frac{1}{\tanh\left(\Delta(T)/2k_BT\right)}. \tag{1.7}$$

The normal fraction is accordingly replaced by $f(T) = 1 - \frac{\lambda^2(0)}{\lambda^2(T)}$. For magnetic fields parallel to the planes, we assumed that $B_{c2}^2(T) = B_{c2}^2(1 - t^2)/(1 + t^2)$ with $t = T/T_c$ the reduced temperature.

The results, for the same parameters as in figure 1.6, and for $B_{c2} = 120$ Tesla, $T_c = 32$ K are shown in figures 1.5b and 1.5d. U, the parameter which sets the energy scale for depinning is taken as 1.5 eV Tesla. Although there is no exact agreement, the general tendency of the magnetic field effect is reproduced quite well.

1.3.4 Summary

We presented measurements of the c-axis reflectance in $La_{1.85}Sr_{0.15}CuO_4$ from 6 to 70 cm^{-1} in fields up to 25 Tesla. A small renormalization of the plasma edge is observed. No significant change in the plasma frequency nor in the absorption at the plasma frequency is found. This demonstrates that near the plasma edge one cannot neglect the displacement current due to bound charges as assumed in existing models. The various results are fairly consistent and all imply a rather strong pinning of the vortices.

1.4 Theoretical description

The appearance of the *c*-axis plasma edge is intimately related to the supercurrent which can flow in the *c*-direction. This is illustrated by the following argument based on the Kramers-Kronig relations [28]. These relations state that causality closely links the real and imaginary parts of the conductivity spectrum in linear response theory. If the real part is known for all frequencies then the imaginary part can be calculated and vice-versa. Therefore, if there is a dissipationless dc supercurrent, described by a delta function at zero frequency in $\sigma_1(\omega)$ then it follows from the Kramers-Kronig relations that there should be a corresponding contribution to the imaginary part $\sigma_2(\omega)$ proportional to $1/\omega$. With $\epsilon(\omega) = \epsilon + i\sigma(\omega)/\omega$ this directly gives a plasmon-type of dielectric function.

Moreover, this reasoning shows that the presence of a plasma edge is not restricted to the specific type of interlayer coupling. In the classical bulk superconductors the same argument applies, but because the metallic conductivity is usually much larger, a pole would occur at frequencies far above the gap, and the response in the superconducting state is very similar to that of the normal state. Note that in the latter case the plasma edge is due to a resonance in the charge density oscillation, in contrast to the Josephson case described below where the plasma edge is due to resonant oscillations of the local phase of the order parameter.

Below we will show how the *c*-axis plasmon in the high T_c cuprates can be described by a Lawrence-Doniach type of model [29] if we assume that the superconducting CuO_2 layers are Josephson coupled. This assumption is not unreasonable since the thickness of the poorly conducting layers separating the superconducting planes is of atomic dimensions, so that Cooper pairs can tunnel or diffuse from one CuO_2 plane to another, thereby establishing phase coherence. A similar model has been proposed by Bulaevskii *et al.* [30].

In section 1.4.1 we present this Josephson model and show that the plasmon appears naturally in this model as an oscillation of the order parameter phase difference between adjacent layers. In section 1.4.2 we investigate the behaviour of this plasmon in a magnetic field. In particular, we will calculate the extra dissipation in the mixed state due to vortices moving under the influence of the Lorentz force. The usual starting point in literature is a London approximation for the complex conductivity.

However, in this approximation one neglects the polarization current due to bound charges. We will show that the inclusion of the polarization current is essential at frequencies near the plasma edge.

1.4.1 Josephson plasmon

In this section we will show that a small interlayer coupling in a layered superconductor will give rise to a low frequency plasmon in the out-of-plane response. We start from a Lawrence-Doniach [29] picture *i.e.* we assume that the material can be treated as a stack of quasi two dimensional superconductors at a periodic distance d. The macroscopic wave function of layer n can be written as: $\Psi_n = \Delta_0 e^{i\phi_n}$. The superconducting layers are separated by weakly metallic or dielectric layers through which Josephson coupling is established. As a consequence, the supercurrent density j_s and the potential difference V between adjacent layers are connected by the Josephson relations:

$$j_s = j_c \, sin(\phi_n - \phi_{n+1}) = j_c \, sin(\varphi) \tag{1.8}$$

$$V = \frac{\hbar}{2e}\frac{d\varphi}{dt} \tag{1.9}$$

We will assume that the dc Josephson relation for the supercurrent remains valid at finite frequencies ω much smaller than the gap frequency ω_g. At the end of this section we will come back to the regime $\omega \approx \omega_g$ where this assumption is no longer valid.

The total ac current $j(t)$ induced by the electromagnetic field can be written as $j(t) = j_s + j_{qp} + j_p$ where j_s is the Josephson supercurrent, j_{qp} is the dissipative current due to excited quasiparticles, and j_p, is the polarization current due to the bound carriers and is thus proportional to the dielectric susceptibility of the material for this field direction, χ_c. Using the Josephson equations we can write:

$$j_s = j_c \sin\varphi \tag{1.10}$$

$$j_{qp} = V\sigma_{qp} = \frac{\hbar\sigma_{qp}}{2e}\frac{d\varphi}{dt} \tag{1.11}$$

$$j_p = \frac{\epsilon_0\chi_c}{d}\frac{dV}{dt} = \frac{\epsilon_0\chi_c}{d}\frac{\hbar}{2e}\frac{d^2\varphi}{dt^2}\,, \tag{1.12}$$

where the quasiparticle conductivity σ_{qp} is, in principle, temperature and frequency dependent. At low current densities we can linearize equation (1.10) with respect to φ. For solutions that have the same harmonic $e^{-i\omega t}$ time dependence for $j(t)$ and φ, we obtain:

$$j(t) = j_c\varphi(1 - \omega^2 L_J \frac{\epsilon_0\chi_c}{d} + L_J\sigma_{qp}) \quad (1.13)$$

$$V(t) = -i\omega j_c L_J\varphi \ , \quad (1.14)$$

where $L_J = \hbar/2ej_c$ is the nonlinear Josephson inductance. Using $j = \sigma V/d$ and $C = \epsilon_0(\chi_c + 1)/d = \epsilon_0\epsilon_c/d$, it is straightforward to deduce the complex conductivity $\sigma_J(\omega)$,

$$\sigma_J(\omega) = \epsilon_0\epsilon_c\left(\gamma + i(\frac{\omega_{ps}^2}{\omega} - \frac{\epsilon_0\chi_c}{Cd})\right) \ . \quad (1.15)$$

The corresponding dielectric response $\epsilon_J(\omega) = \epsilon_0 + i\sigma_J(\omega)/\omega$ is,

$$\epsilon_J(\omega) = \epsilon_0\epsilon_c(1 - \frac{\omega_{ps}^2}{\omega^2} + \frac{i\gamma}{\omega}) \ . \quad (1.16)$$

In the last two equations we have introduced the screened plasma frequency $\omega_{ps} = 1/\sqrt{L_J C}$ and the damping $\gamma = \sigma_{qp}C^{-1}$.

The reflectance $\mathcal{R}$ can now be calculated from:

$$\mathcal{R} = \left|\frac{1 - \sqrt{\epsilon_J(\omega)/\epsilon_0}}{1 + \sqrt{\epsilon_J(\omega)/\epsilon_0}}\right|^2 \quad (1.17)$$

From this derivation it is clear that any layered superconductor with a sufficiently weak (Josephson) coupling between the planes will have a plasma resonance at frequencies below the energy gap. The electrodynamic properties are completely analogous to the classical results derived for large single junctions, with the exception that the effective width of the junction $d + 2\lambda$ is replaced by the interlayer distance.

When we want to calculate the actual value of ω_{ps}, we need to know the size of the dc critical current density j_c. For simplicity, we will determine j_c from the Ambegaokar-Baratoff relation for Josephson tunnel junctions [17]:

$$j_c = \frac{\pi\Delta(T)}{2eR_n}\tanh\frac{\Delta(T)}{2k_BT}. \quad (1.18)$$

In this equation, R_n is the characteristic normal state resistance of the junctions which we put equal to the normal state resistivity ρ_n times the layer separation d. Using typical parameters for $La_{1.85}Sr_{0.15}CuO_4$ ($\epsilon_c = 30, \rho_n = 0.00125\ \Omega^{-1}m^{-1}$, $T_c = 34$ K) and a BCS weak coupling order parameter $\Delta_0 = 1.76 k_B T_c$, we find $\omega_{ps} = 46\ cm^{-1}$ at low temperatures, which is indeed close to the experimental result for this material (see section 1.2).

In $La_{1.85}Sr_{0.15}CuO_4$ the screened plasma frequency ω_{ps} is approximately half the BCS weak coupling gap frequency ω_g. It is thus not evident that we can use the simple relation (1.10) to describe the Josephson current near this frequency.
To check this, we use the model developed by Ferrell [31]. He derived the generalized ac response of a Josephson junction at arbitrary frequency and $T = 0$ using standard BCS expressions and causality arguments. The basic result for the dielectric function at zero applied dc current which can be derived from this model is

$$\epsilon_F(\omega) = \epsilon_0 \epsilon_c \left(1 - \frac{\omega_g}{\rho_n \epsilon_c \omega^2} E(\omega/\omega_g)\right) , \qquad (1.19)$$

in which E is the complete elliptic integral of the second kind. Figure 1.7 shows the reflectance following from equation (1.19) together with that from our simple dielectric function with no damping. We used the same parameters as above and a BCS weak coupling gap frequency $\omega_g = 3.52 k_B T_c$. It is clear that for this parameter range the deviations between the two reflectance curves are marginal which shows that it is indeed valid to use equation (1.10) up to frequencies $\omega \approx \frac{1}{2}\omega_g$.

1.4.2 Influence of vortices

In this section we will evaluate the effect of a finite magnetic field B parallel to the wave vector of the incident light. Vortices will enter the sample preferentially between the superconducting layers. Again we will assume $\omega \ll \omega_g$ and we will neglect pair breaking effects of B. When the barrier layers are (weakly) metallic there will be a proximity induced order parameter and the vortices will be Abrikosov-like in nature rather than Josephson-like. Nevertheless, we will neglect the possible influence of the

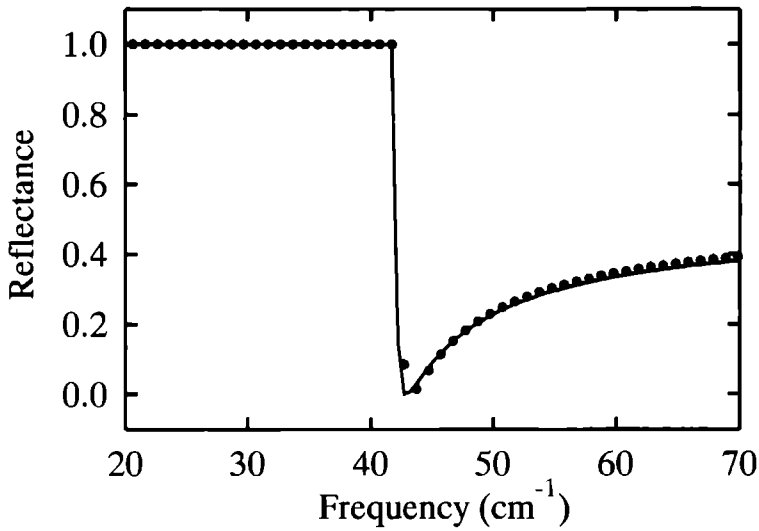

Figure 1.7 *Computed reflectance curves at zero magnetic field. The circles are calculated with the model presented here (equation 1.16) and the solid line represents a calculation with Ferrell's model (equation 1.19).*

vortex cores on the dielectric response. As usual, we will characterize the vortices by a phenomenological vortex mass per unit length M, a vortex viscosity η and a pinning force constant $\kappa_{\rm p}$.

In the present geometry, the vortices will be accelerated by the Lorentz force $F_{\rm L}$ that is exerted by the current $j(t)$. The influence of Lorentz force driven vortex motion on the electromagnetic response of a superconductor was studied in many papers [24–26, 32, 33]. In all these papers the London approximation was used and, thus, the effects of the polarization current $j_{\rm p}$ were neglected. This is perfectly valid when describing the electromagnetic response of superconductors at frequencies much lower than either $\omega_{\rm g}$ or $\omega_{\rm ps}$. This approach fails however for the c-axis response of high temperature superconductors in which the highly unusual situation is encountered that the plasma frequency is *smaller* than the gap frequency. This means that when we want to study the effect of moving vortices on the low frequency plasma mode, near which $j_{\rm s} \approx -j_{\rm p}$, polarization effects may not be neglected. In particular, the polarization current should be included in the expression for $F_{\rm L}$. This leads to the following harmonic equation of motion

for the vortices [25],

$$M\frac{d^2u}{dt^2} + \eta\frac{du}{dt} + \kappa_p u = (j_s + j_{qp} + j_p)\Phi_0 \ , \tag{1.20}$$

in which u is the displacement of the vortices from their equilibrium positions. We neglect forces related to deformation of the vortex lines which are brought about by *e.g.* the finite wavelength of the light in the sample and a nonuniform pinning force constant along the length of the vortex.

Below we will calculate the extra absorption due to moving vortices following the Josephson model described in the previous section. Note, however, that the effect of the polarization currents is more general and not restricted to specific assumptions regarding the coupling of the layers.

Moving vortices cause a change in the phase difference between two adjacent layers given by,

$$\dot{\varphi} = 2\pi\dot{u}\frac{B}{\Phi_0}d \ . \tag{1.21}$$

Together with the equation of motion (1.20) and $j = \sigma V/d$ we obtain for the conductivity of the vortex system $\sigma_v(\omega)$:

$$\sigma_v(\omega) = \frac{1}{\Phi_0 B}(\eta + i\frac{\kappa_p}{\omega} - M\omega) \ . \tag{1.22}$$

We account self-consistently for the current changes due to the vortex motion by taking $\sigma_v(\omega)$ electrically in series with the Josephson conductivity (1.15). The total conductivity follows in a straightforward way,

$$\begin{aligned} \sigma_t(\omega) &= \sigma_J(\omega)\left(1 + \frac{1}{\sigma_J(\omega)/\sigma_v(\omega)}\right) = \\ &= -i\omega(\epsilon_J(\omega) - \epsilon_0)\left(1 + \frac{(\epsilon_J(\omega) - \epsilon_0)B\Phi_0}{M - \frac{\kappa_p}{\omega^2} + i\frac{\eta}{\omega}}\right)^{-1} \ , \end{aligned} \tag{1.23}$$

and yields a total dielectric function

$$\epsilon_t(\omega) = \epsilon_0 + (\epsilon_J(\omega) - \epsilon_0)\left(1 + \frac{(\epsilon_J(\omega) - \epsilon_0)B\Phi_0}{M - \frac{\kappa_p}{\omega^2} + i\frac{\eta}{\omega}}\right)^{-1} \tag{1.24}$$

If we neglect the polarization current in equation (1.20), $\sigma_v(\omega)$ will only be in series with the inductive part of the Josephson conductance $\epsilon_0\epsilon_c(\gamma +$

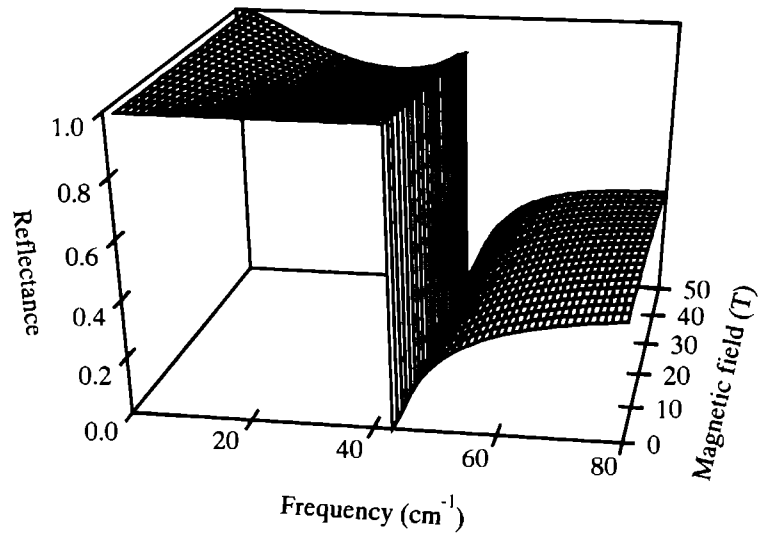

Figure 1.8 *Reflectance versus frequency and magnetic field using the model presented here.*

$i\omega_{ps}^2/\omega^2$). If we further neglect any damping and add a separate capacitive response, equation (1.24) reduces to the TKT result [26]:

$$\epsilon_T(\omega) = \epsilon_0\epsilon_c - \epsilon_0\epsilon_c\frac{\omega_{ps}^2}{\omega^2}\left(1 + \frac{B\Phi_0\epsilon_c\omega_{ps}^2}{\kappa_p - M\omega^2 - i\eta\omega}\right)^{-1}, \qquad (1.25)$$

with $\epsilon_c\omega_{ps}^2$ the unscreened plasma frequency used in Ref. 26.

The reflectances calculated with the model presented above and with the TKT model are given in figures 1.8 and 1.9, respectively, for the case of low damping. In both figures the following parameters were used: $M = 0$, $\kappa_p = 500$ Pa, $\eta = 1.85 \times 10^{-10}$ Pa s, $\epsilon_c = 30$, and $\omega_{ps} = 42.5$ cm^{-1}. Our result in figure 1.8 shows almost no changes in reflectance near ω_{ps} as the field increases, only some increased absorption at frequencies away from ω_{ps} is observed. The field induced effect on the plasma frequency itself is very small. This is exactly what one should expect near the plasma frequency: The polarization current and the free carrier supercurrent are out of phase and nearly cancel when $\omega \approx \omega_{ps}$ which results in a zero Lorentz force on the vortices and, hence, no extra dissipation.

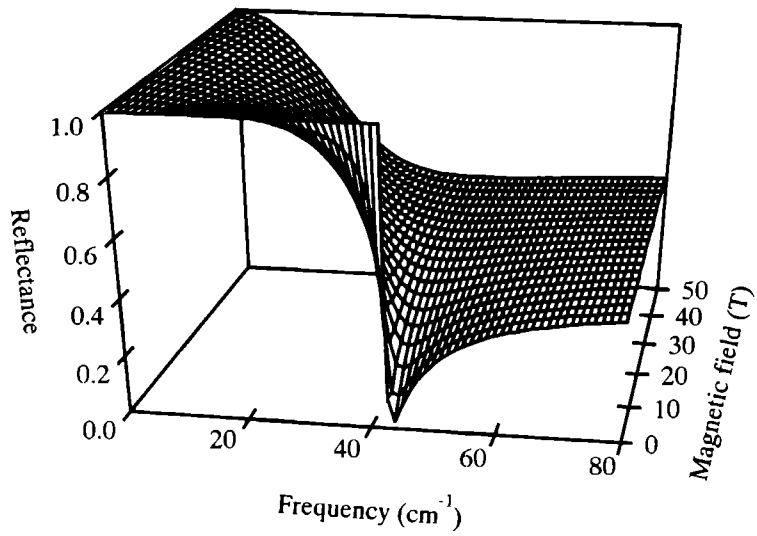

Figure 1.9 *Reflectance versus frequency and magnetic field using the TKT model [26].*

1.4.3 Summary

We presented a simple model which describes the electromagnetic response of Josephson coupled layered superconductors. The model is applicable to *e.g.* the *c*-axis response of high temperature superconductors and provides an elegant description of the low frequency plasmon that was observed in these materials. In a parallel magnetic field, we find that, in contrast to recent predictions, vortex motion does not have an appreciable influence on the plasma frequency itself nor on the damping near the plasma frequency. The reason for this is that the supercurrent and the polarization current cancel each other at frequencies near the plasma frequency.

References

1. J.G. Bednorz and K.A. Müller, Z. Phys. B **64**, 189 (1986).
2. A. Schilling, M. Cantoni, J.D. Guo, and H.R. Ott, Nature **362**, 56 (1993).
3. I. Tanaka and H. Kojima, Nature **337**, 21 (1989).
4. S.L. Cooper and K.E. Gray, in *Physical Properties of High Temperature Superconductors IV*, edited by D.M. Ginsberg (World Scientific, Singapore, (1994).
5. Z. Schlesinger, R.T. Collins, M.W. Shafer, and E.M. Engler, Phys. Rev. B **36**, 5275 (1987); D.A. Bonn, J.E. Greedan, C.V. Stagar, T. Timusk, M.G. Doss, S.L. Herr, K. Kamaras, C.D. Porter, D.B. Tanner, J.M. Tarascon, W.R. McKinnon, and L.H. Greene, Phys. Rev. B **35**, 8843 (1987); M.S. Sherwin, P.L. Richards, and A. Zettl, Phys. Rev. B **37**, 1587, (1988).
6. T.W. Noh, S.G. Kaplan, and A.J. Sievers, Phys. Rev. B **41**, 307 (1990).
7. K. Tamasaku, Y. Nakamura, and S. Uchida, Phys. Rev. Lett. **69**, 1455 (1992).
8. J. Bardeen, L.N. Cooper, and J.R. Schrieffer, Phys. Rev. **108**, 1175 (1957).
9. P.W. Anderson, Phys. Rev. **112**, 1900 (1958).
10. C.C. Homes, T. Timusk, R. Liang, D.A. Bonn, and W.N. Hardy, Phys. Rev. Lett. **71**, 1645 (1993).
11. D.N. Basov, T. Timusk, B. Dabrowski, and J.D. Jorgensen, Phys. Rev. B **50**, 3511 (1994).
12. S. Tajima, G.D. Gu, S. Miyamoto, A. Odagawa, and N. Koshizuka, Phys. Rev. B **48**, 16164 (1993).
13. B.D. Josephson, Adv. Phys. **14**, 419 (1965).
14. See *e.g.* J.R. Clem, Physica A **200**, 118 (1993).
15. R. Kleiner and P. Müller, Phys. Rev. B **49**, 1327 (1994).
16. V.H.M. Duijn, N.T. Hien, A.A. Menovsky, and J.J.M. Franse, Physica C **235-240**, 559 (1994).
17. V. Ambegaokar and A. Baratoff, Phys. Rev. Lett. **10**, 486 (1963); erratum, **11**, 104 (1963).

18. K. Kishio, Y. Nakayama, N. Motohira, T. Noda, T. Kobayashi, K. Kitazawa, K. Yamafuji, I. Tanaka, and H. Kojima, Supercond. Sci. Technol. **5**, Iss S1, S69 (1992).
19. R. Landauer, J. Appl. Phys. **23**, 779 (1952).
20. K. Maki, in *Superconductivity* edited by R.D. Parks, (Marcel Dekker, New York, 1969).
21. See *e.g.* M. Tinkham, in *Introduction to Superconductivity*, (McGraw-Hill, New York, 1975).
22. T.W. Noh, S.G. Kaplan, and A.J. Sievers, Phys. Rev. B **41**, 307 (1990).
23. C.P. Bean, Phys. Rev. Lett. **8**, 250 (1962).
24. E.H. Brandt, Phys. Rev. Lett. **67**, 2219 (1991).
25. M.W. Coffey and J.R. Clem, Phys. Rev. Lett. **67**, 386 (1991).
26. M. Tachiki, T. Koyama, and S. Takahashi, Phys. Rev. B **50**, 7065 (1994).
27. J. Bardeen and M.J. Stephen, Phys. Rev. **140**, A1197 (1965).
28. N.W. Ashcroft and N.D. Mermin, in *Solid State Physics* (Saunders College, Philadelphia, 1976).
29. W.E. Lawrence and S. Doniach, in *Proceedings of the 12th International Conference on Low Temperature Physics, Kyoto, 1970*, edited by E. Kanda (Keigaku, Tokyo, 1970), p. 361.
30. L.N. Bulaevskii, M. Zamora, D. Baeriswyl, H. Beck and J.R. Clem, Phys. Rev. B **50**, 12831 (1994).
31. R.A. Ferrell, Physica C **152**, 10 (1988).
32. M.W. Coffey and J.R. Clem, Phys. Rev. B **48**, 342 (1993).
33. N.C. Yeh, Phys. Rev. B **43**, 523 (1991).

Chapter 2

Far-infrared reflectance of $YBa_2Cu_3O_7$ at high magnetic fields

Parts of this chapter have been published in:
- Physica C **235-240**, 1115 (1994).

2.1 Introduction

It was shown by Glover and Tinkham [1] that the electromagnetic absorption of conventional superconductors at low energies is reduced when they enter the superconducting state. In many cases, the absorption even completely vanishes below a certain threshold energy $\hbar\omega_g$ called the quasiparticle gap or superconductive gap. This discovery played a central role in establishing the validity of the Bardeen, Cooper and Schrieffer (BCS) theory [2]. In this theory, the gap energy $\hbar\omega_g$ is equal to $3.52k_BT_c$ at low temperatures. The lost spectral weight in the real part of the conductivity is transferred by coherence effects to a delta function at zero frequency. This delta function represents the energy absorption from a dc electric field in order to accelerate the superconducting condensate.

In view of the success of infrared studies on classical superconductors, many similar studies were undertaken on the CuO_2 or *ab* planes of the high temperature superconductors. As these planes are a common feature of these compounds, studying their conductivity may provide clues on the mechanism causing the extremely high critical temperatures observed in these materials. Results on the *ab* optical properties of several high T_c compounds were recently reviewed by Tanner and Timusk [3].

In the high T_c compound most intensively studied, $YBa_2Cu_3O_7$, many groups have observed a clear 'knee'-like feature at 400-500 cm^{-1} in infrared reflectivity spectra. This feature had a large temperature dependence near T_c and a gap-like structure could be seen in the conductivity. As a consequence, a number of groups attributed this feature to the quasiparticle gap [4–6]. Many arguments have been brought up against this assignment because the feature showed very anomalous behaviour for a superconductive gap. The 'knee' appeared at an unusually high frequency ($\hbar\omega_g/k_BT_c \approx 8$) and did not shift as a function of temperature. Furthermore it did not change its frequency in materials with doping-reduced T_c and it was visible in the spectra above T_c.

Another objection against the gap assignment was that the *ab* plane electrodynamics of the high temperature superconductors is in the clean limit *i.e.* the electronic mean free path l is (much) larger than the coherence length ξ and that therefore the superconductive gap can not be seen. The reason for this is that when such a clean superconductor enters the superconducting state, nearly all spectral weight of the conductivity vanishes

into the delta function at zero frequency leaving only a marginal conductivity above the gap which is therefore difficult to detect [7,8].

Direct absorption measurements by Pham *et al.* [9] indicated, with an order of magnitude better accuracy than the reflectivity data, a finite *ab* conductivity at least down to 80 cm^{-1}. The absorption increased considerably above 500 cm^{-1}, but there was no sharp feature which one could identify with the gap. The classical BCS *s*-wave order parameter proposed for $YBa_2Cu_3O_7$ in Refs. 4–6 is not in agreement with these observations. The results of Pham *et al.* are not inconsistent with a *d*-wave order parameter: in this case low energy excitations are possible and the onset of absorption at ω_g is less pronounced. Recently, a number of experiments have yielded strong evidence that the order parameter in the *ab* planes indeed has this *d*-wave symmetry. In one of these experiments, Hardy *et al.* observed a linear temperature dependence of the magnetic penetration depth [10] which is characteristic for a superconductor having an order parameter with nodes such as a *d*-wave order parameter. A *d*-wave order parameter should moreover change sign across these nodes. Experiments based on the Josephson effect are the only ones that can show whether the order parameter actually does this. The observation of a Josephson supercurrent minimum at zero magnetic field in Pb-$YBa_2Cu_3O_7$ SQUIDs [11,12] and the observation of spontaneous magnetization of a three junction ring with half a flux quantum [13] both gave strong evidence for these sign changes.

Because the 'knee'-like feature appears both above and below T_c, and is insensitive to changes in the doping level, Timusk, Porter and Tanner (TPT) [14] suggested that its origin should be phononic rather than electronic. They proposed that the explanation of the 'knee' should be found in a mechanism similar to what they called the charged-phonon mechanism. This mechanism was originally discussed by Rice [15] (who used the term 'phase phonons') to explain anomalous phonon features commonly seen in the spectra of quasi one-dimensional organic conductors [16] and describes how normally forbidden phonons can become visible with unusually large oscillator strengths by coupling to the electronic system via charge density wave distortions. TPT argued that, in the high T_c compounds, the phonons coupled to bound carriers responsible for the mid-infrared absorption band [3] commonly observed in these materials. The origin of the cou-

pling itself was supposed to be related to an incipient structural instability or to spin fluctuations [17].

It is well known that the normal state properties of the high T_c superconductors such as the electronic relaxation rate and the phonon dynamics are strongly temperature dependent. Thus, an intrinsic problem of using temperature to drive the material superconducting is that reflectance changes due to the normal state properties obscure those due to superconductivity. One way to influence only the superconductivity of a material without affecting its normal state properties is to apply a magnetic field because it changes the coupling between the superconducting pairs. We will use just this method in the present chapter.

In the BCS theory superconducting singlet pairs are formed in a time reversed way *i.e.* by coupling a quasiparticle with wave vector $\vec{k}$ to a quasiparticle with wave vector $-\vec{k}$. When a magnetic field is applied time-reversal symmetry is broken. This has the effect that the wave vector of one paired quasiparticle in a Cooper pair is changed with $\delta\vec{k}$ with respect to the wave vector of its 'mate' which results in a net momentum of the Cooper pairs transverse to the field direction. At a critical value of the magnetic field $\delta\vec{k}$ becomes too large and the pairs break apart. This process, called orbital frustration or diamagnetic pair breaking, is one example of a pair breaking effect caused by a perturbation which destroys time reversal degeneracy of the paired states. Pair breaking was first treated by Abrikosov and Gor'kov [18] for the case of a superconductor containing magnetic impurities (which also break time-reversal symmetry) and was later generalized by Maki [19] and de Gennes [20] for other pair breaking perturbations such as an applied magnetic field. It is found that the presence of these pair breaking perturbations will cause superconducting quantities such as the order parameter Δ and the gap frequency ω_g to decrease [21]. Tinkham and coworkers [22] were very successful investigating this effect on the far-infrared and millimeter wave absorption of classical superconductors.

When the critical magnetic fields for diamagnetic pair breaking are very large or when the Meissner effect is only partial because of geometrical reasons another effect becomes important. The magnetic field will split the quasiparticle density of states (QP-DOS) by the Zeeman energy which leads, for a finite spin-flip scattering time, to an additional decrease of ω_g by $2\mu_B B$ and to additional fine structure in the conductivity. For finite spin-orbit coupling this simple picture is no longer valid but the effect on ω_g

will be basically the same. This Zeeman splitting of the QP-DOS has been observed by van Bentum and Wyder [23] in infrared experiments on thin superconducting Al films in a parallel magnetic field and this observation confirmed the spin singlet state of the condensed pairs. Before it had been demonstrated very convincingly in the tunneling experiments of Tedrow and Mersevey [24]. At very high magnetic fields, when the pairs are not already broken by orbital effects, it becomes energetically more favourable for all spins to align than to pair antisymmetrically into Cooper pairs. This effect is called Pauli pair breaking.

The pair breaking effect of a magnetic field on the high temperature superconductors has not been studied intensively. This is partly because the critical magnetic fields are much larger than any available laboratory magnet can supply stationarily.

In this chapter we investigate the *ab* plane reflectance of $YBa_2Cu_3O_7$ in perpendicular magnetic fields. The field, although it enters in the form of Abrikosov vortices (see chapter 1), is almost uniform inside the film. This is because the penetration depth is much larger than the inter-vortex distance at typical magnetic field values used (up to 15.5 Tesla). and thus diamagnetic pair breaking effects are rather small. Although these fields are still far below the critical field for $YBa_2Cu_3O_7$($B_{c2\perp} \approx$ 60-100 T) it is estimated that pair breaking effects and the paramagnetic shift due to the Zeeman splitting of the QP-DOS are sufficiently strong to cause a noticeable shift of the gap structure(s).

2.2 Experimental details

Our experiments were done on a 2000 Å thick microtwinned $YBa_2Cu_3O_7$ thin film grown by laser ablation onto a (100) $SrTiO_3$ substrate. The spectrometer used was a Bruker IFS113v. Infrared measurements as a function of temperature at $B = 0$ were done using a cold finger cryostat (Oxford CF1104) with polyethylene windows. Field dependent measurements at 1.2 K were done in a ^{3}He system equipped with a bolometer at 0.4 K which had been placed in a superconducting magnet system. The magnetic field was oriented perpendicular to the *ab* planes.

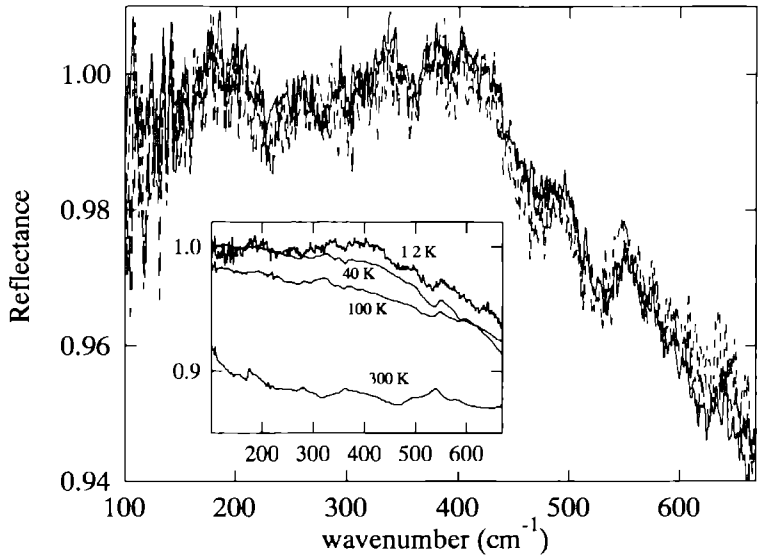

Figure 2.1 *In-plane reflectance of $YBa_2Cu_3O_7$ at magnetic fields of 0, 5, 10 and 15.5 Tesla (all at 1.2 K). Inset: zero field reflectance at 1.2, 40, 100, and 300 K.*

2.3 Results and discussion

In the inset of figure 2.1 we show the reflectance spectra of the film at $B = 0$ at different temperatures. Part of the structure visible at room temperature is due to substrate phonons. With decreasing temperature, most structure disappears but a clear absorption edge develops at 400-500 cm^{-1}, in accordance with spectra measured by many other groups. When the temperature is lowered to 1.2 K this edge sharpens into a sharp kink. Note that such a clear kink in the reflectance can only be due to the opening of an energy gap if the material is in the dirty limit [7]. If this feature was attributed to the superconductive gap, both the size of this gap (which would correspond to a value $2\Delta/k_BT_c \approx 6.4$), and its temperature dependence would be distinctly non-BCS. An independent test for this possible assignment is to investigate the magnetic field dependence of the feature. To estimate the diamagnetic pair breaking effect for the particular geometry of a thin superconducting film in a perpendicular magnetic field we use the work of Hendriks [25]. Assuming that the critical field perpendicular to the *ab* planes is of order 80

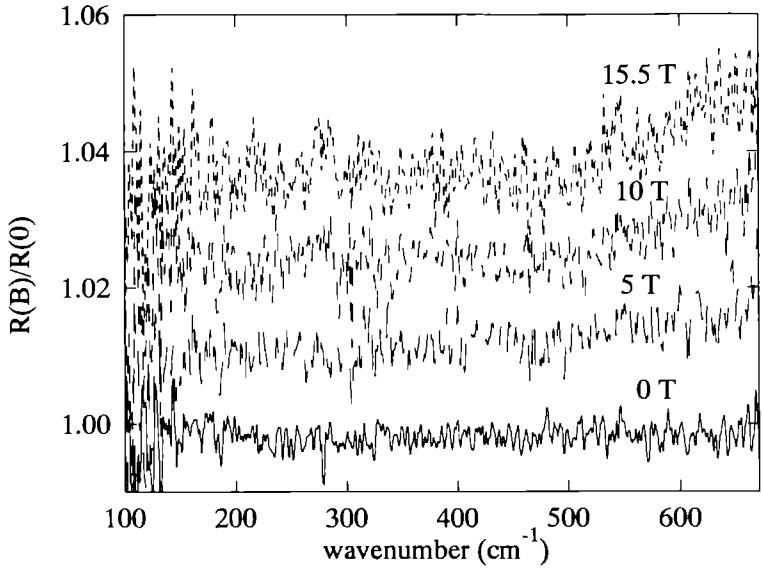

Figure 2.2 *$YBa_2Cu_3O_7$ reflectance at various different magnetic fields normalized to the reflectance in zero field. The spectra are offset for clarity.*

Tesla, we expect the kink to shift about 10 cm^{-1} to lower energies due to pair breaking effects for the maximum fields used and about 15 cm^{-1} due to the Zeeman splitting of the QP-DOS.

The reflectance spectra with applied magnetic field are shown in figure 2.1. Within the experimental accuracy (0.5 % in relative intensity, resolution 1 cm^{-1}) the 400 cm^{-1} kink is found at the same frequency ($\pm$ 10 cm^{-1}) in fields up to 15.5 Tesla.

In order to enhance any field possible dependence we have normalized the spectra taken in a magnetic field B on a zero field spectrum and have plotted the resulting spectra in figure 2.2. The curves are offset for clarity. As indicated before, no change in reflectivity is observed near 400 cm^{-1}. However, we do find a weak shoulder above approximately 500 cm^{-1} which increases with increasing magnetic field but which cannot be due to an isotropic superconductive gap because the absorption onset is clearly below this frequency. The field independence of the 400 cm^{-1} edge favours explanations of this feature which are not directly related to superconductivity such as the charged-phonon model.

The absence of a clear gap structure is in agreement with a combination of both the proposed clean limit *ab* plane electrodynamics of $YBa_2Cu_3O_7$ films and a considerable (anisotropic) spreading of the gap value as expected in a very anisotropic *s*-wave or *d*-wave symmetry ground state. In both cases, one does not expect a clear reflectivity edge which would shift in field but rather a small decrease of reflectivity in the whole subgap region. Although the absolute accuracy in our data does not allow distinct conclusions one could speculate that the $\vec{k}$-dependent gap has a fairly flat distribution up to about 500 cm^{-1}.

2.4 Summary

We observed that the reflectance edge of $YBa_2Cu_3O_7$ at 400 cm^{-1} develops into a distinct kink when the temperature is lowered to 1.2 K. This absorption edge is, within the experimental accuracy, independent of the magnetic field up to 15.5 Tesla. This observation favours explanations of the absorption edge such as given in the charged-phonon model. The absence of clear field induced changes in the reflectance is consistent with both clean limit electrodynamics and a considerable spread in the value of the gap.

References

1. R.E. Glover and M. Tinkham, Phys. Rev. **104**, 844 (1956); **108**, 243 (1957).
2. J. Bardeen, L.N. Cooper, and J.R. Schrieffer, Phys. Rev. **108**, 1175 (1957).
3. D.B. Tanner and T. Timusk, in *Physical Properties of High Temperature Superconductors III* (World Scientific, Singapore 1992).
4. Z. Schlesinger, R.T. Collins, F. Holtzberg, C. Feild, S.H. Blanton, U. Welp, G.W. Crabtree, Y. Fang, J.Z. Liu, Phys. Rev. Lett. **65**, 801 (1990).
5. J. Schützmann, W. Ose, J. Keller, K.F. Renk, B. Roas, L. Schultz, and G. Saemann-Ischenko, Europhys. Lett. **8**, 679 (1989).
6. D. van der Marel, M. Bauer, E.H. Brandt, H.-U. Habermeier, D. Heitmann, W. König, and A. Wittlin, Phys. Rev. B **43**, 8606 (1991).
7. T. Timusk, S.L. Herr, K. Kamarás, C.D. Porter, D.B. Tanner, D.A. Bonn, J.D. Garrett, C.V. Stager, J.E. Greedan, and M. Reedyk, Phys. Rev. B **38**, 6683 (1988).
8. K. Kamarás, S.L. Herr, C.D. Porter, N. Tache, D.B. Tanner, S. Etemad, T. Venkatesan, E. Chase, A. Inam, X.D. Wu, M.S. Hedge, and B. Dutta, Phys. Rev. Lett. **64**, 84 (1990); erratum **64**, 1692 (1990).
9. T. Pham, M.W. Lee, H.D. Drew, U. Welp, and Y. Fang, Phys. Rev. B **44**, 5377 (1991).
10. W.N. Hardy, D.A. Bonn, D.C. Morgan, Ruixing Liang, and Kuan Zhang, Phys. Rev. Lett. **70**, 3999 (1993).
11. D.A. Wollman, D.J. van Harlingen, W.C. Lee, D.M. Ginsberg, and A.J. Leggett, Phys. Rev. Lett. **71**, 2134 (1993).
12. D.A. Wollman, D.J. van Harlingen, J. Giapintzakis, and D.M. Ginsberg, Phys. Rev. Lett. **74**, 797 (1995).
13. C.C. Tsuei, J.R. Kirtley, C.C. Chi, Lock See Yu-Jahnes, A. Gupta, T. Shaw, J.Z. Sun, and M.B. Ketchen, Phys. Rev. Lett. **73**, 593 (1994).
14. T. Timusk, C.D. Porter, and D.B. Tanner, Phys. Rev. Lett. **66**, 663 (1991).
15. M.J. Rice, Phys. Rev. Lett. **37**, 36 (1976).

16. M.J. Rice, L. Pietronero, and P. Brüesch, Solid State Commun. **21**, 757 (1977).
17. M. Reedyk, T. Timusk, and D. Basov, Phys. Rev. Lett. **71**, 2677 (1993).
18. A.A. Abrikosov and L.P. Gor'kov, Zh. Eksperim. i. Teor. Fiz. **39**, 1781 (1960) [Sov. Phys. JETP **12**, 1243 (1960).
19. K. Maki, Prog. Theoret. Phys. (Kyoto) **29**, 10 (1963).
20. P.G. de Gennes, Phys. Kondens. Mat. **3**, 79 (1964).
21. S. Skalski, O. Betbeder-Matibet, and P.R. Weiss, Phys. Rev. **136**, A1500 (1964).
22. R.H. White and M. Tinkham, Phys. Rev. **136**, A203 (1964);
J. Millstein and M. Tinkham, Phys. Rev. **158**, 325 (1967);
W.S. Martin and M. Tinkham, Phys. Rev. **167**, 421 (1968).
23. P.J.M. van Bentum and P. Wyder, Phys. Rev. B **34**, 1582 (1986).
24. R. Mersevey, P.M. Tedrow, and P. Fulde, Phys. Rev. Lett. **25**, 1270 (1970);
P.M. Tedrow and R. Mersevey, *ibid.* **27**, 919 (1971).
25. J.W. Hendriks, Ph.D. thesis, University of Nijmegen (1976).

Chapter 3

c-axis infrared response of $Tl_2Ba_2Ca_2Cu_3O_{10}$ studied by oblique-incidence polarized-reflectance measurements

The work presented in this chapter was done in cooperation with Jae H. Kim, B.J. Feenstra, H.S. Somal, and D. van der Marel from the University of Groningen and parts of it have been published in:

- Phys. Rev. B **49**, 13065 (1994).

3.1 Introduction

In the previous chapter we have introduced the charged-phonon model which was proposed by Timusk, Porter and Tanner [1] as an explanation for the 400-500 cm^{-1} 'notch'-like absorption feature in the optical *ab* conductivity of high temperature superconductors and which describes the coupling of phonons to the bound charge carriers responsible for the mid-infrared absorption in these compounds. Shortly after the appearance of Ref. 1, Reedyk and Timusk (RT) [2] demonstrated a remarkable correspondence between the structure in the *ab* conductivity and peaks in the *c*-axis dielectric loss function $\mathrm{Im}(-\epsilon_c^{-1})$ caused by the longitudinal optic (LO_c) phonons. From this correspondence it was concluded that the bound carriers couple specifically to these LO_c phonons. Momentum conservation implies that the incident light can only couple to the LO_c phonons when its wave vector $\vec{q}$ has a component parallel to the crystal *c*-axis. Indeed, no 'notches' were found for $\vec{q} \perp \vec{c}$.

In a Comment on the RT paper, van der Marel *et al.* [3] showed both theoretically and experimentally that a similar correspondence between *ab* response and *c*-axis dielectric loss function can be expected if one assumes that the incident radiation has an electric field component parallel to the *c*-axis. In the reflectance set-ups commonly used, this component is always present because the (unpolarized) light beam is not strictly normal to the surface. Instead it is focused rather strongly on the sample with an average angle of incidence of about 10°. From this point of view it is expected that the features related to the *c*-axis dielectric function should only be observed with *p*-polarized light and not with *s*-polarized light. Reedyk, Timusk and Basov showed, however, in their reply [4] that the same structures are observed with both *p*- and *s*-polarized light.

In another paper opposing the RT interpretation, Leskova *et al.* [5] suggested that the observed structures were caused by surface roughness. Roughness breaks the translational symmetry of a surface. By coupling to this roughness, a photon can acquire an additional wave vector parallel to the surface. As a result, the photon can excite normally non-optically active surface polaritons which would give rise to the observed features. This mechanism may qualitatively explain the *c*-axis features in most data shown in Ref. 2. It would be very interesting to extend Leskova's work to other crystal faces and see whether surface polaritons can also account for

the RT results in the $\vec{q} \perp \vec{c}$ geometry.

Although the explanation by van der Marel *et al.* could not account for the presence of the *c*-axis phonon features in *s*-polarized geometry in Ref. 4, it does hint towards a technique to study the anisotropy of the electronic properties of the cuprate high T_c superconductors and, more specifically, the *c*-axis response of these compounds. In most cases a direct study of the *c*-axis optical properties requires preparation of single crystal samples with large faces containing this axis. Such an analysis has been carried out with normal-incidence infrared reflectometry for $La_{2-x}Sr_xCuO_4$ [6], $YBa_2Cu_3O_{7-\delta}$ [7,8], $Pb_2Sr_2DyCu_3O_8$ [2], and $Bi_2Sr_2CaCu_2O_8$ [9]. Although larger single crystals gradually become available for this kind of studies, it is useful to have an experimental technique for determining the dielectric function along the *c*-axis for those materials of which only thin films or thin single crystal platelets exist. Such a technique may also serve as a second complementary approach since, for example, in epitaxially grown thin films it is often easier to obtain a homogeneous oxygen distribution than in single crystals.

In this chapter we introduce this experimental technique which was developed in the group of van der Marel at the university of Groningen and is based upon reflectance measurements at oblique angles of incidence with two different polarizations of the light. Using Kramers-Kronig relations for the experimentally measured $R_s(\omega)$ and $R_p(\omega)$ (the reflectance measured with *s*- and *p*-polarized light, respectively), it is possible to calculate the tensor components $\epsilon_{ab}(\omega)$ and $\epsilon_c(\omega)$ of the complex dielectric function for the directions parallel and perpendicular to the *ab* plane, respectively. It is demonstrated both theoretically and experimentally that indeed this method gives reasonable results for the dielectric loss function along the *c*-axis even if only the *ab* faces of the crystal are available for reflectance measurements. The physical mechanism behind this technique is in fact similar to that causing the Berreman effect [10] for dielectric layers on metallic substrates but this time used for anisotropic solids.

The technique bears a great resemblance to standard ellipsometric techniques [11]. A disadvantage of our technique with respect to normal ellipsometric techniques is that we have to rely on Kramers-Kronig calculations to obtain the desired dielectric function which implies that we need to measure the reflectance in a frequency range as broad as possible and

have to rely on extrapolations outside this range. On the other hand, our technique is rather easy to implement, and instead of two polarizers and a compensator only one polarizer is needed.

As an example we study a c-axis oriented epitaxial thin film of the high T_c superconductor $Tl_2Ba_2Ca_2Cu_3O_{10}$, for which single crystals were synthesized only recently and the typical c-axis dimension of the platelet-like crystals is again much smaller than 1 mm. Hence, most optical studies of this material were limited to the *ab* plane response and only a glimpse of the c-axis response is present in early studies of ceramic samples [12]. Although it has been shown that the optical anisotropy of thin platelets of $YBa_2Cu_3O_{7-\delta}$ [13] and $Bi_2Sr_2CaCu_2O_8$ [14] can be determined with an infrared microscope with the light beam focused to a very small region (typically 200 μm) on the *ac* face, the operational wavelengths were diffraction-limited to the mid-infrared region. Such limitations do not occur if oblique-incidence reflection spectroscopy of the much larger *ab* face is employed.

3.2 Outline of the Method

The complex reflection coefficients for a uniaxial crystal in air, with its optical axis oriented perpendicularly to the surface of reflection, are given by the expressions [11, 15, 16]

$$\begin{aligned} r_s &= \frac{\cos\theta - \sqrt{n_o^2 - \sin^2\theta}}{\cos\theta + \sqrt{n_o^2 - \sin^2\theta}}\,, \\ r_p &= \frac{n_o n_e \cos\theta - \sqrt{n_e^2 - \sin^2\theta}}{n_o n_e \cos\theta + \sqrt{n_e^2 - \sin^2\theta}}\,, \end{aligned} \tag{3.1}$$

for s- and p-polarized light, respectively. Here θ is the angle of incidence and n_o and n_e are the complex refractive indices for the ordinary and extraordinary rays, respectively.

Experimentally one has to determine the reflected *intensities* $R(\omega)$ for a wide range of frequencies. Hence, one has $r^2 = Re^{2i\phi}$ of which only R is measured experimentally, while the phase ϕ is calculated from R using the Kramers-Kronig relations. For s-polarized light the usual convention is to have ϕ restricted to the interval from 0 to π. Due to experimental

uncertainties negative values of ϕ may arise, leading to spurious negative values of the real part of the *ab*-plane optical conductivity $\sigma_{ab}(\omega)$ which one obtains by inverting the expression for r_s. For *p*-polarized light the situation is different, as even in the absence of experimental errors the phase may become negative.

Once the coefficients r_s and r_p are known, the indices n_o and n_e, or the corresponding complex dielectric functions ϵ_o and ϵ_e can be found by solving equation (3.1) for them in terms of r_s and r_p:

$$\begin{aligned} \epsilon_o &= \sin^2\theta + \cos^2\theta \left(\frac{1-r_s}{1+r_s}\right)^2 , \\ \epsilon_e &= \sin^2\theta \left[1 - \epsilon_o \cos^2\theta \left(\frac{1-r_p}{1+r_p}\right)^2\right]^{-1} \end{aligned} \tag{3.2}$$

Given ϵ_o and ϵ_e, it is possible to derive all other spectral functions such as optical conductivity and loss functions.

Our method can be applied directly to reflectance measurements on *c*-axis oriented high T_c superconducting thin films. This is allowed provided that the film is optically 'thick' (for our $Tl_2Ba_2Ca_2Cu_3O_{10}$ films of thickness $\sim$ 5000 Å this condition is reasonably satisfied). For thinner films, the equations 3.1 are no longer appropriate and should be replaced by more complicated expressions involving the index of refraction of the substrate and multiple reflections inside the film [11]. The quantities with subscript o (for 'ordinary') then correspond to the in-plane (the *ab* plane) parameters (we assume a tetragonal crystal structure) and those with subscript e (for 'extraordinary') correspond to the axial (the *c*-axis) parameters. As for these materials the conduction parallel to the planes is known to be metallic, with an almost insulating or semiconducting behavior along the *c*-axis, we can derive an approximate expression of the reflectance for *p*-polarized light when the sample surface corresponds to the *ab* plane. Let us first introduce the complex parameters $l \equiv (\cos\theta)^{-1}\sqrt{1 - \epsilon_c^{-1}\sin^2\theta}$ and $x = n_{ab}^{-1}$, with the help of which we can write the corresponding absorptivity for the *p*-polarized light in the form

$$1 - R_p = 4\frac{\mathrm{Re}(x \cdot l^*)}{|1 + x \cdot l^*|^2} ,$$

in which the asterisk denotes the complex conjugate. As $\mathrm{Im}\, n_{ab} \gg 1$ in the limit of metallic conductivity along the *ab* plane, we can use $1/\mathrm{Im}\, n_{ab}$ as the

expansion parameter of a Taylor series. Furthermore we make an expansion for $|\sin^2\theta/\epsilon_c| \ll 1$, so that the leading term of the series expansion is given by

$$1 - R_p = \frac{2}{\mathrm{Im}\, n_{ab}} \frac{\sin^2\theta}{\cos\theta} \mathrm{Im}\left(-\frac{1}{\epsilon_c}\right) . \tag{3.3}$$

We see that, for a smoothly varying n_{ab}, the absorptivity of p-polarized light has peaks which are essentially the peaks in the loss function along the c-axis. Although we will use the full inversion formulas of equation 3.2, equation 3.3 already shows that the c-axis loss function obtained from such an inversion is less prone to experimental errors than *e.g.* the c-axis conductivity.

3.3 Experimental details

With this motivation, we have undertaken a study of optical anisotropy in $Tl_2Ba_2Ca_2Cu_3O_{10}$, for which high-quality large-area c-axis oriented thin films are available. Our superconducting c-axis oriented $Tl_2Ba_2Ca_2Cu_3O_{10}$ thin films were grown by Lee *et al.* [17] using a sputter deposition technique at ambient temperature in a symmetrical RF diode sputtering system from two identical 1/2 inch targets. The films are typically 5000 Å thick and have critical temperatures in the range 120-123 K.

Our oblique-incidence reflectance measurements were carried out in a Bruker IFS113v Fourier Transform Infrared Spectrometer with a CryoVac variable temperature exchange gas cryostat. The infrared spectra were acquired at temperatures of 108, 163, and 300 K. The samples and the reference Au mirrors are mounted together inside the cryostat for calibration of reflectance at each temperature during the measurement.

3.4 Results and Discussions

In figure 3.1 we present the reflectance spectra for s- and p-polarization at various temperatures. As expected, the reflectance R_s for s-polarized light is higher than the reflectance R_p for p-polarized light throughout the frequency and temperature range of our measurement. The R_s spectra of $Tl_2Ba_2Ca_2Cu_3O_{10}$ are quite representative of the ab-plane response of high

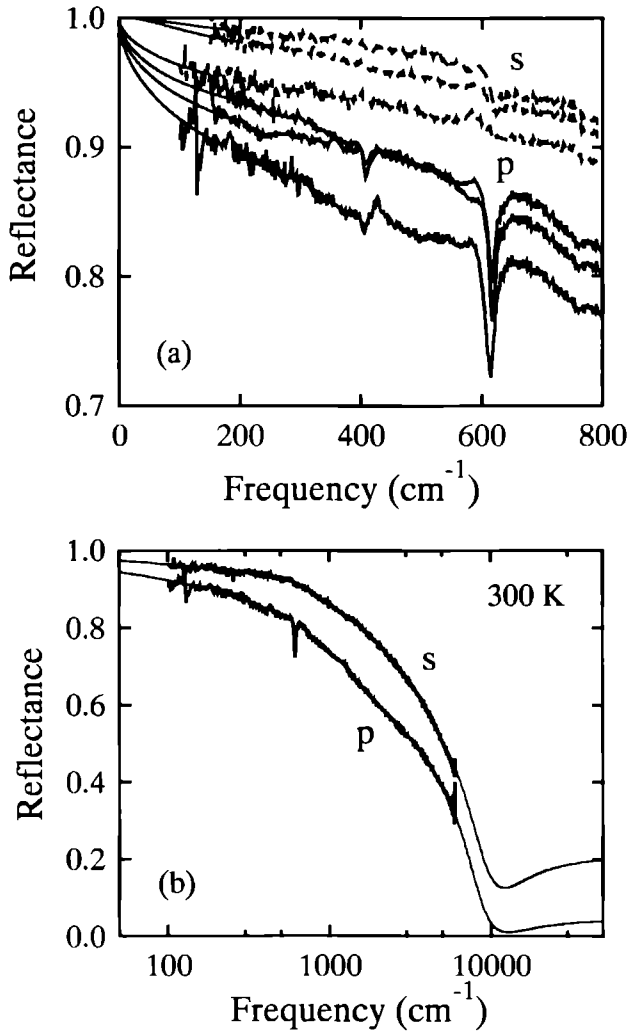

Figure 3.1 *(a) Reflectivity of $Tl_2Ba_2Ca_2Cu_3O_{10}$ for s-polarized light (the top three curves) and p-polarized light (the bottom three curves), measured at 45° angle of incidence. The temperatures are 108, 163 and 300 K from top to bottom for each set of three curves. (b) Room temperature reflectance (thick curves) measured at the University of Groningen with s-polarized (top) and p-polarized (bottom) light and high- and low-frequency extrapolations used for the Kramers-Kronig analysis (thin curves) above 6000 cm^{-1} and below 100 cm^{-1}.*

T_c superconductors in general. The more or less featureless, quasi-linear frequency dependence is quite evident.

A marked difference between our R_s and R_p spectra is the existence of strong absorption features in R_p positioned at 400 and 620 cm^{-1} due to the excitation of c-axis longitudinal optical phonons. This assignment is supported by the absence of these fairly strong features in the R_s spectra. Furthermore, from the reflectance spectra of ceramic $Tl_2Ba_2Ca_2Cu_3O_{10}$ samples [12] where a number of c-axis longitudinal optical phonons clearly appear in the infrared range, one can easily identify the two phonon peaks positioned near 400 and 620 cm^{-1}. The lattice dynamics calculation for $Tl_2Ba_2Ca_2Cu_3O_{10}$ by Kulkarni *et al.* [18] also predicts two c-axis A_{2u} longitudinal optical modes situated at 421 and 616 cm^{-1}. The former corresponds to vibration along the c-axis of the oxygen atoms in the CuO_2 and BaO planes against Ca atoms. The latter corresponds to vibration along the c-axis of the oxygen atoms in the BaO planes and Ca atoms against the oxygen atoms in the central CuO_2 planes.

In figure 3.2 we display the c-axis loss function of $Tl_2Ba_2Ca_2Cu_3O_{10}$ at various temperatures. We can easily recognize the two corresponding features due to the aforementioned c-axis longitudinal optical phonons. These phonon modes do exhibit some change with temperature. Both the 400 cm^{-1} and 620 cm^{-1} shift to higher frequencies by about 5 cm^{-1} as the temperature changes from 300 K to 108 K. The electronic background in the c-axis loss function is more or less flat at room temperature and the 163 K spectra are not much different from the 300 K case. However, in the case of 108 K (below T_c), there is a rise in the electronic-background intensity in the low frequency region. This can be interpreted as the high-frequency tail of the loss function peak due to the formation of the c-axis optical plasmon of the superconducting electrons. Based on this observation, we place an upper limit of 200 cm^{-1} or 25 meV on the c-axis plasmon energy.

Let us compare our findings with the experimental reports on other high T_c superconductors. Even though all of $La_{2-x}Sr_xCuO_4$, $YBa_2Cu_3O_{7-\delta}$, $Bi_2Sr_2CaCu_2O_8$, and $Tl_2Ba_2Ca_2Cu_3O_{10}$ have an in-plane optical plasmon at about 1 eV [19], the energy of the c-axis plasmon varies from one system to another. In the case of $YBa_2Cu_3O_{7-\delta}$ there is a zero-crossing of ϵ_c at around 100 cm^{-1}, *i.e.* below the lowest transverse optical mode, corresponding to a longitudinal mode of mixed vibrational and electronic character [7]. At higher temperatures this zero-crossing shifts to lower frequencies

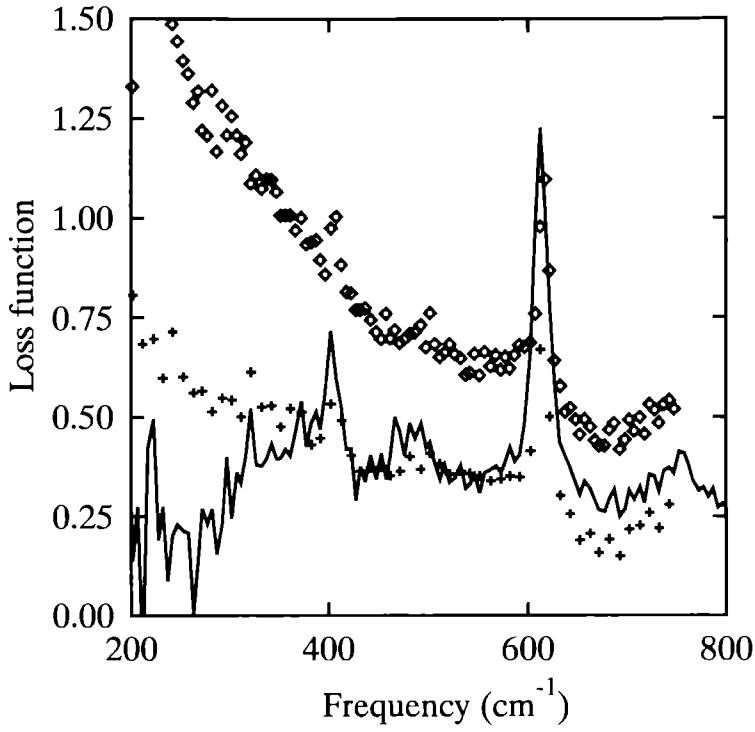

Figure 3.2 *The loss function for $\vec{E} \parallel \vec{c}$. The temperatures are 108 (diamonds), 163 (crosses) and 300 K (solid curve).*

and eventually disappears, apparently due to enhanced damping. A similar behaviour has been observed in $La_{2-x}Sr_xCuO_4$ [6], where the lowest longitudinal out-of-plane mode is found at 30 cm^{-1}. $Bi_2Sr_2CaCu_2O_8$ [9] does not show any trace of an out-of-plane plasmon either at room temperature or well below T_c even down to 30 cm^{-1}, which is then taken as an experimentally determined upper limit.

One can use band structure calculations based on the local density approximation (LDA) to determine the normal state intra- and interband plasmon frequencies. Calculations for $Bi_2Sr_2CaCu_2O_8$ were done by Ushpenskii and Rashkeev [20], who obtained plasmon energies of 3.3 and 0.9 eV for $\vec{E} \perp \vec{c}$ and $\vec{E} \parallel \vec{c}$ respectively, and about 1.5 eV for the screened in-plane plasmon. The calculation of Maksimov *et al.* for $YBa_2Cu_3O_{7-\delta}$ gives unscreened intra-band plasma frequencies (determined from a properly

weighted Fermi velocity) of 3.5, and 4.2 and 1.05 eV for $\vec{E}$ parallel to the a, b and c directions [21], respectively, which should be scaled with a factor of 0.5 to obtain the screened plasma frequencies ($\omega_p^{scr} = \omega_p/\sqrt{\epsilon_\infty}$, with $\epsilon_\infty \approx 4$). For $La_{2-x}Sr_xCuO_4$ the LDA result for the screened in-plane and out-of-plane plasmons is 1.9 eV and 0.4 eV, respectively [22,23]. So we see, that the experimental value of the in-plane plasmons of optimally doped samples is about half the value of the LDA calculation. This discrepancy is not surprising since LDA calculations do not take into account strong electron-electron interactions which are known to exist in the CuO_2 planes.

In the c-direction the discrepancy is even more dramatic. The optical c-axis conductivity in the normal state is phonon-dominated; no plasmon is observed above T_c. One reason for this could be that the plasmon in the normal state is strongly overdamped [24] and thus hard to detect. In an interpretation by Anderson [25], the dynamics inside the ab planes involves spin-charge separation which leads to confinement of the carriers in these planes. The finite conductivity in the c-direction is then caused by incoherent hopping which means that no properly defined band structure exists in this direction. Coherent transport only sets in below T_c [6].

Regardless of the reason why the normal state plasmon is absent in the infrared spectra, the plasmon which appears in the superconducting state can be explained by oscillations of phase difference of the superconductive order parameter (see chapter 1). This Josephson effect based interpretation gives a natural explanation as to why the c-axis plasmon appears at such low frequencies and why it is only visible below T_c.

In figure 3.3 we display the c-axis conductivity for our $Tl_2Ba_2Ca_2Cu_3O_{10}$ sample at various temperatures. As we mentioned previously the c-axis conductivity is more susceptible to errors than the c-axis loss function. However, one can see that below T_c there is a tendency of depression in the c-axis conductivity below 600 cm^{-1}. We can compare our results with the c-axis conductivity of $YBa_2Cu_3O_{7-\delta}$ above and below T_c determined from reflection measurements on the ac plane of single crystals by Bauer [7] and Homes *et al.* [8]. According to these authors, there is a gap-like depression of conductivity at low temperatures below 600 cm^{-1} but there is no clear evidence of a true BCS-like gap. Hence the situation for $YBa_2Cu_3O_{7-\delta}$ is quite similar to what we found in our own investigation of $Tl_2Ba_2Ca_2Cu_3O_{10}$.

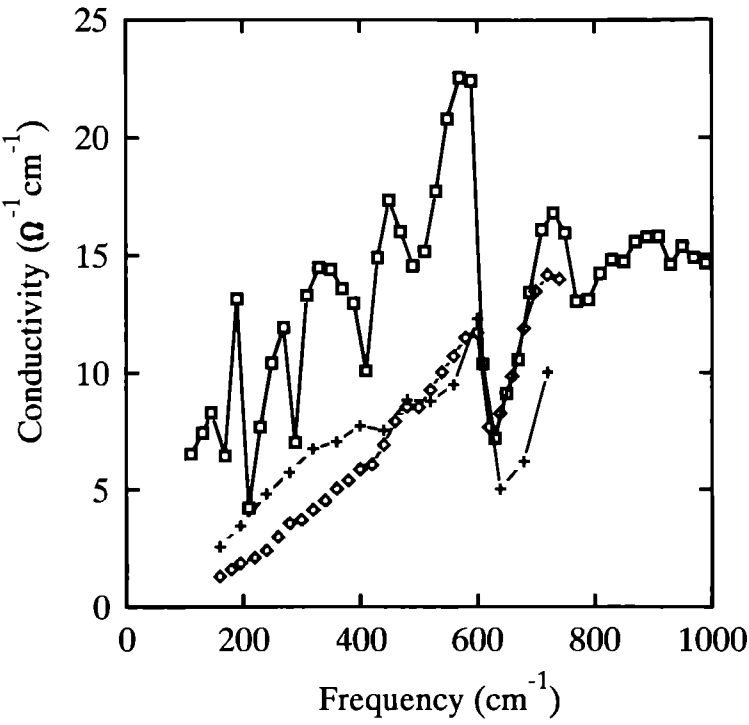

Figure 3.3 *The conductivity for $\vec{E} \parallel \vec{c}$, for $T = 108$ K (diamonds), 163 K (crosses), and 300 K (squares).*

3.5 Summary

We demonstrated the feasibility of an experimental technique to obtain the dielectric function in the direction parallel and perpendicular to the optical axis of a uniaxial sample by oblique-incidence polarized reflectometry. We applied this technique to a thin film of $Tl_2Ba_2Ca_2Cu_3O_{10}$ in order to study the *c*-axis infrared response. For this material no single crystals are available which are sufficiently elongated along the *c*-axis to allow a direct scattering experiment on the *ac* face. Although the longitudinal optical phonons in the *c*-axis are clearly present, no plasma-related zero crossing of ϵ_c is found above 200 cm^{-1}, which indicates that 200 cm^{-1} is an upper limit for the out-of-plane plasmon.

Acknowledgment: This work was part of the research program of the "Stichting voor Fundamenteel Onderzoek der Materie", which is financially supported by the "Nederlandse Organisatie voor Wetenschappelijk Onderzoek".

References

1. T. Timusk, C.D. Porter, and D.B. Tanner, Phys. Rev. Lett. **66**, 663 (1991).
2. M. Reedyk and T. Timusk, Phys. Rev. Lett. **69**, 2705 (1992).
3. D. van der Marel, J.H. Kim, B.J. Feenstra, and A. Wittlin, Phys. Rev. Lett. **71**, 2676 (1993).
4. M. Reedyk, T. Timusk, and D. Basov, Phys. Rev. Lett. **71**, 2677 (1993).
5. T. Leskova, J. Keller, and K. Renk, Physica C **225**, 190 (1994).
6. K. Tamasaku, Y. Nakamura, and S. Uchida, Phys. Rev. Lett. **69**, 1455 (1992).
7. M. Bauer, Ph.D. Thesis, University of Tübingen, (1990).
8. C.C. Homes, T. Timusk, R. Liang, D.A. Bonn, and W.N. Hardy, Phys. Rev. Lett. **71**, 1645 (1993).
9. S. Tajima, G.D. Gu, S. Miyamoto, A. Odagawa, and N. Koshizuka, Phys. Rev. B **48**, 16164 (1993).
10. D.W. Berreman, Phys. Rev. **130**, 2193 (1963).
11. R.M.A. Azzam and N.M. Bashara, in *Ellipsometry and Polarized Light*, (North-Holland, Amsterdam, 1987).
12. T. Zetterer, M. Franz, J. Schützmann, W. Ose, H.H. Otto, and K.F. Renk, Phys. Rev. B **41**, 9499 (1990).
13. I. Bozovic, K. Char, S.J.B. Yoo, A. Kapitulnik, M.R. Beasley, T.H. Geballe, Z.Z. Wang, S. Hagen, N.P. Ong, D.E. Aspnes, and M.K. Kelly, Phys. Rev. B **38**, 5077 (1988).
14. J.H. Kim, I. Bozovic, D.B. Mitzi, A. Kapitulnik, and J.S. Harris, Jr., Phys. Rev. B **41**, 7251 (1990).
15. A.B. Winterbottom, The Royal Norwegian Science Scociety Report No. 1 1955 (unpublished).
16. J.C. Decius, R. Frech, and P. Brüesch, J. Chem. Phys. **58**, 4056 (1973).
17. W.Y. Lee, J. Vazquez, T.C. Huang, and R. Savoy, J. Appl. Phys. **70**, 3952 (1991).
18. A. Kulkarni, F.W. de Wette, J. Prade, U. Schröder, and W. Kress, Phys. Rev. B **41**, 6409 (1990).
19. J.H. Kim, I. Bozovic, J.S. Harris, Jr., W.Y. Lee, C.B. Eom, and T.H.

Geballe, in *Proceedings of the Universty of Miami Workshop on Electronic Structure and Mechanism for High Temperature Superconductivity*, Coral Gables, Florida, 1991, edited by J. Ashkenazi, (Plenum Press, New York, 1991), p. 251.

20. Yu.A. Uspenskii, and S.N. Rashkeev, Phys. Lett. A **153**, 373 (1991).
21. E.G. Maksimov, S.N. Rashkeev, S.Yu. Savrasov, and Yu.A. Uspenskii, Phys. Rev. Lett. **63**, 1880 (1989).
22. E.G. Maksimov, I.I. Mazin, S.N. Rashkeev, S.Yu. Savrasov, and Yu.A. Uspenskii, Int. J. Mod. Phys. B **2**, 883 (1988).
23. M. Czyzyk, and D. van der Marel, unpublished (1993).
24. J.H. Kim, H.S. Somal, M.T. Czyzyk, D. van der Marel, A. Wittlin, A.M. Gerrits, V.H.M. Duijn, N.T. Hien, and A.A. Menovsky, Physica C, in press (1995).
25. P.W. Anderson, Science **256**, 1526 (1992).

Chapter 4

Magneto-optic study of the quasi-1D organic conductor $(TMTSF)_2ClO_4$

The work presented in this chapter has been done in cooperation with J.S. Brooks and A.S. Perel from Boston University and the F.B. National Magnet Laboratory, MIT, USA.

Parts of this chapter have been published in the following papers:

- Phys. Rev. B **46**, 8663 (1992).
- Journal de Physique IV (France) **3**, C2-299 (1993).
- Proceedings of the International Conference on Science and Technology of Synthetic Metals, Seoul, 1994, to be published in Synth. Met.

and have been presented in:

- T.J.B.M. Janssen, Ph.D. thesis, University of Nijmegen (1994).

4.1 Introduction

The charge-transfer salts of the Bechgaard family [1], $(TMTSF)_2X$ (where TMTSF is tetramethyltetraselenafulvalene, and X is ClO_4, PF_6, ReO_4 etc.), have a unique set of properties which depend on temperature, magnetic field and pressure. The discovery of superconductivity in these materials marked the onset of extensive research, devoted to the understanding of the physical properties of these quasi-one-dimensional organic conductors [2–4]. Besides superconductivity, these quasi-one-dimensional conductors show Quantum hall-like behaviour, spin-density-wave (SDW) states and field-induced spin-density-wave (FI-SDW) states.*

The Bechgaard Salts consist of large organic TMTSF molecules, the cations, and smaller inorganic monovalent anions *e.g.* PF_6 or ClO_4. The crystal structure of $(TMTSF)_2X$ consists of stacks of the large planar TMTSF molecules in the a-direction with a slight tendency towards dimerization. The anions are ordered in sheets separating the TMTSF stacks in the c-direction and accept one electron from each donor pair of TMTSF molecules. The delocalized states necessary for metallic conductivity are formed by the overlap of molecular orbitals. In the a-direction this overlap is largest (predominantly via Selenium π-orbitals in the TMTSF molecules). The transfer energies t in the different directions as calculated within the tight binding approximation [6–8] bear the following proportions to one another: $t_a : t_b : t_c = 1 : 0.1 : 0.001$. One usually neglects the overlap in the c-direction. The above band parameters lead to an open Fermi surface consisting of two parallel, slightly warped planes (see figure 4.2). The degree of warping is proportional to t_b (= interaction between the stacks) and determines the 'degree' of two-dimensionality.

$(TMTSF)_2PF_6$ is a prototypical member of the Bechgaard salt family; it exhibits a transition to a spin-density-wave insulator at 12 K at ambient pressure. This state is suppressed above 6 kbar at which pressure superconductivity sets in. This can in turn be suppressed by a small magnetic field. At much higher fields (> 3 T) a cascade of field-induced spin-density-wave

*For a long time, the Bechgaard salt family was the only class of compounds known to exhibit the FI-SDW state. Recently, Oshima *et al.* observed FI-SDW-like behaviour in the magnetoresistance and magnetization of $(DMET\text{-}TSeF)_2X$ (X = AuI_2, $AuBr_2$, $AuCl_2$) [5]. The effect in these materials is however less pronounced than in the Bechgaard salts.

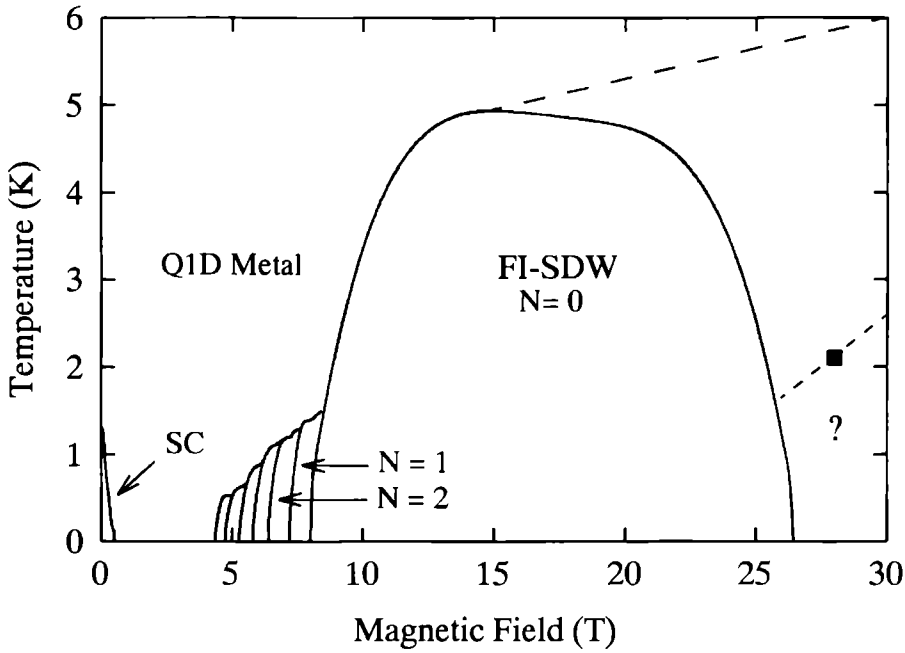

Figure 4.1 *A schematic phase diagram of $(TMTSF)_2ClO_4$ (solid line), based on a compilation of calorimetric [9] and magnetization [10, 11] measurements. The final FI-SDW state is referred to as the $N = 0$ state, the one before $N = 1$ state, etc.. The question mark indicates another possible state observed by Yu et al. [12]. SC denotes the superconducting phase. 'The Standard Model' (see text) is shown as a long dashed line and does not cover the experimental data at very high fields.*

transitions is found.

The PF_6 anion is octahedral. When the anion is of tetrahedral symmetry (*e.g.* ClO_4) it can take two orientational positions with respect to the crystal lattice. When $(TMTSF)_2ClO_4$ is cooled down slowly (0.1 K/min) below 24 K, the anions take alternating orientations along the *b*-direction which leads to a doubling of the unit cell in this direction and a halving of the Brillouin zone. At more rapid cooling rates (> 50 K/min), no anion ordering takes place and $(TMTSF)_2ClO_4$ enters a SDW insulating state at 6 K [13]. In the ordered state $(TMTSF)_2ClO_4$ at ambient pressure has a very complex phase diagram (see figure 4.1) with FI-SDW's [14, 15],

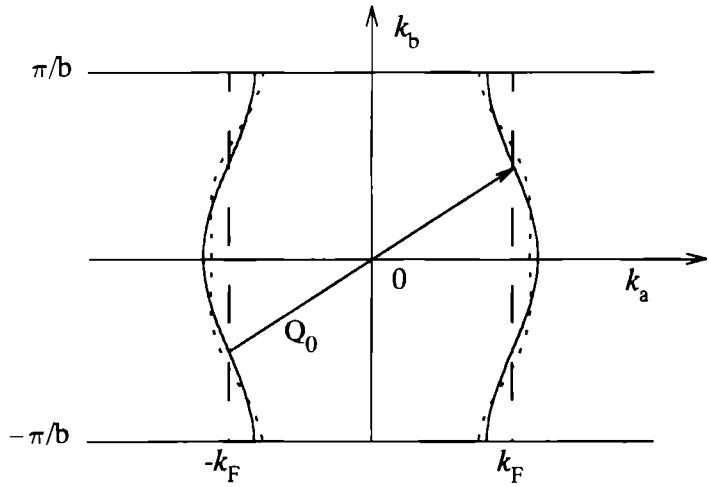

Figure 4.2 *Fermi surface for a quasi-1D conductor $(TMTSF)_2X$ (solid line) and a truly 1D conductor (long dashed line) in the k_a-k_b plane. The dotted lines show the deviation of the Fermi surface from this simple form as a result of higher harmonic components. $\vec{Q}_0 = (2k_F, \pi/b)$ is the nesting vector discussed in the text.*

reentrance to a metallic state [11]. Shi *et al.* reported many sharp peaks in this high field phase boundary [16]. A controversial 'insulating phase' above 27 T was reported in Refs. 12 and 17. The ordering of the ClO_4 ions is considered crucially important for these features [18], and are the subject of ongoing controversy and considerable theoretical attention [19–22].

Peierls instability

It is well known that in quasi-1D conductors such as the Bechgaard salts the electronic system is subject to a nesting or Peierls instability [23]. Peierls showed that in these systems any perturbation of amplitude Δ and wave vector $\vec{Q}_0 = (2k_F, \pi/b)$ will couple (or 'nest') a large number of degenerate states which results in a strongly peaked response (infinite at $T = 0$) to perturbations with this wave vector. To avoid this instability, the system sets up an electronic modulation of wave vector $\vec{Q}_0$ and as a result, a gap $2|\Delta|$ opens up across the entire Fermi surface (see figure 4.2). The physical principle behind the opening of the gap is basically the same as that causing Bragg scattering [24]. Peierls first demonstrated that below a critical

temperature T_P the energy gain of opening the gap will always exceed the energy cost of creating a modulated distortion with wave vector $\vec{Q}_0$. Hence, all 1D conductors have this Peierls instability towards an insulating state at low temperatures.

When only nearest neighbour interactions are taken into account (solid lines in figure 4.2) the Fermi surface has a sinusoidal shape and the vector $\vec{Q}_0$ will nest the entire Fermi surface. However, when next nearest neighbour corrections are included (dotted lines in figure 4.2) the surfaces are more corrugated and become less prone to nesting instabilities. This correction is proportional to $t_b^2/t_a = t_b'$ [25] and hence increases when the system becomes more 2D-like. With these corrections complete nesting of the warped Fermi surface will not be possible. In this case a gap may open only on a restricted part of the Fermi surface.

In most quasi-1D conductors the low temperature state is a charge-density-wave (CDW) state; a periodic density modulation with wave vector $\vec{Q}_0$ of the electronic density which is usually accompanied by a lattice modulation. However, in the Bechgaard salts the low temperature insulating state cannot be a CDW since the relevant lattice modulations are not observed. Instead this state was shown to be antiferromagnetic by the observation of a characteristic anisotropy of the magnetic susceptibility [26] and a strong inhomogeneous line broadening of the ^{77}Se NMR line [27] indicating the existence of strong local magnetic fields. The state is known as a spin-density-wave (SDW) state; a periodic modulation with wave vector $\vec{Q}_0$ of the electronic spin density. The driving mechanism for this state is the on-site Coulomb interaction which in the anisotropic Bechgaard salts is relatively large with a magnitude comparable to the electronic bandwidth. This is a result of the limited screening of the Coulombic charge due to restraints on the electronic movements [28]. In addition, the electron-phonon coupling which leads to a modulation of charge density is opposed by this large on-site Coulombic repulsion [29].

The different ground states among the various members of the Bechgaard salt family can be qualitatively understood from their degree of one-dimensionality and hence the nesting properties of the Fermi surface. ClO_4 is the smallest anion in the Bechgaard salt family and as a result the transfer energy t_b is largest and at low temperatures the Peierls instability does not occur. The PF_6 ion, which is larger, leads to a slightly smaller t_b in $(TMTSF)_2PF_6$, and thus, there is a transition to the SDW state below

12 K. When pressure is applied the transfer energy t_b is increased, which makes the band structure more quasi-2D: this results in a suppression of the SDW state.

Field Induced Spin-Density-Waves

One of the most special properties of $(TMTSF)_2X$ is that a series of SDW phase transition can be induced by applying a magnetic field parallel to the least conducting c'-axis [30,31]. This leads to a cascade of SDW phase transitions manifested by nearly quantized steps in the Hall voltage and related features in the magnetoresistance, heat capacity, and magnetization [9,10,32,33].

As stated previously, application of pressure makes the band structure more two-dimensional and decreases the degree of nesting. In contrast, a simple semi-classical picture due to Chaikin [34] shows that the SDW formation is favoured in magnetic field because it makes the system effectively more one-dimensional. Chaikin pointed out that the nearly sinusoidal band structure leads to a zig-zag like motion of the carriers in real space perpendicular to the applied magnetic field. It is easy to show that the amplitude A of the zig-zag motion is equal to $4t_b b/\hbar\omega_c$ with $\omega_c = eB/m^\star$ the cyclotron frequency. Increasing the magnetic field will decrease A and make the carrier motion more one-dimensional.

Of course, more profound models have been proposed to explain the FI-SDW formation in the $(TMTSF)_2X$ salts. Gor'kov and Lebed' [35] first tackled the problem by calculating the nesting vector dependent spin susceptibility $\chi(\vec{Q})$. They showed that in a magnetic field orbital effects can improve the nesting conditions making $\chi(\vec{Q}_0)$ (with $\vec{Q}_0$ the optimum nesting vector defined above) periodically divergent in $1/B$ even if it remains finite in zero field.

Later, Montambaux, Héritier and Lederer [36, 37] put forward the quantized nesting mechanism which was based on a mean field approximation. In this model, which later became known as the standard model, the mechanism of successive field-induced SDW (FI-SDW) transitions can be described naively in the following way. With the imperfect nesting such as shown in figure 4.3 translating one sheet of the Fermi surface with the wave vector $\vec{Q}$ leaves an area A between this sheet and the other one. The total energy is minimized when A is quantized in units of $2\pi eB/\hbar$ and contains

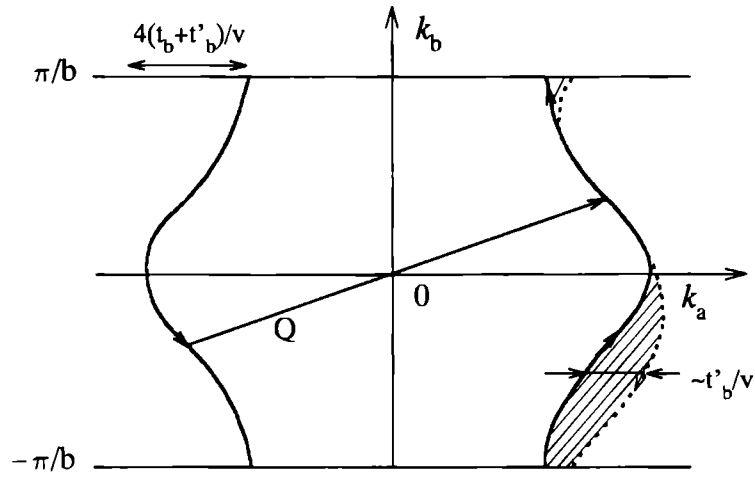

Figure 4.3 *SDW wave vector $\vec{Q}$ for which the left hand side of the Fermi surface is translated so that it is tangent to the right hand side. In a magnetic field, $\chi(\vec{Q})$ has a maximum when the area of the hatched part is quantized in terms of $2\pi eB/\hbar$. For clarity, the width of the pocket $\sim t'_b/v$ (v is the Fermi velocity) has been exaggerated and in reality it only spans $\approx 1\%$ of the Brillouin zone. The arrows indicate semi-classical trajectories of electrons at the Fermi surface in momentum space. After Ref. 37.*

an integer number of completely filled Landau levels and, hence, the system still conducts. Because the degeneracy of the Landau levels increases linearly with the field, so does the carrier density. This is made possible thanks to small variations of the nesting vector with the field $\vec{Q}(B)$. There is then a critical field above which the nesting deteriorates so much that the quantum number N decreases by one unit to get back to the better nesting condition. This mechanism describes a cascade of subphases each of them characterized by an integer number N of completely filled Landau levels. The Hall voltage is then quantized in each subphase, and due to the discontinuity of the number of carriers, there is a first order transition between the subphases. When the last $N = 0$ phase is entered no Landau levels are contained in A and the system is insulating.

The standard model has been very successful in explaining many of the features observed in the Bechgaard salts in particular for $(TMTSF)_2PF_6$. It nicely demonstrates the opposite effects of pressure and magnetic field on

the dimensionality of the Fermi surface. The observation of a well developed quantum Hall effect (QHE) with a transition to the insulating $N = 0$ state at high fields strongly supports the assumption of completely filled Landau bands around the Fermi level. However, deviations from the usual QHE observed in 2D-electron gasses occur in that the ratios between quantized plateaux depend strongly on pressure [38].

The $(TMTSF)_2ClO_4$ compound shows strong deviations from the standard model. At high fields it shows a reentrance from the FI-SDW into the metallic state [11]. Furthermore, the insulating phase at low temperatures and high magnetic fields and the oscillating high field phase boundary cannot be explained within this framework. The large and extremely stable state between 8 and 27 T was first thought to be the final $N = 0$ SDW phase. However, this phase is not an insulator and a lot of the discussions in the literature centered on the correct assignment of it ($N = 0$ [39], $N = 1$ [21], and even $N = 1/3$ [14]). Up to now no conclusive assignment has been possible. The reentrant behaviour is generally thought to be intimately related with the anion ordering in this compound. This could give rise to an additional periodic potential in the crystal which might suppress the $N = 0$ phase [20, 21]. It must be noted that neither of the two models mentioned above is yet capable of predicting the correct shape of the phase diagram of $(TMTSF)_2ClO_4$. In addition, the QHE is poorly developed in this compound and at certain magnetic field values the Hall-voltage even changes sign (the 'Ribault anomaly' [40]).

The fact that the band parameters of the ClO_4 and PF_6 compounds only differ by a few percent [7] and that yet their phase diagrams do not universally converge to that predicted by the standard model, is an indication that there are some essential parts missing in the theory. Certainly the ClO_4 compound seems to require additional ingredients, or maybe a completely different approach [19]. In a recent report [18] on the complete phase diagrams of the PF_6 and ClO_4 compounds versus magnetic field, temperature and pressure, it was found that above a critical pressure of 5 kbar the anion ordering is suppressed, and it was suggested that above this pressure $(TMTSF)_2ClO_4$ does show normal standard model behaviour like $(TMTSF)_2PF_6$. However, the magnetic fields available currently are too low to justify such a conclusive assignment.

We now discuss the predictions of the standard model for the single particle excitation spectrum in the FI-SDW phase. According to Refs. 41

and 42 this spectrum consists of a series of Landau-like bands separated by more or less equidistant gaps. The main SDW gap is predicted to occur at the Fermi level. An important point is the proportionality relation between T_{SDW} and the magnetic field dependent ground-state properties formulated by Montambaux *et al.* [43]. This relation is based on a very general model-independent thermodynamic description of a system with many gaps. It is found that in such a system there still exists a BCS-like proportionality between the gap at the Fermi level and $T_{SDW}(B)$. This means that the ground state SDW gap should roughly follow the contour of the phase diagram in figure 4.1). Therefore, measuring this energy gap and establishing its magnetic field and temperature dependence could give a conclusive verification of the standard model.

Sofar, the FI-SDW formation was mainly studied with techniques probing the dynamics *at* the Fermi surface. The advantage of using an optical technique is that energies comparable to the SDW gaps are available allowing a very direct way of probing gaps in the electronic density of states. A large number of Bechgaard salts has been optically investigated [44] in the past but up until now there have been no reports of studies of the SDW excitation spectrum in magnetic field. This is probably due to the considerable complexity of combining an optical measurement on these small opaque crystals with both high magnetic fields and low temperatures.

In this chapter we report an extensive optical study of the excitation spectrum of the magnetic-field-induced spin-density-wave phases in the quasi-1D organic conductor $(TMTSF)_2ClO_4$. By the use of several experimental techniques we have been able to investigate the magnetic field-, energy-, and temperature-dependence of the spectrum, covering a large part of the phase diagram at ambient pressure. We find good general agreement of the optical features with the phase diagram, well established from *non-optical* experimental studies. However, the specific information which is derived from the current *optical* study is in serious disagreement with the accepted theoretical understanding of the magnetic field dependent band structure of quasi-1D organic conductors. In section 4.2 we present the evolution of the excitation spectrum in the various SDW subphases. The main result of this study is that a gap opens up that is independent of magnetic field and subphase index. The temperature dependence of the excitation spectrum is investigated in section 4.3. In addition to the energy gap we report the observation of a pinned collective mode resonance, which suggests

a coupling between the SDW condensate and the lattice.

4.2 FIR spectroscopy of the FI-SDW gap in $(TMTSF)_2ClO_4$

In the past decade a large number of extensive spectroscopic studies have been performed on the Bechgaard salts [44], however, none were performed in magnetic fields strong enough to induce the FI-SDW states. Instead these investigations concentrated on the low temperature conductivity in the metallic, density-wave (SDW or CDW), and superconductive states. The conductivity in the metallic state is in general very different from the Drude-type conductivity observed in ordinary metals and is strongly anisotropic in the *ab*-plane. A discrepancy is observed between the high dc conductivity above the density wave transition temperature and a depressed optical conductivity in the FIR regime. This discrepancy has been generally explained in terms of a narrow zero-frequency mode with very large effective mass. This mode would get weakly pinned at low temperatures [45] removing the disagreement between infrared and dc transport results. A second explanation that is widely accepted is in terms of a single particle picture of carriers with a very long mean free path [46,47]. The reduction in low frequency conductivity is then attributed to extrinsic causes such as a damaged surface which is then not representative for the bulk properties of the material [48].

In the group of materials with octahedral anions (AsF_6, SbF_6, PF_6) a SDW transition takes place at $\sim$ 12 K. In the spectra clear changes are observed when passing the transition temperature, corresponding to a developing gap in the density of states [45,47,49]. However, the conductivity below the gap energy does not vanish completely as expected, suggesting that the gap is anisotropic with parts of the Fermi surface being gapless [44,45,49]. Quinlivan *et al.* [50] investigated the microwave and submillimeter properties of the SDW state in $(TMTSF)_2PF_6$. They observed a conductivity edge in the spectra which was interpreted as evidence for the opening of a SDW gap, accompanied by the appearance of a collective mode resonance of the SDW condensate. Later the former statement was recalled because the conductivity edge was seen up to room temperature [51]. It was furthermore stated that the gap cannot be visible in the spectra because the material

shows clean limit electrodynamics in the a-direction (see also page 36).

In addition, Eldridge *et al.* [52] measured the absorption spectra of a large number of powdered Bechgaard salts. From these spectra a large number of low energy phonon modes could be identified. Most interesting are the low frequency phonon modes which only appear after the structural ordering in the salts with tetrahedral anions and can therefore only be observed in the slow-cooled state of $(TMTSF)ClO_4$.

In the first optical study that did cover the FI-SDW regime, Perel *et al.* concluded that a reversal of the background reflection signal in their optical data indicated the opening of a FI-SDW gap. However, from a few monochromatic energies alone it is impossible to derive the theoretically predicted [43] behaviour of the gap in the various subphases. In this section we present a detailed FIR and microwave study in the range between 1.5 and 45 cm^{-1} in fields up to 20 T, covering both the metallic and FI-SDW states in $(TMTSF)_2ClO_4$ at a temperature of 400 mK. The broad-band interferometer technique allows a detailed investigation of the threshold fields of the FI-SDW subphases which are well separated at this low temperature (*cf.* figure 4.1). We report the spectroscopic observation of the evolution of the excitation spectrum in the various FI-SDW subphases. The main result of this work is that a gap opens up with a magnitude that is independent of magnetic field or subphase index. We interpret this as evidence that the gap is nonuniform in k-space and that the gapped area on the Fermi surface appears to increase discontinuously upon each phase transition to a lower index spin-density-wave state. We will discuss additional observations related to a collective mode excitation in the microwave region and a coupling of low energy phonons to the spin-density modulation.

4.2.1 Experimental details

The samples used in this work were prepared in a standard electrochemical way, yielding very pure crystals with a typical size of $0.5 \times 1 \times 7$ mm^3. In order to enhance the optical signal from these small crystals, we arranged a dozen crystals in a grid like structure, so that the plane of the grid coincides with the ab plane of the crystals. The samples were then placed in a ^3He cooled sample holder, mounted in the bore of either a 10 T superconducting magnet or of a 20 T Bitter magnet. The magnetic field direction was chosen along the c'-axis, perpendicular to the grid. We used different FIR set-ups;

an optically-pumped molecular FIR-laser, providing approximately 20 lines in the submillimeter range (10-30 cm^{-1}), several microwave klystrons in the frequency range between 30 and 70 GHz (1-2.5 cm^{-1}), a set of microwave pumped diode frequency multipliers, yielding a nearly continuous output between 2 and 15 cm^{-1} and a Bruker IFS 113v Fourier Transform IR spectrometer. All sources could be connected to the insert using light guides and could be interchanged without affecting the sample conditions. The combination of these different sources allows a quasi-continuous spectroscopy from the infrared range down to approximately 1.0 cm^{-1}.

The FIR light intensity was measured with Si bolometers cooled to 1.2 K. The sample was cooled at a rate of 30 mK/min through the anion ordering transition at 24 K and was kept at 400 mK during the experiment. Both reflection and transmission of the sample grid could be measured simultaneously, a technique first exploited by Ng *et al.* [54] on these materials. Because of the large conductivity along the *a*-axis, the reflectivity is close to unity and field dependent changes in the extreme FIR are difficult to detect. The basic reason for using a grid arrangement is that transmission is restricted to a polarization along the less conducting *b*-axis and multiple reflections will enhance the effect of changes in conductivity. Therefore the signal measured by the transmission bolometer basically corresponds to the sample *b*-axis *reflectivity*. A disadvantage of this configuration is that it is difficult to calibrate the absolute value of the sample absorption and perform Kramers Kronig analysis. The linear polarization of the transmitted light in the spectral region of interest (below 30 cm^{-1}) was confirmed in a separate experiment for temperatures down to 4 K using a commercial metal grid polarizer.

A second sample was placed outside the optical path but in good thermal contact with the holder. The magnetoresistance of this reference sample was used to monitor the formation of FI-SDW states.

4.2.2 Results

Figure 4.4(a) shows the normalized transmission through the sample grid versus magnetic field for several monochromatic FIR energies. Here the transmission (T) taken in an applied field B is divided by the transmission in zero field. Large changes are found in $T(B)/T(0)$ at the various phase transitions. At this low temperature the transmission changes in a step-like

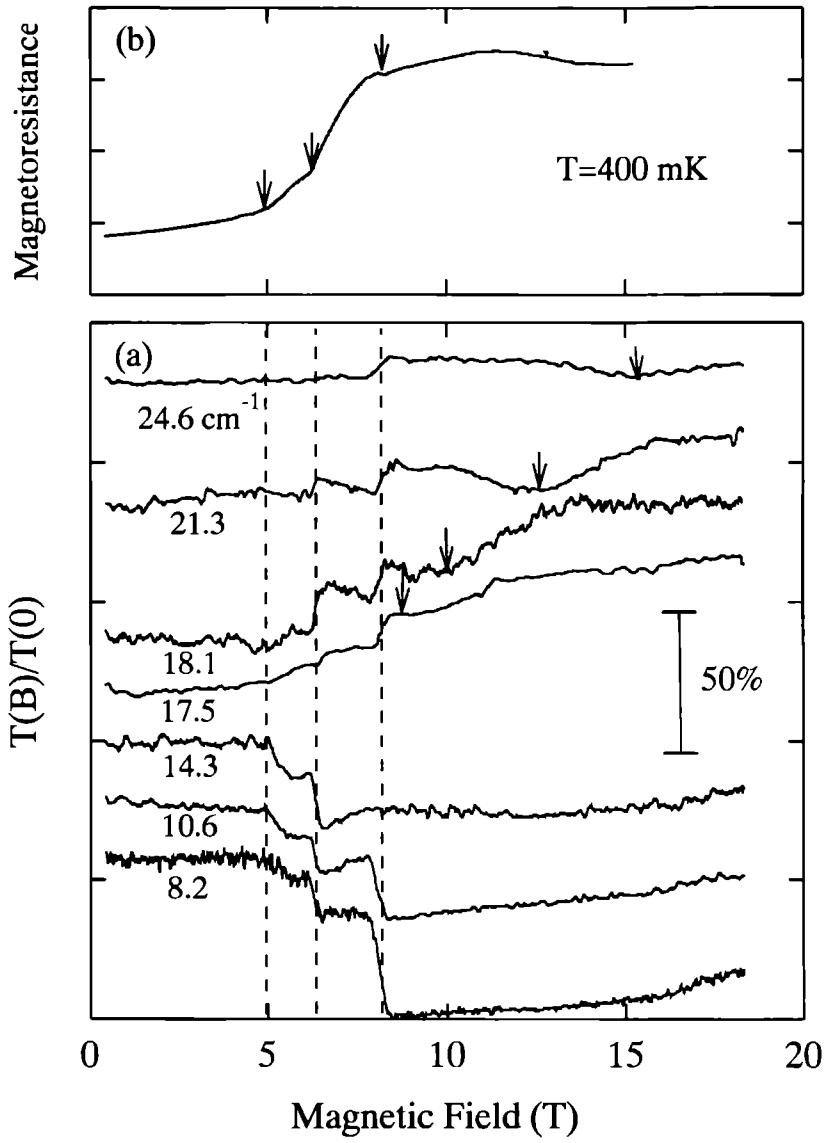

Figure 4.4 *(a) Transmission (normalized to transmission at $B = 0$) versus magnetic field for different frequencies both below and above the SDW gap. The arrows indicate the cyclotron resonance. Dashed lines correspond to the fields where magnetoresistance steps were observed, as shown in (b). (b) Magnetoresistance of the reference sample, where arrows indicate the phase transitions between the FI-SDW subphases.*

fashion with nearly field independent plateaux in between. With the help of the magnetoresistance data (figure 4.4(b)) taken on the reference sample these steps can be identified to correspond with transitions between different FI-SDW subphases. Above 7 T the spectra exhibited a large hysteresis depending on the magnetic field history. Because of this effect only traces recorded with increasing field are shown. Some of the microwave-energy $T(B)/T(0)$ traces are shown figure 4.6.

The most interesting aspect of these traces at fixed radiation energy is that the changes near the phase transitions are quasi-steplike, reminiscent of the steps in the Hall voltage. At low frequencies the sample reflectivity, proportional to $T(B)/T(0)$, generally decreases with field. This would indicate a smaller conductivity, in agreement with the opening of a (partial) gap in the excitation spectrum. A remarkable exception is the behaviour in a narrow range around 2.4 cm^{-1}, where $T(B)/T(0)$ increases sharply. At frequencies above 14 cm^{-1}, $T(B)/T(0)$ increases at the phase transitions, which could possibly be related to a piling up of the single particle density of states above the gap edge. Normalized FIR spectra are shown in figure 4.5, showing the complete energy dependence. The spectra in magnetic field are normalized to the zero field transmission spectrum. The data taken with monochromatic energy sources (laser or klystron) are indicated by the different symbols. For values of the field between the thresholds for different phase transitions the spectra were virtually identical, so we have limited the data to the three generic spectra that are shown in this figure. For historical reasons we labeled the FI-SDW phases with index N=2,1,0 corresponding to fields of 6, 7.5, and 8 T. More spectra at fields up to 15 T have been taken but these did not differ substantially from the 8 T spectrum. In figure 4.5 several features can be identified:(a) a large decrease is found for $T(B)/T(0)$, below approximately 14 cm^{-1} in all FI-SDW phases, indicating the opening of a (partial) gap. Note that the energy of the gap is the same in all subphases. (b) Sharp spectral features at 17 and 32 cm^{-1} appear suddenly with the formation of each SDW subphase. A smaller structure appears near 23 cm^{-1}. (c) Finally, a resonance peak at 2.4 cm^{-1} is found. All features become more pronounced at higher fields or, equivalently, for lower FI-SDW index. However, none of them tend to shift in energy with increasing magnetic fields.

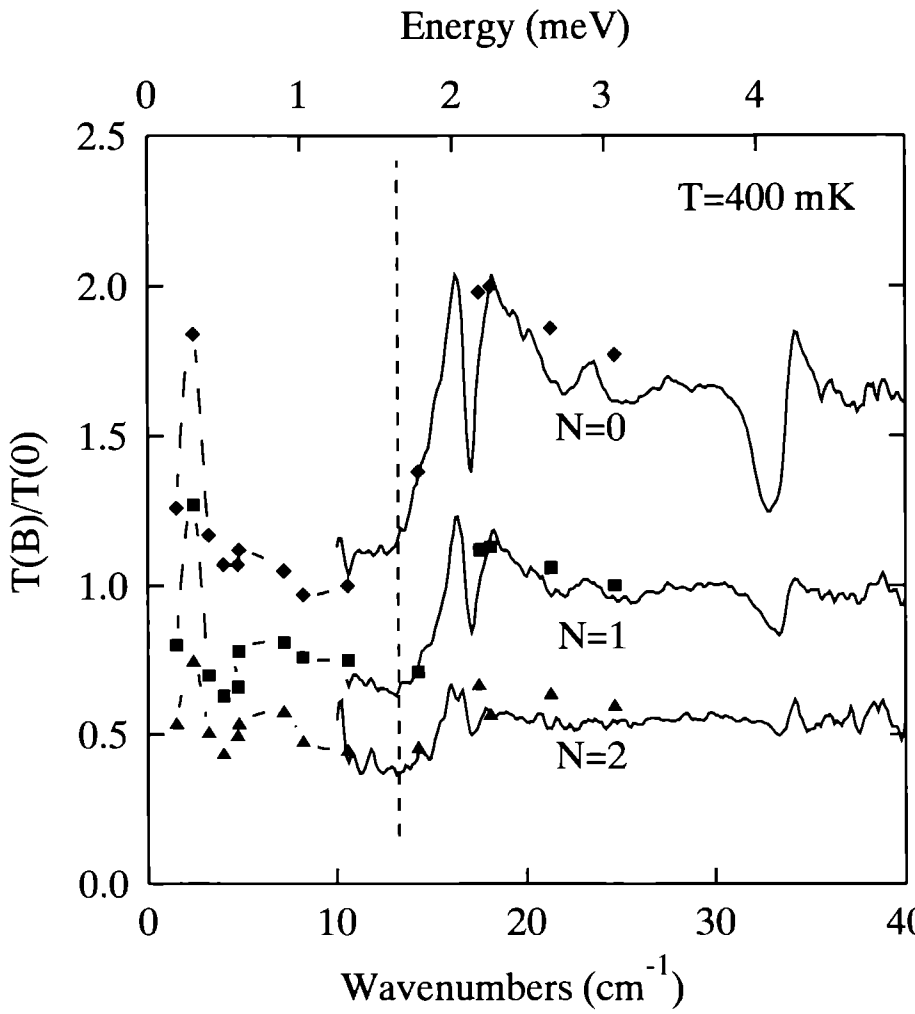

Figure 4.5 *FIR transmission spectra (normalized to the $B = 0$ spectrum) for three different magnetic fields corresponding to the $N = 0, 1,$ and 2 FI-SDW subphases. The microwave and FIR laser data are indicated by the different symbols. The upper (lower) spectrum has been offset by $+(-)0.5$ for clarity.*

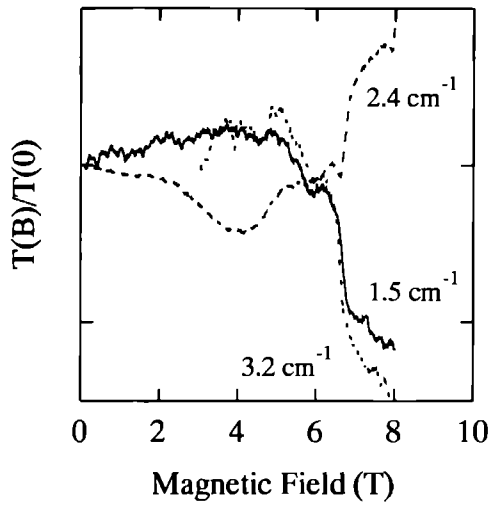

Figure 4.6 *Field dependence of the normalized transmission through the grid of samples for three frequencies in the microwave regime.*

4.2.3 Discussion

The main feature in the spectra is the opening of a gap below 14 cm^{-1}. This value is slightly higher than that estimated from the 1.2 K reflectivity in Perel's work [53], however still within the accuracy which can be expected from the monochromatic experiment.

We have already mentioned the work of Montambaux *et al.* [37] who, trying to explain the quasi-quantized Hall behaviour, assumed a constant carrier density and concluded that a multiplet of gaps would form, separating Landau-like bands. As a consequence the magnitude of the gaps would be strongly field dependent and should even show small discontinuities between the various SDW subphases.

Our spectroscopic results do not confirm this picture. We find no evidence for multiple gaps, and more specifically, our data show that the fundamental gap is independent of the magnetic field or subphase index. However, the signal strength in the gap is not zero but does depend on the subphase index. We must conclude that the gap is not uniform in k-space.

To explain the data we propose the following simple qualitative model: When the field increases, the system will become more sensitive to a nesting

instability, part of the charge carriers condense into a collective SDW ground state and it will take a finite amount of energy (the gap) to create a free electron excitation. In the original treatment of Gor'kov and Lebed' [35] the free energy of the system is lowest if the area of the normal carrier pockets on the Fermi surface is quantized. The total gapped area, or equivalently the density of electrons in the collective state will increase discontinuously upon each phase transition. (This agrees with the general observation of an increase of the magnetoresistance and a stepwise increase of the Hall voltage.)

The fact that, in contrast to Donovan *et al.* [55], we do see the gap is most likely related to the fact that we mainly probe the *b*-axis conductivity which is more a hopping type of conductivity and does not show the same clean limit electrodynamics. Moreover, the clear gap feature suggests an anomalous enhancement of the SDW dynamical mass (see page 79) which could be due to higher-order electron-phonon interactions.

We associate the low frequency resonance at 2.4 cm^{-1} in figure 4.5 with the collective mode of the SDW condensate. Both the extremely low frequency (well inside the SDW gap) and the magnetic field dependent behaviour of the resonance support this assignment. A somewhat surprising result is the fact that the collective mode appears at a rather high frequency (still much lower than the phonon modes) in comparison with the collective mode observed in $(TMTSF)_2PF_6$ [50, 55]. This would indicate a strong pinning of the electronic spin modulation to the lattice.

The change in the phonon response, especially near 32 cm^{-1}, demonstrates an appreciable interaction of the SDW formation with the lattice. The 32 cm^{-1} phonon is expected to be basically an acoustic mode, which becomes FIR active because of the zone folding caused by the ClO_4 anion ordering transition [52]. This mode is depicted in more detail in figure 4.7, where the transmission signal is normalized to the transmission of the same sample after it had been coating with gold. The 32 cm^{-1} phonon mode is distorted from a simple Lorentzian, partly due to the varying dielectric constant in this frequency region. However, it is clear that, especially in the $N = 0$ SDW state the phonon lineshape changes and becomes more asymmetric. This indicates an enhanced coupling of this phonon to the electronic system in the SDW state. Part of this coupling could result from the opening of the gap, which shifts electronic spectral weight to higher frequencies closer to the phonon frequency.

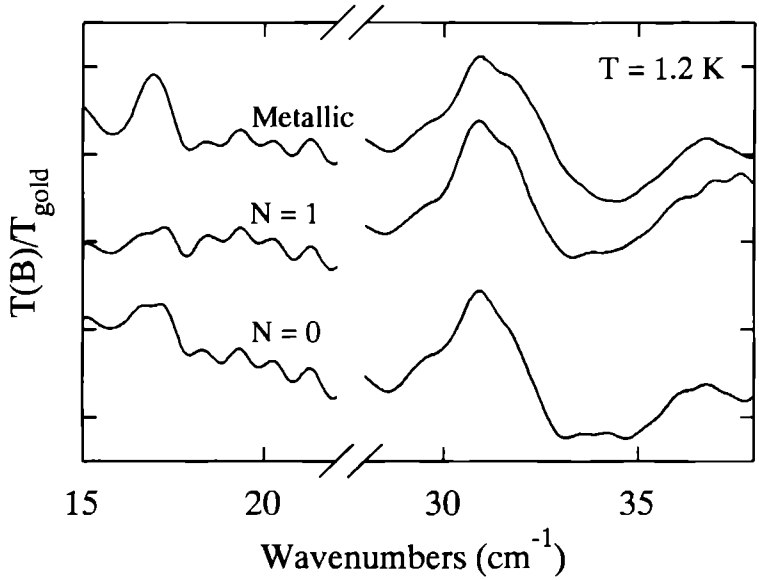

Figure 4.7 *Normalized transmission spectra (using a reference spectrum taken on a gold coated sample) in two FI-SDW states and the low field metallic state.*

The origin of the feature around 17 cm^{-1} is not understood. One could speculate that the additional incommensurate periodicity of the spin-density-wave leads to additional minigaps in the phonon dispersion and induces new FIR active modes that correspond to the original acoustic mode. Such phenomena have been observed in the related material MEM(TCNQ)$_2$ (which exhibits a spin-Peierls transition below 19 K) [56] and in incommensurately modulated crystals such as calaverite [57]. For a quarter filled band and a $2k_F$ modulation this would lead to additional modes at about half of the zone folding 32 cm^{-1} mode induced by the anion ordering. The observation of this phonon mode in the zero field (metallic state) spectra in figure 4.7 contradicts this supposition. The mode slightly shifts in frequency with magnetic field and becomes very asymmetric in the SDW phases. These facts make a mechanism via double folding due to SDW formation unlikely. This phonon is therefore more likely another zone folded acoustic phonon not previously observed by other workers [52, 58, 59]. It probably appears distorted at higher fields due to large changes in the dielectric response very close to the gap.

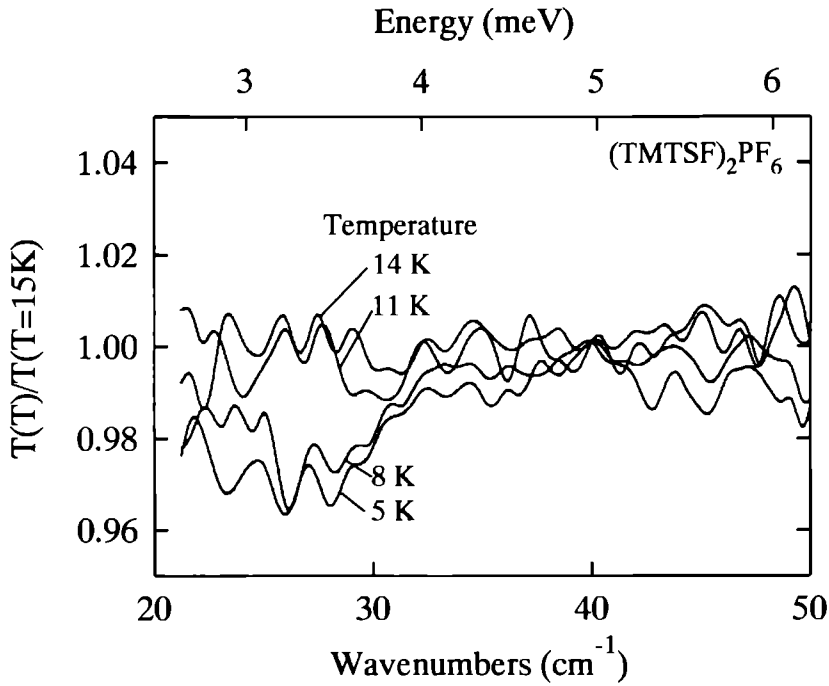

Figure 4.8 *Normalized transmission spectra (using 15 K spectra) through a grid of $(TMTSF)_2PF_6$ crystals at 4 different temperatures around the SDW phase transition.*

In order to check the assignment of the 14 cm^{-1} edge to the SDW gap we performed FIR measurements on a similar grid of $(TMTSF)_2PF_6$ crystals, which exhibit a SDW state at low temperatures in zero field. In figure 4.8 several spectra are shown, measured both above and below the SDW ordering temperature which is 12 K at ambient pressure for this material. The spectra are of considerable lower quality than those obtained on $(TMTSF)_2ClO_4$ crystals due to the poor crystal quality of the $(TMTSF)_2PF_6$ batch we had available. Below the SDW ordering temperature a decrease of the transmission signal below ~ 30 cm^{-1} is observed. Near this edge we find no visible phonon structure in the spectra, and this absence is indeed expected as there is no anion disorder in the centro-symmetric PF_6 compound and, thus, no zone folding. Assigning this edge to the opening of the SDW gap, we indeed find that the size of the gap is about twice as large as for the sharp edge in the $(TMTSF)_2ClO_4$ spectra, in accordance

with the twice larger value of T_{SDW} in $(TMTSF)_2PF_6$.

Further confirmation of our observations was given recently by Lefebvre *et al.* [60] who performed far infrared photoconductivity (PC) measurements on $(TMTSF)_2ClO_4$ in the FI-SDW regime. Their results show a large PC peak at 19 cm^{-1} (stretched from 14 to 20 cm^{-1}) caused by resonant photon absorption near the SDW gap. The PC peak does not shift as a function of field or temperature.

A final remark concerns the appearance of broad shallow dips in the field dependent data, marked in figure 4.4(a) by arrows. When compared with the work in Ref. 53 at higher temperature, the number and sharpness of these features, which are interpreted as the cyclotron resonance of free carriers, is considerably reduced. This result is consistent with the general observation [15] that Landau level type behaviour is thermally activated below $T_{SDW}(B)$ in this material. We calculate the effective mass to be $m^* = 0.7m_e$ which is in the range of values found in Ref. 53. The observation of a cyclotron resonance in these open orbit systems is quite astonishing and was recently discussed by Gor'kov and Lebed' [61].

4.2.4 Summary

Spectroscopic evidence has been presented that the gap in the field induced spin-density-wave state is independent of the value of the magnetic field. The data are consistent with a stepwise increase of the carrier density in the condensed SDW ground state upon each phase transition into a lower index subphase. In addition, the first indication of a pinned collective mode excitation in the microwave region is reported, and of an enhanced coupling of the 32 cm^{-1} zone folding phonon mode with the electronic system as a result of SDW formation.

4.3 Temperature dependence of the excitation spectrum in $(TMTSF)_2ClO_4$

In the previous section we established the low temperature magnetic field induced excitation spectrum of $(TMTSF)_2ClO_4$. In principle, the spectrum was found to consist of two parts; a contribution from single particle excitations across the SDW gap, and a collective mode resonance originating

from the excitation of the density-wave itself at a pinning frequency inside the SDW gap. This spectrum is in many respects similar to that known from CDW compounds [62]. However, such a spectrum is not theoretically expected for SDW systems [63]. A review on the dynamics of spin-density-waves was given by Grüner [64].

Grüner, following the work of Lee, Rice, and Anderson [63], defines the dynamical mass m^* of a density-wave as the band mass times the ratio of the total spectral weight in the metallic state (which is assumed Drude-like) and the total spectral weight of the density wave. In a CDW, m^* is strongly enhanced over the band mass m_b, because it is associated with a large lattice distortion. The CDW collective mode resonance appears with weight m_b/m^* at zero frequency or at a finite frequency if pinned to lattice imperfections. The single particle excitations occur with oscillator weight $(1 - m_b/m^*)$ commencing at the gap. In the ideal SDW case m^* equals m_b, because the SDW does not interact with the lattice. Hence, the single particle contribution to the excitation spectrum would be zero with all oscillator strength concentrated at the zero frequency collective mode. As shown in the previous section this is far from being the case since we do observe both collective and single particle contributions. Other experiments also indicate that the SDW is strongly pinned to the lattice [65] and has a SDW dynamical mass enhanced over the band mass [50]. One generally assumes that the SDW pinning is established via impurities in the lattice [66]. Alternatively, it has been predicted that Coulomb repulsion could raise the collective contribution to finite frequencies [67]. However, the understanding of these mechanisms is still far from complete.

In this section we present a magneto-optical study of the excitation spectrum of $(TMTSF)_2ClO_4$ covering the phase diagram around the FI-SDW threshold fields. The observed transition temperatures of the various FI-SDW subphases follow closely the phase diagram derived from transport data. From the excitation spectra we derive the magnitude of the SDW gap as a function of temperature. In addition we find evidence of a developing collective mode excitation in the gap with decreasing temperature, confirming the relatively strong pinning of the SDW to the lattice. Finally we present novel hysteresis and memory effects near the FI-SDW phase transitions which might point to a possible new mechanism for coupling between the condensed SDW electrons and the lattice.

4.3.1 Experimental details

Basically the experimental setup was identical to the one described in section 4.2.1 except that a heater, capacitance sensor and calibrated Allen-Bradley temperature sensor were incorporated, which allowed precise control of the sample temperature in a range from 0.4 to 7 K without essentially affecting the bolometer sensitivity. In addition we used a slow-scan Grubb-Parsons interferometer with either a 50 μm beamsplitter, or a 250 μm beamsplitter which enabled us to measure down to 2 cm^{-1}.

4.3.2 Results

In figure 4.9 normalized transmission spectra taken at monochromatic energies are shown for a set of temperatures covering the phase diagram of $(TMTSF)_2ClO_4$. The laser was tuned to 8.3 cm^{-1} which corresponds to an energy well within the SDW gap. With increasing temperature the number of FI-SDW phase transitions decreases and those still present move to higher magnetic fields. The transition field at each temperature is taken as the midpoint of the steps in the transmission signal. The points thus acquired in the phase diagram have been plotted in figure 4.10, together with the specific heat data of Fortune *et al.* [17].

In figure 4.11 we show the complete energy spectrum as a function of temperature for a magnetic field of 10 T measured with a slow-scan Fourier interferometer optimized in the long wavelength region. At this field we probe only the $N = 0$ FI-SDW phase. The spectra were normalized using zero field spectra taken at the same temperature, hence dividing out any temperature dependence in the bolometer sensitivity. The signal strength inside the gap remains nearly constant with increasing temperature until the transition temperature is reached. This sharp transition is more evident from the inset in figure 4.11 where the normalized signal intensities at 9.5 cm^{-1} well within the gap are plotted versus temperature. Note the remnants of a shallow structure above T_{SDW} in the main part of figure 4.11.

After all measurements were performed a layer of gold was evaporated onto the sample. This was done from different angles to obtain complete coverage also in between the crystals. All measurements were then repeated in order to obtain reference spectra. Unfortunately, due to small alignment and source intensity changes in the time elapsed between the sample and reference spectra, the quality of the normalized spectra was poor. In spec-

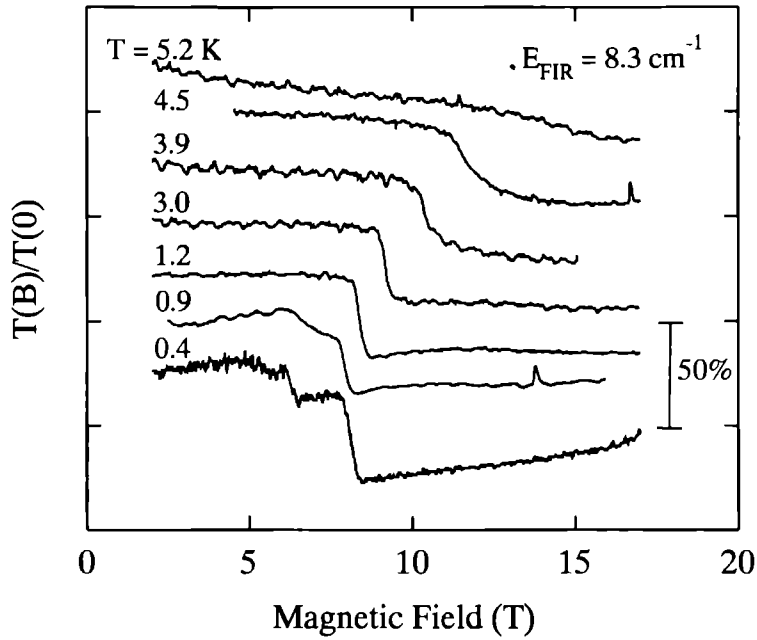

Figure 4.9 *Normalized transmission spectra $T(B)/T(0)$ versus magnetic field at different sample temperatures at 8.3 cm^{-1}. The traces are offset for clarity.*

troscopic studies of organic materials it is common practice to perform a Kramers-Kronig analysis on the normalized spectra obtained with a reference spectrum of a gold coated sample. However, the conductivities thus obtained are not very accurate and show a large difference in magnitude due to irregular crystal surfaces and open spaces between the separate crystals [44]. For a transmission-type experiment on a grid of crystals as used by us these effects would be even more severe. Therefore we have not pursued such an analysis and only base our analysis on the changes directly observable in the spectra. Nevertheless, the normalized spectra do reveal a clear change in phonon lineshape when the temperature changes through the phase transition. This is demonstrated in figure 4.12 where the details of the 17 and 32 cm^{-1} phonon modes are shown for a few temperatures above and below T_{SDW} at 10 T.

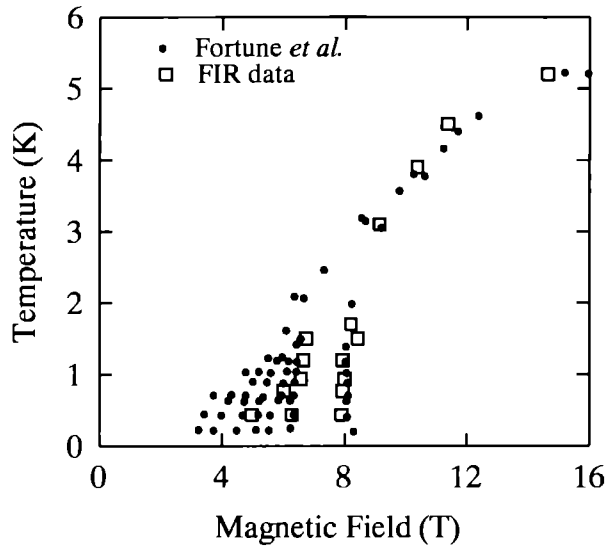

Figure 4.10 *Phase diagram composed of the FIR transmission data. Here the midpoints of the transitions such as in figure 4.9 have been used. The specific heat data reproduced from Fortune et al. [17] are shown for comparison.*

4.3.3 Discussion

The monochromatic data summarized in figure 4.9 for different temperatures show a behaviour identical to that of the data presented in figure 4.4(a) in section 4.2.2. With increasing temperature we find that the number of resolved FI-SDW phase transitions decreases and that they shift to higher fields. At low temperatures the transitions are almost discontinuous and occur within a very narrow field range, indicative of a first order nature of these phase transitions. At higher temperatures the transitions are broadened and the change in the FIR transmission becomes smaller, probably related to the presence of thermally excited carriers above the SDW gap. The overall agreement with the specific heat data (see figure 4.10) is quite good, giving confidence that we are indeed optically probing the SDW formation. The conclusion of the previous section was that the gap is not uniform in k-space, and that in all subphases there is a remaining free carrier density, related to the non-gapped area of the Fermi surface. The present data are consistent with this conclusion.

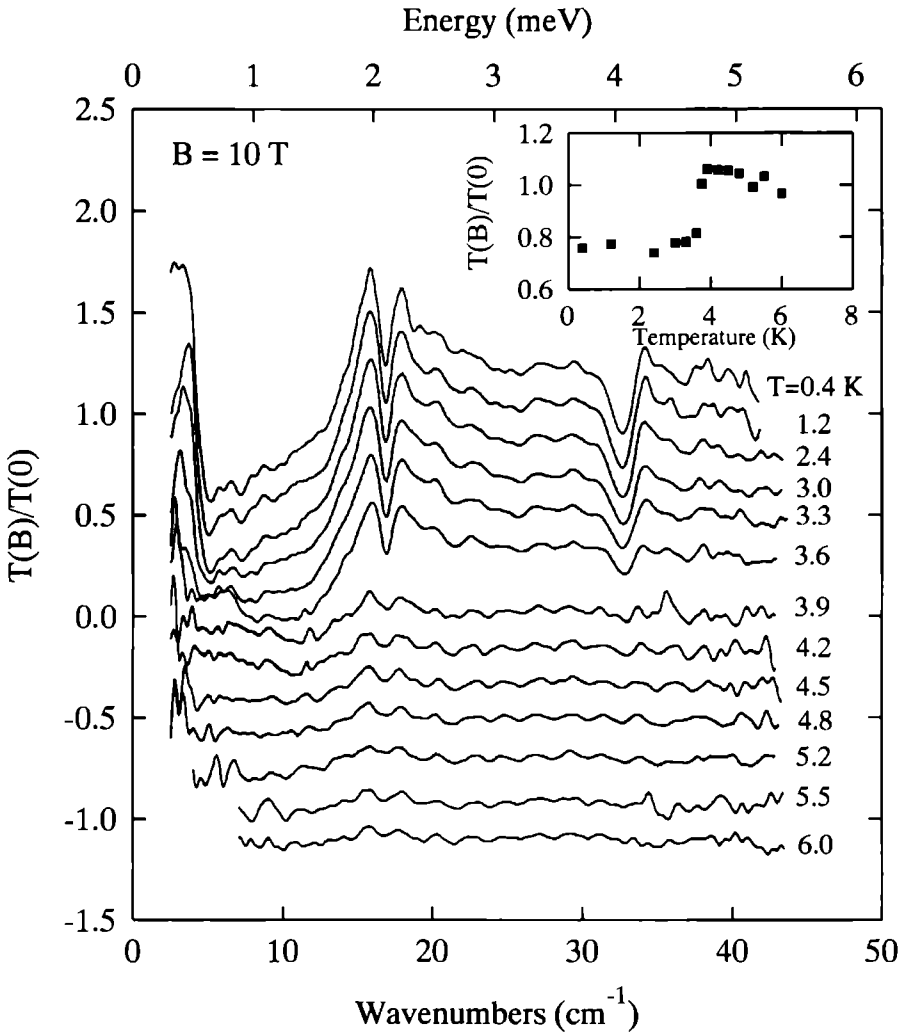

Figure 4.11 *Normalized spectra (using zero field spectra at the same temperature) as a function of frequency at various temperatures and a magnetic field of 10 T. The spectra taken with 50 and 250 μm beamsplitter are merged together. The traces are offset for clarity. Inset: Plot of the signal intensities at (9.5 cm^{-1}) within the SDW gap as a function of temperature.*

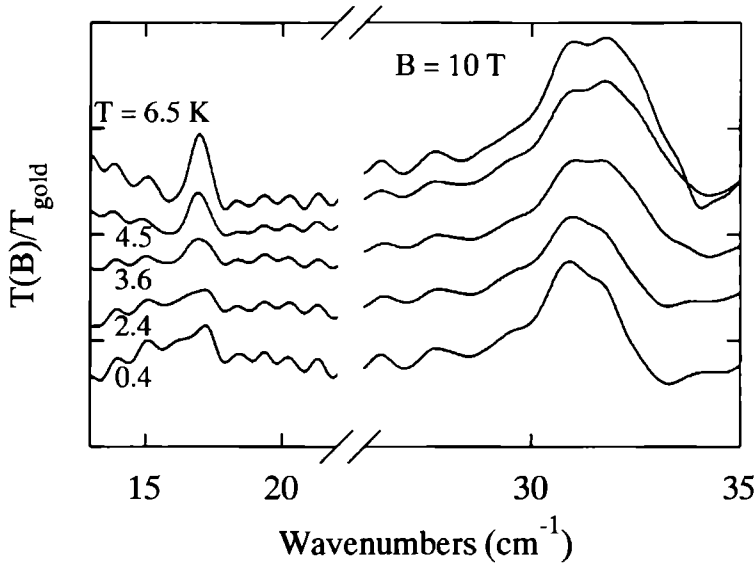

Figure 4.12 *Normalized spectra (using reference spectra on a gold coated sample at the same temperature) at 10 T for several different temperatures both above and below the SDW phase transition temperature. The spectra are offset for clarity.*

In the energy spectra in figure 4.11 we observe a gap-like structure below 14 cm^{-1} similar to the low temperature data in figure 4.5 for the $N = 0$ FI-SDW phase. With increasing temperature the gap edge does not shift to lower energies, as one would expect in a mean field picture, but remains at a fixed position. The signal strength inside the gap depicted in the inset of figure 4.11 remains nearly constant with increasing temperature up to the phase transition. Again, this behaviour is quite different from BCS-like mean field predictions. A similar sharp decrease of the order parameter was found in the muon spin resonance data by Le *et al.* [68].

The fact that, above T_{SDW}, shallow remnants of the gap remain visible is unexpected in a mean field model and indicates the possible presence of SDW fluctuations with no long range magnetic order. Fluctuations are an issue which have lead to a lot of debate in the past [3,13]. Evidence is conclusive that the phase boundary of $(TMTSF)_2ClO_4$ is second order up to a temperature of 3 K where the subphases disappear; the subphase transitions themselves are thought to be first order [9,10]. Above 3 K the magnetization data indicate a first order phase transition [10], contradicting the specific

heat measurements which point to a second order transition [17]. On the other hand, we observe hysteresis in our data at the phase transition also above 3 K like for the subphase transitions, and this points rather to a first order transition. Fluctuations are predicted to be present in anisotropic conductors but would be strongly suppressed for first order phase transitions. One could argue that the origin of the shallow structure is less subtle than proposed above, and caused by the inability of the heater to reach the proper sample temperature at the highest temperatures during the measurement. However, the fact that in the experiments with monochromatic energies the exact phase diagram can be reproduced, indicates that the sample temperature is correct. On the other hand, temperature gradients may exist in the samples because they are not cooled by exchange gas but by contact with a cold finger. However, because the material is still a good conductor in the $N = 0$ phase we do not expect that these gradients are significant.

At low frequencies we find in figure 4.11 a strong excitation mode which slightly hardens when going to lower temperatures. This confirms the earlier observation of this mode with monochromatic microwave sources shown in figure 4.6 of section 4.2.2. Although the relative accuracy decreases near the extreme low frequency end of the spectrum, it is clear that the intensity of this mode is weakly temperature dependent until it vanishes near the critical temperature. This is in agreement with its interpretation as a collective mode excitation of the SDW state, where the hardening at low temperatures is due to a more effective pinning of the condensate. To observe this hardening unequivocally, additional measurements down to lower frequencies will be necessary.

The phonon features observed in the spectra in figure 4.11 also change when going from the metallic state to the SDW state below T_{SDW}. As mentioned before, these are probably both related to zone folding due to the anion ordering superlattice. We find a strong change in the phonon lineshape when lowering the temperature into the SDW state. When the spectra are normalized to the reference spectrum taken on the gold-coated sample (figure 4.12) it is indeed clear that the 17 cm^{-1} phonon peak decreases in intensity and becomes strongly asymmetric, again similar to the case where the magnetic field changes the SDW subphases (figure 4.7). This could be due to an increased coupling to the electronic excitations just above the SDW gap. A similar effect appears at the high energy side of the 32 cm^{-1}

phonon structure. These changes, although unexpected for SDW systems, are in themselves not very surprising given the additional incommensurate modulation which breaks the translation symmetry and changes the selection rules for optically active ($k = 0$) phonon modes. However, it must be noted that both phonons are also present in the metallic state and the major effect of the SDW formation is a change in lineshape.

4.3.4 Hysteresis and memory effects

In this last section we want to discuss some interesting hysteresis and memory effects observed in the experiments taken with microwave sources at energies well within the SDW gap. Normally the hysteresis observed in magnetotransport measurements at the last SDW phase transition depends on how far the magnetic field has been swept beyond the threshold field. In figure 4.13(a), a field sweep at 7.2 cm^{-1} is shown. When the field was swept up, we found the signal to show the usual steps at the FI-SDW transition fields. Just after the $N = 0$ SDW state was entered, the magnetic field sweep was stopped, and the field was held constant at 8.0 T. During the pause the transmission signal relaxed back very slowly (on a time scale of minutes) to the level corresponding to the previous $N = 1$ subphase. When after about 20 minutes the field was swept down, the signal was found to drop again to the level of the $N = 0$ state. At even lower fields the transmission rose again and after this the usual steps of the phase transition were observed. Figure 4.13(b) shows the signal intensity at a magnetic field of 8.0 T versus time for an initial sweep rate of 0.04 T/min. At this slow sweep rate induction effects in the magnetic field or temperature changes due to sweeping of the magnetic field are, to our estimates, insignificantly small.

The time scale for the relaxation is very long, in the order of minutes; this suggests besides simple heating effects either the presence of domain formation or possibly some sort of coupling to the nuclear spins of the organic molecules. The fact that the system relaxes back to the $N = 1$ state after it already made the transition to the $N = 0$ state rules out hysteresis effects and heating. The nucleation of domain structures also seems unlikely because the system already made the full phase transition. Furthermore, on the down sweep the transition occurs on a much shorter time scale. The appearance of a memory effect while sweeping down in field suggests the build up of an internal magnetic field. A similar sort of effect

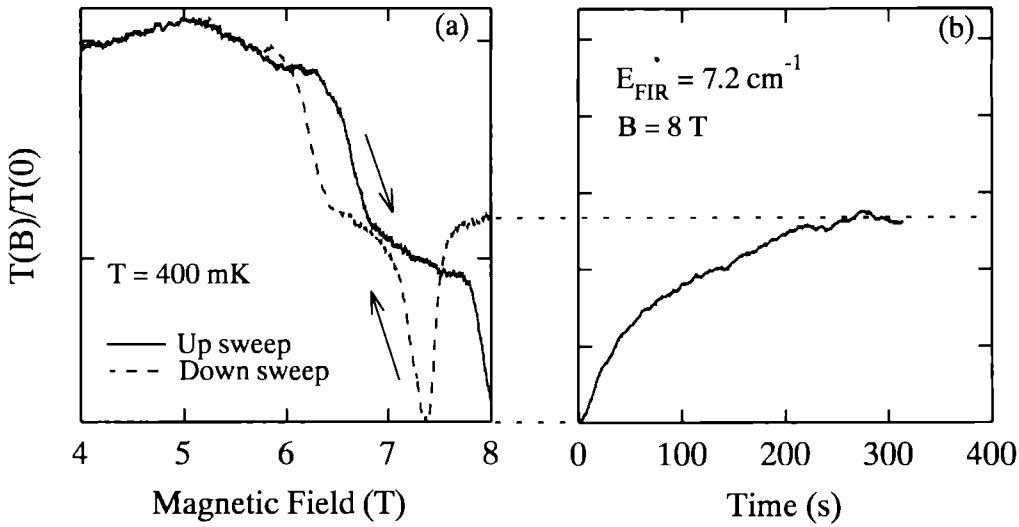

Figure 4.13 *(a) Up and down sweep for the transmission signal at microwave energy of 7.2 cm^{-1}, showing anomalous hysteresis. (b) Transmission signal versus time after an up-sweep to 8 T.*

was first predicted by Overhauser [69] for metallic systems. He suggested that microwave energies are capable of saturating the electronic system via electron-spin-resonance (ESR). The electron system will then effectively polarize the nuclei via paramagnetic relaxation processes that can occur by means of the hyperfine interaction between electrons and nuclei. Such a strong nuclear polarization has been observed by Dobers *et al.* [70] in an ESR experiment on GaAs-(Ga,Al)As heterostructures. In the present system one could envision a similar effect where the electronic system carries a stationary magnetic moment which varies in space. The hyperfine interaction could effectively induce a coupled magnetization of the nuclei (presumably Se or H) with the same periodicity as the electronic SDW. This mechanism implies that memory effects could also appear in non-optical experiments. With NMR experiments, Azevedo *et al.* [71] estimated the local field in $(TMTSF)_2ClO_4$ to be at least of the order of 0.1 T on the Selenium sites. A very slow proton relaxation rate (minutes) was observed in the FI-SDW states indicating a change in relaxation mechanism at the phase transition. Because the FI-SDW formation is the result of a delicate energy balance it is possible that the lowest energy state for a given external field in the presence of the polarized nuclei is different from the state

without polarization. This kind of coupling could also be the origin of the frequently observed hysteresis effects near the SDW transitions. It could also explain the unusual pinning of the SDW electronic ground state to the lattice. A possible check for the mechanism will be to quench the relaxation effect via saturation of the nuclear spins with RF radiation [70]. In that case no spin-flip process can take place due to absence of empty levels in the nuclei, as a result the up and down sweep in the experiment should appear unshifted, without the memory effect.

4.3.5 Summary

We have presented spectroscopic data on the temperature dependence of the FI-SDW formation in $(TMTSF)_2ClO_4$. The value of the SDW gap is relatively insensitive to temperature. The phase transitions as a function of temperature at high magnetic fields, as well as the phase transitions as a function of magnetic field at low temperatures are of first order. The optically detected phase transitions follow closely the phase diagram established from thermodynamic measurements. Above T_{SDW} some shallow gap structure in the spectra remains. This indicates possible fluctuations of the FI-SDW state. We confirm the presence of a collective mode near 2.4 cm^{-1} which is weakly temperature dependent, indicating possible depinning at higher temperatures. In addition we report the measurement of peculiar memory effects near the SDW subphase transitions, which suggest magnetic coupling to the lattice.

Acknowledgment: We are grateful to Paul Chaikin for providing the samples used.

References

1. K. Bechgaard, C.S. Jacobsen, K. Mortensen, J.H. Pederson, and N. Thorup, Solid State Commun. **33**, 1119 (1980).
2. D. Jérome, A. Mazaud, M. Ribault, and K. Bechgaard, J. Phys. (Paris) Lett. **41**, L95 (1980).
3. D. Jérome and H.J. Schulz, Adv. Phys. **31**, 299 (1982).
4. T. Ishiguro and K. Yamaji, *Organic Superconductors*, Springer Series in Solid-State Sciences **88**, (Springer-Verlag, Berlin, 1990).
5. K. Oshima, H. Okuno, K. Kato, R. Maruyama, R. Kato, A. Kobayashi, and H. Kobayashi, in *Proceedings of the International Conference on Science and Technology of Synthetic Metals, Seoul, 1994*, to be published.
6. T. Mori, A. Kobayashi, Y. Sasaki, and H. Kobayashi, Chem. Lett. **1982**, 1923 (1982).
7. P.M. Grant, Phys. Rev. B **26**, 6888 (1982).
8. P.M. Grant, Phys. Rev. Lett. **50**, 1005 (1983).
9. F. Pesty, P. Garoche, and K. Bechgaard, Phys. Rev. Lett. **55**, 2495 (1985).
10. M.J. Naughton, J.S. Brooks, L.Y. Chiang, R.V. Chamberlin, and P.M. Chaikin, Phys. Rev. Lett. **55**, 969 (1985).
11. M.J. Naughton, R.V. Chamberlin, X. Yan, S.Y. Hsu, L.Y. Chiang, M.Y. Azbel, and P.M. Chaikin, Phys. Rev. Lett. **61**, 621 (1988).
12. R.C. Yu, L.Y. Chiang, R. Upasani, and P.M. Chaikin, Phys. Rev. Lett. **65**, 2458 (1990).
13. H. Bando, K. Kajimura, H. Anzai, T. Ishiguro, and G. Saito, Mol. Cryst. Liq. Cryst. **119**, 41 (1985).
14. R.V. Chamberlin, M.J. Naughton, X. Yan, L.Y. Chiang, S.Y. Hsu, and P.M. Chaikin, Phys. Rev. Lett. **60**, 1189 (1988).
15. X. Yan, M.J. Naughton, R.V. Chamberlin, S.Y. Hsu, L.Y. Chiang, J.S. Brooks, and P.M. Chaikin, Phys. Rev. B **36**, 1799 (1987).
16. X.D. Shi, W. Kang, and P.M. Chaikin, Phys. Rev. B **50**, 1984 (1994).
17. N.A. Fortune, J.S. Brooks, M.J. Graf, G. Montambaux, L.Y. Chiang, J.A.A.J. Perenboom, and D. Althof, Phys. Rev. Lett. **64**. 2054 (1990).

18. W. Kang, S.T. Hannash, and P.M. Chaikin, Phys. Rev. Lett. **70**, 3091 (1993).
19. V.M. Yakovenko, Sov. Phys. JETP **66**, 355 (1987).
20. A.G. Lebed' and Per Bak, Phys. Rev. B **40**, 11433 (1989).
21. T. Osada, S. Kagoshima, and M. Miura, Phys. Rev. Lett. **69**, 1117 (1992).
22. L.P. Gor'kov and A.G. Lebed', in *Proceedings of the International Conference on Science and Technology of Synthetic Metals, Seoul, 1994*, to be published.
23. R.E. Peierls, *Quantum Theory of Solids*, (Oxford Univ. Press, London 1955).
24. N.W. Ashcroft and N.D. Mermin, *Solid State Physics* (Saunders College, Philadelphia, 1976).
25. K. Yamaji, J. Phys. Soc. Jpn. **55**, 860 (1986).
26. K. Mortensen, Y. Tomkiewicz, and K. Bechgaard, Phys. Rev. B **25**, 3319 (1982).
27. A. Andrieux, D. Jérome, K. Bechgaard, J. Phys. (Paris) Lett. **42**, L87 (1982).
28. G. Soda, D. Jérome, M. Weger, J. Alizon, J. Gallice, H. Robert, J.M. Fabre, and L. Giral, J. Phys. (Paris) **38**, 931 (1977).
29. J.E. Hirsch, Phys. Rev. Lett. **51**, 296 (1983).
30. J.F. Kwak, J.E. Schirber, R.L. Greene, and E.M. Engler, Phys. Rev. Lett. **46**, 1296 (1981).
31. H. Bando, K. Oshima, M. Suzuki, H. Kobayashi, and G. Saito, J. Phys. Soc. Jpn. **51**, 2711 (1982).
32. P.M. Chaikin, M.Y. Choi, J.F. Kwak, J.S. Brooks, K.P. Martin, M.J. Naughton, E.M. Engler, and R.L. Greene, Phys. Rev. Lett. **51**, 2333 (1983).
33. K. Kajimura, H. Tokumoto, M. Tokumoto, K. Murata, T. Ukachi, H. Anzai, T. Ishiguro, and G. Saito, J. Phys. (Paris) Colloq. **44**, C3-1059 (1983).
34. P.M. Chaikin, Phys. Rev. B **31**, 4770 (1985).
35. L.P. Gor'kov and A.G. Lebed', J. Phys. (Paris) Lett. **45**, L433 (1984).
36. M Héritier, G. Montambaux, and P. Lederer, J. Phys. (Paris) Lett. **45**,

L943 (1984).

37. G. Montambaux, M. Héritier, and P. Lederer, Phys. Rev. Lett. **55**, 2078 (1985).
38. J.F. Kwak, J.E. Schirber, P.M. Chaikin, J.M. Williams, H.H. Wang, and L.Y. Chiang, Phys. Rev. Lett. **63**, 972 (1986).
39. A. Virosztek, L. Chen, and K. Maki, Phys. Rev. B **34**, 3371 (1986).
40. M. Ribault, D. Jérome, J. Tuchendler, C. Weyl, and K. Bechgaard, J. Phys. (Paris) Lett. **44**, L953 (1983).
41. K. Yamaji, J. Phys. Soc. Jpn. **54**, 1034 (1985).
42. G. Montambaux and D. Poilblanc, Phys. Rev. B **37**, 1913 (1988).
43. G. Montambaux, M.J. Naughton, R.V. Chamberlin, X. Yan, P.M. Chaikin, and M.Y. Azbel, Phys. Rev. B **39**, 885 (1989).
44. T. Timusk and C.S. Jacobsen, in: *Low Dimensional Conductors and Superconductors*, edited by D. Jérome and L.G. Caron (Plenum, New York, 1987) p. 253 and p. 275.
45. H.K. Ng, T. Timusk, D. Jérome, and K. Bechgaard, Phys. Rev. B **32**, 8041 (1985).
46. R.L. Greene and P.M. Chaikin, in *Proceedings of the 17th International Conference on Low Temperature Physics*, edited by U. Eckern, A. Schmidt, W. Weber, and H. Wühl (North-Holland, Amsterdam, 1984).
47. K. Kornelsen, J.E. Eldridge, and G.S. Bates, Phys. Rev. B **35**, 9162 (1987).
48. S. Marianer, M. Kaveh, and M. Weger, Phys. Rev. B **25**, 5197 (1982).
49. H.K. Ng, T. Timusk, and K. Bechgaard, Phys. Rev. B **30**, 5842 (1984).
50. D. Quinlivan, Y. Kim, K. Holczer, G. Grüner, and F. Wudl, Phys. Rev. Lett. **65**, 1816 (1990).
51. S. Donovan, Y. Kim L. Degiorgi, and G. Grüner, J. Phys. (Paris) I **3**, 1493 (1993).
52. J.E. Eldridge, C.C. Holmes, F.E. Bates, and G.S. Bates, Phys. Rev. B **32**, 5156 (1985).
53. A.S. Perel, J.S. Brooks, C.J.G.N. Langerak, T.J.B.M. Janssen, J. Singleton, J.A.A.J. Perenboom, and L.Y. Chiang, Phys. Rev. Lett. **67**, 2072, (1991).
54. H.K. Ng, T. Timusk, J.M. Delrieu, D. Jérome, K. Bechgaard, and

J.M. Fabre, J. Phys. (Paris) Lett. **43**, L513 (1982).

55. S. Donovan, Yong Kim, L. Degiorgi, M. Dressel, G. Grüner, and W. Wonneberger, Phys. Rev. B **49**, 3363 (1994).
56. Y. Tanaka, N. Satoh, and K. Nagasaka, J. Phys. Soc. Jpn. **59**, 319 (1990).
57. P.H.M. van Loosdrecht, A.M. Gerrits, K. Balzuweit, W. König, A. Wittlin, and P.J.M. van Bentum, J. Phys.: Cond. Mat. **5**, 3977 (1993).
58. H.K. Ng, T. Timusk, and K. Bechgaard, J. Phys. (Paris) Colloq. **44**, C3-867 (1983).
59. C.S. Jacobsen, D.B. Tanner, K. Bechgaard, Phys. Rev. B **28**, 7019 (1983).
60. J. Lefebvre, J. Beerens, C. Bourbonnais, L.G. Caron, C. Lenoir, and P. Batail, Phys. Rev. Lett. **72**, 3417 (1994).
61. L.P. Gor'kov and A.G. Lebed', Phys. Rev. Lett. **71**, 3874 (1993).
62. G. Grüner, Rev. Mod. Phys. **60**, 1129 (1988).
63. P.A. Lee, T.M. Rice, and P.W. Anderson, Solid State Commun. **14**, 703 (1974).
64. G. Grüner, Rev. Mod. Phys. **66**, 1 (1994).
65. G. Kriza, Yong Kim, and G. Mihaly, Phys. Rev. B **45**, 1466 (1992).
66. W. Kang, S. Tomić, and D. Jérome, Phys. Rev. B **43**, 1264 (1991).
67. K. Maki and G. Grüner, Phys. Rev. Lett. **66**, 782 (1991).
68. L.P. Le, A. Keren, G.M. Luke, B.J. Sternlieb, W.D. Wu, Y.J. Uemura, J.H. Brewer, T.M. Riseman, R.V. Upasani, L.Y. Chiang, W. Kang, P.M. Chaikin, T. Csiba, and G. Grüner, Phys. Rev. B **48** 7284 (1993).
69. A.W. Overhauser, Phys. Rev. **92**, 411 (1953).
70. M. Dobers, K. von Klitzing, J. Schneider, G. Weimann, and K. Ploog in: *High Magnetic Fields in Semiconductor Physics II*, edited by G. Landwehr, Springer Series in Solid State Sciences **87**, 396 (1989).
71. L.J. Azevedo, J.M. Williams, and S.J. Compton, Phys. Rev. B **28**, 6600 (1983).

Chapter 5

Far-infrared studies of the metal-insulator transition in $PrNiO_3$ and $NdNiO_3$

This work was done in cooperation with X. Granados, J.L. Garcia-Muñoz and J. Fontcuberta from the Institut de Ciència de Materials de Barcelona, Consejo Superior d'Investigaciones Científicas, Bellaterra, Spain. Parts of this chapter have been published in:

- Physica C **235-240**, 1289 (1994).

5.1 Introduction

There has recently been a revival of interest in the properties of transition metal oxides and related compounds. The interest was triggered by the discovery of high temperature superconductivity of several copper oxide compounds and recent progress in the understanding of electronic correlations in narrow-band transition metal systems [1,2].

In 1985, Zaanen, Sawatzky and Allen (ZSA) [1] proposed a simple, and yet powerful, framework to describe the nature of the different states of various transition metal (TM) compounds (see figure 5.1). Two types of charge fluctuations are considered in this framework and the relative positions of the electronic bands involved determine the actual state in which these materials are found.

The first type of fluctuation considered by ZSA is the transfer of one electron at a TM site i to a neighbouring TM site j. In the presence of sufficiently delocalized d-states and in the absence of strong Coulomb repulsion this leads to d-type metallic conductivity (the far right of figure 5.1). Double occupancy of the transition metal sites will be suppressed when the on-site Coulomb repulsion U is large. As a result, the d-band splits in two subbands (the upper and lower Hubbard band)* separated by an energy U. We assume a half filled d-band (*i.e.* a completely filled lower Hubbard band and an empty upper Hubbard band) and thus arrive at an insulating state, the so-called Mott state or Mott-Hubbard state.

The other charge fluctuation considered and which is mainly of importance in the late (Mn-Cu) transition metal compounds is the transfer of an electron from an anion p-state to an empty TM d-state. When the anion p-band and the TM d-band overlap, one has a semi-metallic conductor (far left side of figure 5.1. On the other hand, when the charge transfer energy Δ is larger than the electronic bandwidth W, the charges are localized and the system is called a charge transfer insulator. The undoped parent compounds of the superconducting copper oxides are generally regarded as charge transfer insulators.

A schematic phase diagram which results from these considerations is given in figure 5.2.

Although the copper oxides are doped with carriers to make them

*These subbands are not strictly one electron bands but for the present purpose this one electron picture is sufficient.

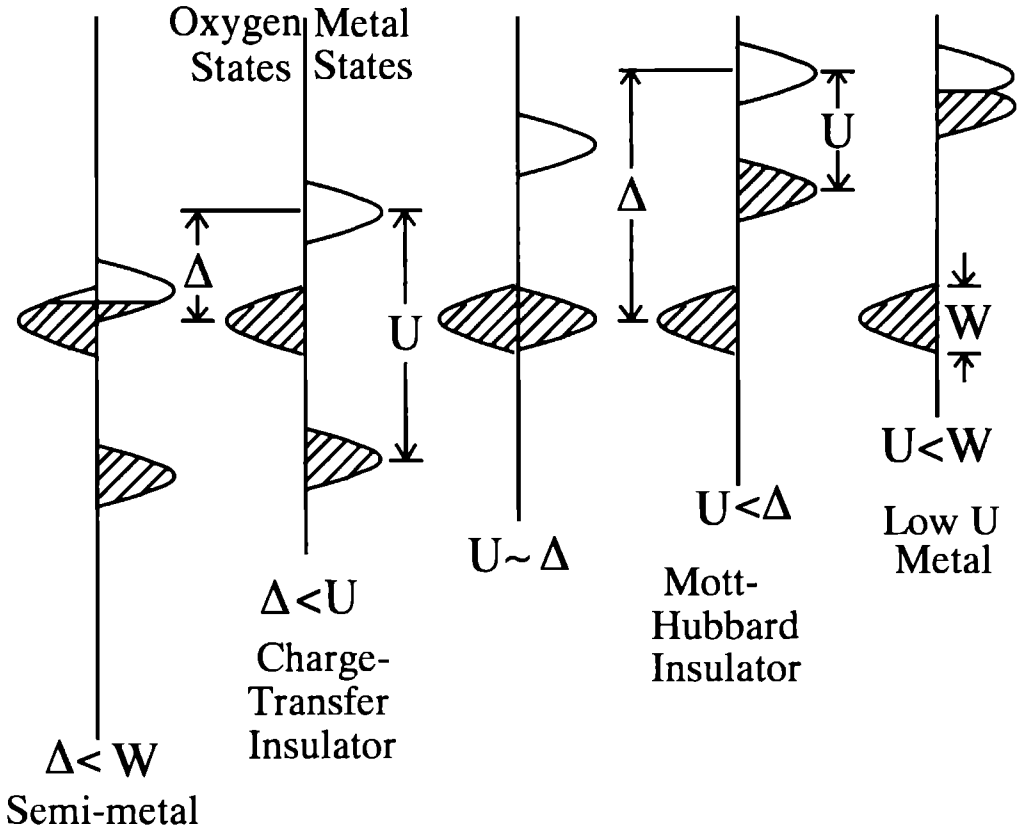

Figure 5.1 *This diagram shows various possible states that can occur in transition metal compounds. The anion (for our material Oxygen) p-states are shown on the left sides of the vertical lines. The transition metal d-states are shown on the right sides. The hatched parts represent filled states. Δ is the charge transfer energy and U is the on-site Coulomb repulsion on the transition metal sites. For simplicity we took the width of all bands involved equal to W. After Ref. 4.*

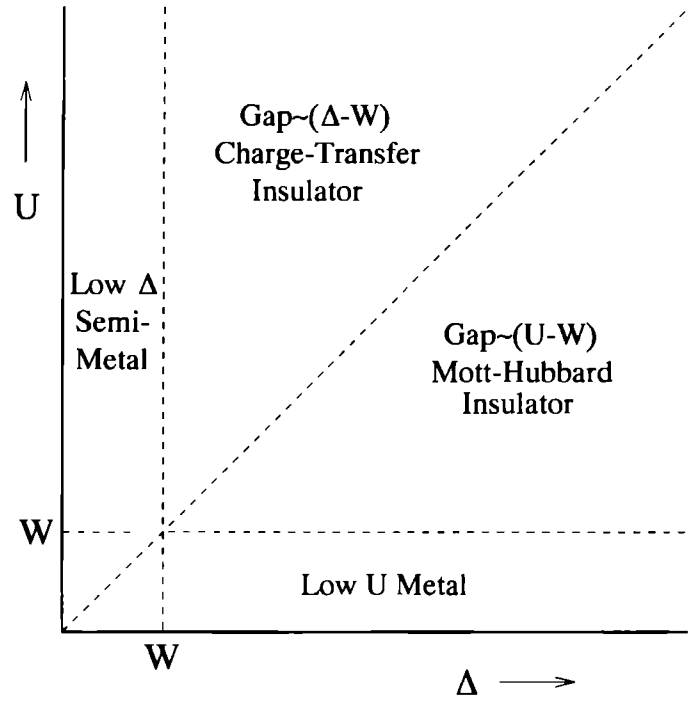

Figure 5.2 *Schematic phase diagram showing the different regions in which the transition metal compounds may lie, depending on their values of U and Δ. After Ref. 4.*

conducting, a charge transfer insulator can also become conducting when, due to an increased bandwidth W, the p- and d-bands start to overlap. Such MI transition has been proposed recently by Torrance *et al.* [3] for the $R\mathrm{NiO_3}$ (R = La, Pr, Nd, Sm, Eu) family. From an extensive study on numerous transition metal oxides [4,5] they found that the position of the $R\mathrm{NiO_3}$ system in a U versus Δ phase diagram is close to the metal-insulator boundary (see figure 5.2) where charge transfer energies are small. On the other hand, $\mathrm{V_2O_3}$, which is well known for exhibiting a Mott-Hubbard metal-insulator transition, is close to the metal-insulator boundary at which the Coulomb repulsion is small.

$R\mathrm{NiO_3}$ compounds have the $\mathrm{GdFeO_4}$ structure. This structure is close to the ideal cubic perovskite structure but the $\mathrm{NiO_6}$ octahedra are slightly tilted with respect to each other. This distortion comes about because the

size of the rare earth ion is relatively small so that the NiO_6 octahedra tilt and rotate to fill the space available around the rare earth ion [6, 7]. A decrease of the ionic radius of the rare earth (and also a decrease of the temperature) causes further buckling of the NiO_6 octahedra and a decrease of the Ni-O-Ni bond angle. It was further known that the electronic bandwidth decreases with decreasing Ni-O-Ni bond angle [8]. These observations lead Torrance *et al.* to propose the metal-insulator transition mechanism of Ref. 3.

The metal-insulator transition temperature in $R\mathrm{NiO_3}$ was found to rise systematically with decreasing rare earth ion size from Pr to Eu. $LaNiO_3$, which has the smallest distortion, is found to remain metallic down to 0.5 K (nevertheless, low temperature specific heat, magnetization and transport data point to a correlated behaviour of the $3d$ electrons [9]). For the other rare earth elements the MI transition temperatures are 135, 200, 400 and 460 K, respectively. A hysteretic behaviour has been found, associated with a first order phase transition. From a structural point of view no change in lattice symmetry at T_{MI} has been seen up to now but the transition is accompanied by a very slight expansion of the unit cell ($\Delta V/V \approx 0.25\%$) with a subtle increase of Ni-O distances of $\Delta d_{\mathrm{Ni-O}} \approx +0.004$ Å. Furthermore, this effect is accompanied by tilts of the NiO_6 octahedra and hence changes in the Ni-O-Ni angles ($\Delta\Theta_{\mathrm{Ni-O-Ni}} \approx -0.5°$) which govern the transfer integral between the nickel $3d$ and the oxygen $2p$ orbitals [7].

Resistivity data show semiconducting behaviour of $PrNiO_3$ [10] and $NdNiO_3$ [11] in the insulating state with an activation energy of 22 and 25-28 meV respectively, which decreases slightly with increasing temperature. When the temperature rises above T_{MI}, the resistivity drops about three orders of magnitude. In the metallic state, dc-transport and thermopower measurements show that the dc-resistivity and the Seebeck coefficient depend linearly on temperature. This would suggest that the carrier density is constant which is in apparent disagreement with the model suggested by Torrance *et al.* [3] where one would rather expect the carrier density to increase with temperature.

Furthermore, in the regime in which transport properties show hysteretic behaviour (70-130 K for $PrNiO_3$ and 130-205 K for $NdNiO_3$) the metallic and the insulating phases are found to coexist [10, 11]. No dependence of T_{MI} on the cooling or heating rate of the sample was observed. The measured transport properties are the result of the mixing of the contribu-

tions of both phases and have been described within the effective medium approximation.

Finally, muon spin resonance experiments [3] have shown that below T_{MI}, antiferromagnetic ordering occurs in $PrNiO_3$ and $NdNiO_3$ [12]. The Sm and Eu compounds first become paramagnetic insulators just below T_{MI} and antiferromagnetic ordering sets in at a much lower temperatures. The importance of magnetic correlations for the electronic properties is not yet clear.

The understanding of the nature of the band gap and of the contributing terms leading to electronic localization in these oxides requires further work. Besides the dramatic change of dc conductivity at the MI transition, also an interesting and unusual temperature and frequency dependence of the dynamic dielectric function $\epsilon(\omega)$ is expected. Therefore, we study in this work the temperature evolution of the optical conductivity in the far infrared of $R NiO_3$ (R = La, Pr, Nd) and we focus our attention on the spectral changes at the transition from the metallic phase into the insulating phase of the latter two compounds.

5.2 Experimental details

The $LaNiO_3$, $PrNiO_3$ and $NdNiO_3$ polycrystalline samples were prepared at the IBM Almaden Laboratory in San Jose by synthesis under high oxygen pressure. Details of the synthesis can be found elsewhere [6]. X-ray and neutron diffraction experiments show that the samples are well crystallized, single phase and have the structure of a slightly rhombohedral ($LaNiO_3$) or orthorhombically ($PrNiO_3$, $NdNiO_3$) distorted perovskite. Extensive structure analysis, transport and thermodynamic measurements have been reported in Refs. 7 and 11. The samples used for this study were pressed pellets, almost black in color. Unfortunately, their surfaces were brittle and remained rather rough, despite various attempts to polish them. The reflectance measurements over the range from 30 to 5000 cm^{-1} were made with a Bruker IFS113v interferometer in a continuous flow helium cryostat (Oxford model CF1104) at temperatures between 300 K and 15 K. Subsequent spectra were always taken with decreasing temperature. A gold mirror was used as a reference. Subsequently, in order to eliminate the ef-

fect of diffuse scattering due to the sample surface roughness, a gold film was evaporated onto the samples. Then, the reflectance was measured again and the spectra were corrected.

5.3 Results and discussion

Figure 5.3(a) shows the reflectivity of $NdNiO_3$ at several temperatures between 15 K and 225 K in the range 30-700 cm^{-1}. Figure 5.3(b) shows the reflectivity of $PrNiO_3$ between 15 K and 155 K in the same spectral range. The most pronounced feature of these spectra is a rapid change of character from metallic-like to insulator-like over a relatively narrow range of temperatures. Whereas the optical phonons are completely screened by free carriers in the metallic phase, they dominate the spectrum at lower temperatures[†]. For $NdNiO_3$ that change takes place between 195 K and 185 K, for $PrNiO_3$ between 135 K and 125 K. These temperatures are close to the MI transition temperature T_{MI}, defined here as the temperature of the resistivity increase in a cooling down trace. Above 700 cm^{-1} the spectra are featureless. The temperature dependent changes in the spectra extend over a broad energy range, up to $\approx$ 2500 cm^{-1} in $NdNiO_3$ and up to $\approx$ 4000 cm^{-1} in $PrNiO_3$.

From room temperature down to the transition temperature, the spectra show basically no reflectance changes in the entire frequency range measured. Below T_{MI} a trace of metallic reflectivity persists which is in agreement with the presence of both phases in a large temperature interval below T_{MI}. Upon further cooling these traces gradually diminish and, ultimately, below 145 K (75 K) in $NdNiO_3$ ($PrNiO_3$) they vanish. This is more or less in agreement which the lowest temperatures at which hysteresis is observed in dc-transport experiments. It is rather surprising that below T_{MI} no spectral feature is seen at energies comparable to the gap energy as determined by transport measurements. We will come back to this point at the end of this section.

The reflectivity of $LaNiO_3$, for which spectra are shown for comparison in figure 5.3(c), retains quasi-metallic character over the whole temperature

[†]The features visible in the metallic state and the absolute reflectivity were strongly dependent on the surface treatment of the sample and did not reproduce after further polishing. We will therefore focus on the changes observed in the spectra when the material enters the insulating state.

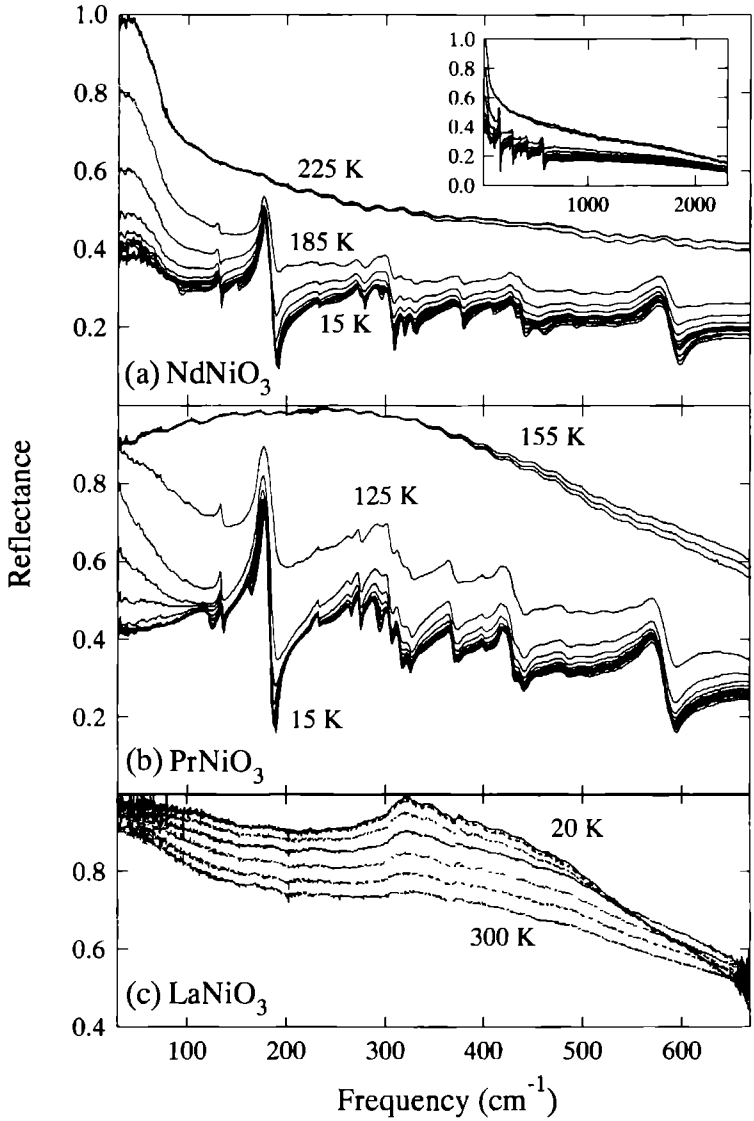

Figure 5.3 *(a) The reflectance of $NdNiO_3$ at 225 K - 125 K (in steps of 10 K), and at 95, 65, and 15 K. (b) The reflectance of $PrNiO_3$ at 155 K - 15 K (in steps of 10 K). (c) The reflectance of $LaNiO_3$ at 300 K - 50 K (in steps of 50 K) and at 20 K. Inset: the reflectivity of $NdNiO_3$ between 30 and 2200 cm^{-1} (at the same temperatures as in (a)).*

range measured.

We used a model dielectric function and applied a multi-oscillator fit to the measured reflectivity. At temperatures below T_{MI} this model dielectric function $\epsilon(\omega)$ was composed of a high frequency electronic part ϵ_∞, a sum of Lorentz oscillators ϵ_{ph}^k representing phonons at frequency ω_k with a strength S_k and damping γ_k. An additional Lorentz oscillator was added representing a mid-infrared absorption band with frequency ω_M, oscillator strength S_M and damping γ_M yielding a total dielectric function,

$$\epsilon(\omega) = \epsilon_\infty + \sum_{k=1}^{n} \epsilon_{ph}^k(\omega) + \epsilon_M(\omega) \ , \tag{5.1}$$

where

$$\epsilon_{ph}^k(\omega) = \frac{S_k\omega_k^2}{\omega_k^2 - \omega^2 - i\omega\gamma_k}, \text{ and } \epsilon_M(\omega) = \frac{S_M\omega_M^2}{\omega_M^2 - \omega^2 - i\omega\gamma_M} \ . \tag{5.2}$$

The structure of the nickelates, determined from neutron diffraction studies is well described by the space group Pbnm, corresponding to an orthorhombically distorted perovskite. This symmetry allows in principle up to 28 infrared-active optical modes [13], of which up to 20 could be resolved in our spectra at the lowest temperature. A satisfactory fit (shown in figure 5.4) was obtained with a sum of phonon modes and a broad mid-infrared band. The phonon parameters of the fit are given in Table 5.1. We want to stress here that because of the limited accuracy of the measured reflectance the absolute values for the oscillator strengths are not well defined. For comparison, recently published [14] phonon frequencies of the weakly metallic isostructural $LaTiO_3$ are also shown. The analysis of Crandles *et al.* [14] of the $LaTiO_3$ phonons, which follows closely Couzi and Huong [13] is, to a large extent, also applicable to nickelates. According to that analysis, the three strongest peaks are attributed to F_{1u} modes of the parent cubic lattice. In $PrNiO_3$ these modes are at 175 cm^{-1}, 286 cm^{-1}, and 567 cm^{-1}. Below T_{MI} the effect of temperature on the phonon spectrum is fairly minor. With increasing temperature the phonon frequencies decrease monotonically. However, even close to T_{MI} we do not observe any significant increase of this phonon softening which could be related to the phase transition. The inset in figure 5.4 shows the temperature dependence of the most pronounced phonon in $PrNiO_3$ at 175 cm^{-1}. The full analysis of the

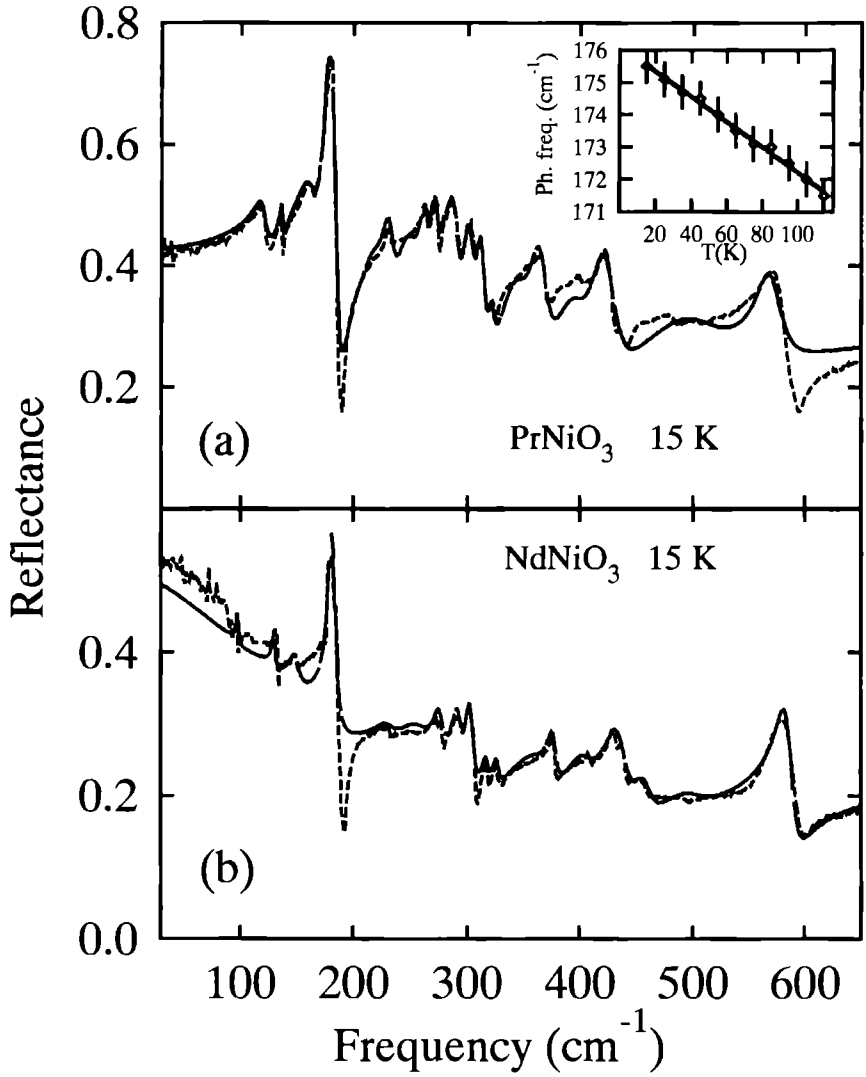

Figure 5.4 *Measured reflectance of $PrNiO_3$ (a) and of $NdNiO_3$ (b) (dashed lines) at 15 K are shown together with fitted curves (solid lines). The model dielectric function used for the fit is shown in equation (5.1) and the phonon oscillator parameters are shown in Table 5.1. The inset in (a) displays the temperature dependence of $PrNiO_3$ phonon at 175 cm^{-1}.*

Table 5.1 *Phonon frequencies ω_i of $NdNiO_3$ and $PrNiO_3$ determined from the least-squares fit of equation (5.1) to the measured reflectance at 15 K, and just below the M-I transition (at the highest temperature where phonon lines could be resolved in the spectra). Other phonon parameters, oscillator strengths S_i and linewidths γ_i are shown for $PrNiO_3$ at 15 K only. For comparison the phonon frequencies of the isostructural compound $LaTiO_3$ are also shown (from Ref. 14).*

Sample	$NdNiO_3$	$NdNiO_3$		$PrNiO_3$		$PrNiO_3$	$LaTiO_3$
T (K)	15	185		15		125	300
Mode	ω_i	ω_i	ω_i	S_i	γ_i	ω_i	ω_i
1	98		120	1.2	12		
2	133	131	137	0.18	2.8	133	
3	149		161	2.2	19		
4	180	176	175.5	2	5	171	169.4
5			220	0.3	18		
6	230		232	0.5	10		
7	257		250	0.7	20		
8			263	0.35	8		
9			271.5	0.42	8		
10	276	272	280	0.12	7	280	245.3
11	292		286	0.65	12		
12	302		301	0.35	10		
13	317	309	311	0.21	8		314.9
14	327		322	0.06	7		
15	360		345	0.44	27		341.8
16	377	375	363	0.4	16	363	377.3
17	405		395	0.3	30		
18	434	428	420	0.42	20	416	410.7
	458						
19	500		500	0.55	80		503.7
							522.9
20	582	580	567	0.25	22	562	556.9

phonon features and lattice dynamics of $PrNiO_3$ and $NdNiO_3$ will be presented elsewhere [15]. Here we only remark, that the phonon frequencies of $PrNiO_3$ and $NdNiO_3$ are almost identical. This is to be expected, regarding the almost identical masses of the Nd and Pr ions.

On the other hand, the parameters of the mid-infrared band used in the fit are quite different. For completeness, we mention here that for $PrNiO_3$ the best fit at 15 K was obtained with $\omega_M = 800$ cm^{-1}, $S_M = 4, \gamma_M = 600$ cm^{-1}, $\epsilon_\infty = 7.5$, and for $NdNiO_3$ with $\omega_M = 140$ cm^{-1}, $S_M = 25, \gamma_M = 400$ cm^{-1}, $\epsilon_\infty = 8.5$. The physical meaning of these band parameters is, however, not so clear because the mid-infrared band feature did not reproduce very well with successive polishing treatments.

As in the hysteretic regime regions of metallic character coexist with regions of insulating character, an effective medium model should be used to analyse the data in this temperature region properly. However, we do not want to investigate this coexistence in detail here and thus, for simplicity we modeled the remaining metallic conductivity below T_{MI} by adding to the model dielectric function (5.1) the following Drude term

$$\epsilon_D(\omega) = \frac{\omega_p^2}{\Gamma - i\omega} \,. \tag{5.3}$$

By increasing gradually both ω_p and Γ and decreasing ω_M we could fit the spectra over the entire temperature range. In figure 5.5(a) we show the results of the fitting procedure for $PrNiO_3$ at 125 K. The fitting parameters are basically unchanged from those at 15 K in figure 5.4, except for the added Drude term and small changes of phonon parameters. We used the Drude parameters: $\omega_p = 4000$ cm^{-1} and $\Gamma = 2500$ cm^{-1}.

Once at temperatures above the hysteretic regime, the effective medium approach is no longer necessary and, within the assumption of a Drude-like free carrier conductivity[‡], the simple addition of $\epsilon_D(\omega)$ is justified. Figure 5.5(b) shows the fit above the MI transition, at 155 K, in which we switched off the phonon part of the dielectric function, We got the following parameters: $\omega_p = 11000$ cm^{-1} , $\Gamma = 16000$ cm^{-1} , $\omega_M = 110$ cm^{-1} , $S_M = 500$ and $\gamma_M = 10$ cm^{-1}.

[‡]It is not evident at all that the conductivity in the metallic state of the present system with partially filled and overlapping *p*- and *d*-bands can be described in a simple one band Drude model.

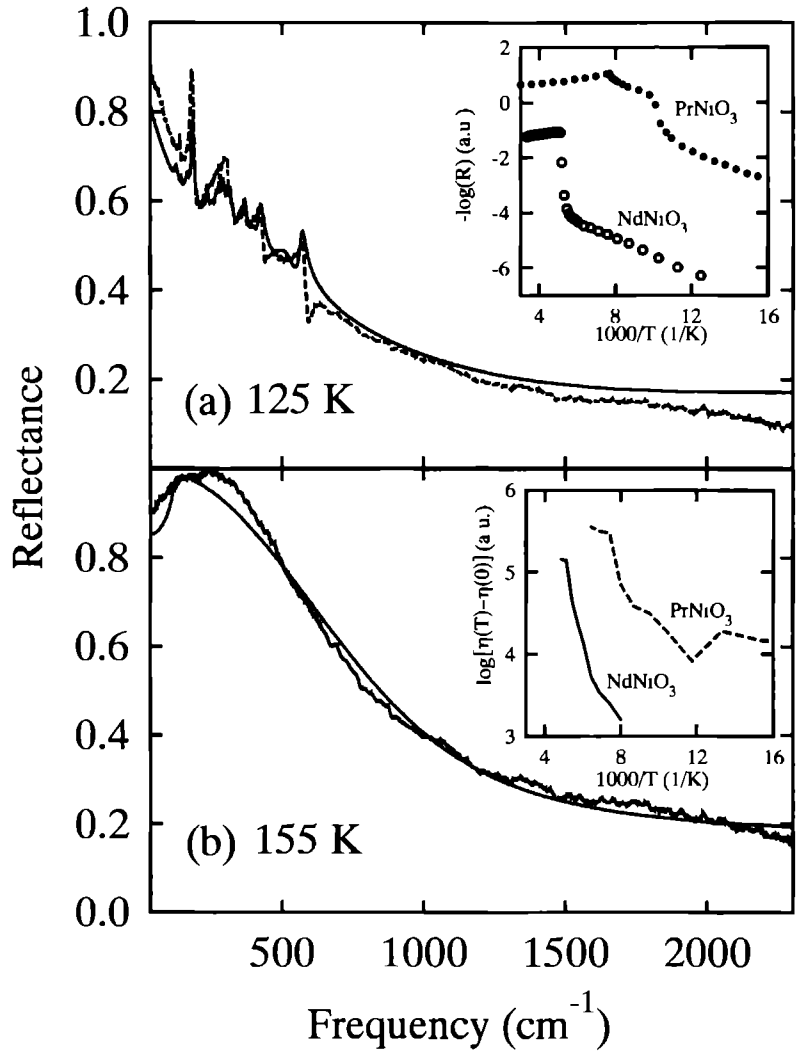

Figure 5.5 *Measured (dashed lines) and fitted (solid line) reflectance of $PrNiO_3$ at 125 K (a) and at 155 K (b). Inset in (a) displays the temperature dependence of $PrNiO_3$ resistivity after Ref. 11, and the inset in (b) shows the temperature dependence of partial f-sum $\eta(T) - \eta(0)$ for $NdNiO_3$ and $PrNiO_3$ obtained from Kramers-Kronig analysis of the spectra. The temperature scale in both plots is in units of 1000/K and both the resistivity and integrated conductivity are shown in logarithmic scale and arbitrary units.*

The plasma frequency values extracted from the fit can be used to get estimates of the n/m^* ratio (m^* is the effective electron mass) by using the classical Drude expression $\omega_p^2 = ne^2/\epsilon_0 m^*$ where n is the charge carrier density. For instance, in $PrNiO_3$ at $T = 155$ K $\omega_p \approx 11000$ cm^{-1} and $n/m^* \approx 1.34 \times 10^{21}$ cm$^{-3}/m_e$ (m_e is the free electron mass). If, according to Ref. 10 one assumes one electron per unit formula participating in electronic conduction, the corresponding electron density is $n \approx 1.8 \times 10^{22}$ cm^{-3}. Consequently, $m^* \approx 13m_e$. In view of the uncertainties in the reflectance measurements and the (in)appropriateness of the Drude model to describe the metallic state, this value for m^* is not very accurate. We believe however, that the value found does illustrate that the effective mass m^* is considerably enhanced above the free electron mass m_e which is an indication for strong correlations between the electrons in the conduction band. Very large mass enhancements ($m^* \approx 9m_e$) were also observed in Seebeck and calorimetric studies [10].

The relaxation rate Γ (≈ 16000 cm^{-1}) can be combined with n/m^* to calculate the Drude conductivity $\sigma = (n/m^*)e^2/\Gamma$. When we insert Γ and the value for n/m^* which has been extracted from ω_p, it turns out that for $PrNiO_3$ the specific resistivity $\rho \approx 1.3$ mΩcm. This value compares favourable with the dc resistivity 2.0 mΩcm [10] and gives confidence that the above analysis is quite reasonable despite the serious assumptions made.

Instead of using a model dielectric function to fit the reflectance, one can use a Kramers-Kronig analysis to obtain the dielectric function $\epsilon(\omega)$ and the conductivity $\sigma(\omega)$. However, due to diffuse scattering in the ceramic samples and the extrapolations needed towards low and high frequencies this method is not likely to produce accurate results. However, it is instructive to follow the *trend* of the integrated conductivity in the vicinity of the MI transition. We will consider a finite-energy *f*-sum

$$\eta(T) = \int_{\omega_{min}}^{\omega_{max}} \sigma(\omega, T)\, d\omega \tag{5.4}$$

as a function of temperature. The integral is cut off at a certain frequency ω_{max} so as to include only intraband contributions to $\sigma(\omega, T)$ but no contributions related to interband transitions. Such a finite *f*-sum is proportional to the density of electrons in the conduction band [16].

In the inset of figure 5.5 we plot $\eta(T)$ for a frequency range between $\omega_{min} = 30$ cm^{-1} and $\omega_{max} = 2500$ cm^{-1}. We subtracted the low temperature conductivity sum $\eta(0)$ for which we used the data measured at the

lowest temperature (15 K). Near T_{MI}, the f-sum or, equivalently, the number of carriers in the conduction band clearly shows a dramatic change. It should be noted that this change extends over a broader range of temperatures than the dc resistivity (also shown in figure 5.5). Moreover, it does not show a semiconductor-like simple activated behaviour. Although it might be tempting to fit $\eta(T) - \eta(0)$ with a straight line (with a single activation energy in the range 10-15 meV, compatible with dc transport measurements), both the dc and the present infrared data indicate, that the MI transition probably has a more complicated character.

An optical sum rule requires that the area under $\sigma_1(\omega)$ integrated over *all* frequencies is proportional to the total number density of electrons in the system and must therefore be constant. This means that across the MI transition the missing conductivity ($50\ \text{cm}^{-1} \leq \omega \leq 2500\ \text{cm}^{-1}$) is shifted to other parts of the spectrum. From the low value of $\epsilon_1(\omega)$ we know that the missing area is not shifted to low frequencies (as happens in a superconductor). Instead, it should be compensated by contributions extending up to very high frequencies, well above our upper limit.

In conventional semiconductors this shifting of spectral weight primarily occurs within a frequency range of the order of several times the gap [17] and, in principle, a clear feature is expected at the gap energy. In the insulating phase of the $R\text{NiO}_3$ system we do not observe any feature that could be related to the gap. This may be due to a conductivity that only has a weak onset above the gap causing the feature to be obscured by the phonons and the mid-infrared band. The value of the activation gap E_g deduced from the transport data is approximately 80 cm^{-1}. One would therefore expect that all spectral weight should be recovered within the explored frequency range. Our data indicate that this is not the case. The physical origin of this very broad frequency-dependent conductivity is not yet clear. Because the samples are ceramic, it could be produced by surface states or impurity states. Another possibility is that this conductivity is of intrinsic origin, like in the high T_c superconductors where the mid-infrared absorption is also observed in high quality single crystals. It could possibly be related to the empty states in the Ni $3d$ band.

5.4 Summary

We have studied the reflectance of $LaNiO_3$, $NdNiO_3$ and $PrNiO_3$ from 30 to 5000 cm^{-1} at temperatures between 300 and 15 K. At temperatures below the metal-insulator transition, the far-infrared spectrum is dominated by phonon structures superimposed on a weak mid-infrared background. We observe a dramatic change of the spectra from nearly insulating to metallic-like in a narrow range of temperatures around the T_{MI} which is consistent which a closing energy gap. In the metallic regime, the infrared data shows that the phonon structures are completely screened. Our results are qualitatively in agreement with the mechanism for the metal-insulator transition proposed by Torrance *et al.* When the data in the metallic state is analyzed within a Drude model the conduction can be understood in terms of rather heavy electrons.

Acknowledgment: We thank J.B. Torrance and P. Lacorre of the IBM Almaden Research Center for providing the $LaNiO_3$, $PrNiO_3$ and $NdNiO_3$ samples.

References

1. J. Zaanen, G.A. Sawatzky, and J.W. Allen, Phys. Rev. Lett. **55**, 418 (1985);
   J. Zaanen and G.A. Sawatzky, J. Solid State Chem. **88**, 8 (1990) and references therein.
2. C.M. Varma, in *Strongly Interacting Fermions and High-T_c Superconductivity*, Proc. Ecole de Physique Théoretique des Houches, August 1991.
3. J.B. Torrance, P. Lacorre, A.I. Nazzal, E.J. Ansaldo, and Ch. Niedermayer, Phys. Rev. B **45**, 8209 (1992).
4. J.B. Torrance, P. Lacorre, C. Asavaroengchai, and R.M. Metzger, Physica C **182**, 351 (1991).
5. J.B. Torrance, J. Solid State Chem. **96**, 59 (1992).
6. P. Lacorre, J.B. Torrance, J. Pannetier, A.I. Nazzal, P.W. Wang, and T.C. Huang, J. Solid State Chem. **91**, 225 (1991).
7. J.L. Garcia-Muñoz, J. Rodríguez-Carvajal, P. Lacorre, and J.B. Torrance, Phys. Rev. B **46**, 4414 (1992).
8. G.A. Sawatzky, W. Geertsma, and C. Haas, J. Magn. Magn. Mater. **3**, 37 (1976).
9. K. Sreedhar, J.M. Honig, M. Darwin, M. McElfresh, P.M. Shand, J. Xu, B.C. Crooker, and J. Spalek, Phys. Rev. B **46**, 6382 (1992).
10. X. Granados, J. Fontcuberta, X. Obradors, U. Mañosa, and J.B. Torrance, Phys. Rev. B **48**, 11666 (1993).
11. X. Granados, J. Fontcuberta, X. Obradors, and J.B. Torrance, Phys. Rev. B **46**, 15683 (1992).
12. J.L. Garcia-Muñoz, J. Rodríguez-Carvajal, and P. Lacorre, Europhys. Lett. **20**, 241 (1992);
    J.L. Garcia-Muñoz, J. Rodríguez-Carvajal, and P. Lacorre to be published.
13. M. Couzi and P. van Huong, J. Chem. Phys. **69**, 1339 (1972).
14. D.A. Crandles, T. Timusk, and J.E. Greedan, Phys. Rev. B **44**, 13250 (1991).
15. W. Kress, to be published.

16. J. Orenstein, G.A. Thomas, A.J. Millis, S.L. Cooper, D.H. Rapkine, T. Timusk, L.F. Schneemeyer, and J.V. Waszczak, Phys. Rev. B **42** 6342 (1990).
17. Z. Schlesinger, Z. Fisk, Hai-Tao Zhang, M.B. Maple, J.F. DiTusa, and G. Aeppli, Phys. Rev. Lett. **71**, 1748 (1993) and reference (13) therein.

Summary

In this thesis we have presented far-infrared studies on a number of solids which exhibit strong electronic correlation effects. The large importance of these correlations is mainly brought about by the reduced dimensionality of the systems, the narrow electronic bands and the low density of electrons. The systems investigated are some high T_c superconductors (chapter 1-3), the organic charge transfer salt $(TMTSF)_2X$ (chapter 4), and some rare earth nickel oxides (chapter 5).

The basic structral building blocks of the high temperature superconductors are the two-dimensional (2D) copper oxide planes which are considered to be responsible for the generation of the extremely high critical temperatures (up to 150 Kelvin) observed in these materials. The physical processes inside these copper oxide planes have been studied much more intensively than the out-of-plane properties. Nevertheless, because bulk (3D) superconductivity is observed in these materials proper knowledge of the out-of-plane dynamics is required to understand thoroughly the superconducting state of the cuprates. Recently it was found that, below the critical temperature and for light polarized perpendicular to the planes, a clear low frequency plasma edge develops in infrared reflectance spectra. In chapter 1 we have investigated the out-of-plane far-infrared response of the high temperature superconductor $La_{1.85}Sr_{0.15}CuO_4$ and have shown that the plasmon can be explained by a Josephson coupled layer model. In a magnetic field study, we have found a small field dependent change of the plasma edge but the screened plasma frequency ω_{ps} itself is basically field independent, in contrast to recent theoretical predictions. Also at ω_{ps} there is no change in the absorption. We have developed a simple model which describes the dielectric response of type II superconductors in the mixed state at frequencies small compared to the gap frequency. Key ingredient of the model is

that the current which exerts the Lorentz force is formed not only by the free carrier current but also by the polarization current. This prevents an appreciable influence of vortex motion near the plasma frequency which is in agreement which the experimental data.

In chapter 2 we report on low temperature far-infrared reflection measurements on the most intensively studied high T_c compound, $YBa_2Cu_3O_7$, at magnetic fields up to 15.5 Tesla. In these experiments the light was polarized parallel to the *ab* planes. Our measurements on thin film $YBa_2Cu_3O_7$ have shown for the superconductive state a clear edge in the reflectance near 400 cm^{-1}, which develops into a distinct kink if the temperature is lowered to 1.2 K. Many groups have argued that this feature is caused by an unusually large superconductive gap ($\hbar\omega_g \approx 8k_BT_c$). We have observed practically no influence of the magnetic field on the infrared reflectance of $YBa_2Cu_3O_7$. In particular we find no field induced shift of the 400 cm^{-1} edge, as would be expected from the effects of pair breaking and Zeeman splitting on a single gap structure. This finding favours non-electronic explanations of this feature such as the charged phonon mechanism. The absence of distinct field-dependent features is consistent clean-limit electrodynamics and a very anisotropic gap in the *ab* plane.

In chapter 3 we have shown that from measurements of the reflectivity of a uniaxial medium taken at a finite angle of incidence using both *s*- and *p*-polarized light it is possible to determine the dielectric function parallel and perpendicular to the optical axis. When applied to layered compounds with the surface parallel to the layers, this technique allows an accurate determination of the loss function perpendicular to the layers. This technique is particularly useful for crystals of which only thin films or thin single crystal platelets exist. High temperature superconductors generally fall into this category although larger single crystals gradually become available. The technique may also serve as a second complementary approach for investigating the out-of-plane response of these materials since, for example, in epitaxially grown thin films it is often easier to obtain a homogeneous oxygen distribution than in single crystals. The technique has been demonstrated for the example of *c*-axis-oriented thin films of the high-T_c superconductor $Tl_2Ba_2Ca_2Cu_3O_{10}$, on which we have carried out polarized reflectivity measurements at 45° angle of incidence above and below T_c. We could clearly observe the longitudinal optical phonons in the *c*-axis. From the behaviour of the *c*-axis dielectric loss function we could

conclude that 200 cm^{-1} is an upper limit for the out-of-plane plasmon.

In chapter 4 we have investigated the FIR excitation spectrum of the compound $(TMTSF)_2ClO_4$, which is a well known member of the quasi-1D family of organic charge-transfer salts, also known as Bechgaard salts. This compound exhibits a complex phase diagram in the presence of a magnetic field. The specific emphasis in our work has been on the details in the excitation spectrum related to a specific kind of antiferromagnetic ordering induced by the magnetic field (the so-called field-induced spin-density-wave (FI-SDW) ordering). We covered large parts of the phase diagram of this charge transfer salt (magnetic field up to 16 T, energy between 0.3 and 6.0 meV, and temperature between 0.3 and 7 K). We have found that the optically detected phase transitions as a function of magnetic field and temperature follow closely the phase diagram established from thermodynamic measurements. The experiments have demonstrated that the cascade of FI-SDW phase transitions can be optically detected. The spectroscopic data has indicated that the gap in the FI-SDW state is independent of the value of the magnetic field and temperature as opposed to the predictions of the standard model. However, this result is consistent with a stepwise increase of the carrier density in the condensed SDW ground state upon each phase transition into a lower index subphase. In addition, the first indication of a pinned collective mode excitation in the microwave region has been reported, and of an enhanced coupling of the 31 cm^{-1} zone folding phonon mode with the electronic system as a result of SDW formation.

Finally, chapter 5 has been dedicated to infrared reflectivity measurements on the rare-earth nickelates $LaNiO_3$, $PrNiO_3$ and $NdNiO_3$ between 30 cm^{-1} and 5000 cm^{-1} at temperatures between 15 K and 300 K. It is known that most members the $RNiO_3$ (R = La, Pr, Nd, Sm, Eu) family exhibit a metal-insulator transition at T_{MI}. It has recently been proposed that this metal-insulator transition is related to the charge transfer gap which opens (closes) when the width of the electronic bands decreases (increases) as the temperature drops (rises). In the insulating state the infrared reflectance of $NdNiO_3$ and $PrNiO_3$ is mainly determined by phonons. We have observed a dramatic change of the spectra from nearly insulating to metallic-like in a narrow range of temperatures around the T_{MI} which is consistent which a closing energy gap. In the metallic regime, the phonon structures are completely screened. $LaNiO_3$ showed metallic behaviour at all tempera-

tures in agreement with previous results of *e.g.* dc transport measurements. Our results are qualitatively in agreement with the above mentioned mechanism for the metal-insulator transition. When the conductivity above T_{MI} is assumed Drude-like the data in the metallic state indicate a rather heavy effective mass of the conduction electrons.

Samenvatting

In dit proefschrift worden ver infrarode onderzoeken beschreven aan een aantal vaste stoffen waarin sterke elektronische correlatie-effecten optreden. De correlatie-effecten zijn juist in deze systemen zo belangrijk vanwege hun lage dimensionaliteit, de smalle elektronische banden en de lage elektronendichtheid. De onderzochte systemen zijn enkele hoge temperatuur supergeleiders (hoofdstuk 1 t/m 3), het organische *charge transfer* zout $(TMTSF)_2X$ (hoofdstuk 4) en enkele zeldzame aard nikkel oxides (hoofdstuk 5).

De structurele basiseenheden waaruit de hoge temperatuur supergeleiders zijn opgebouwd zijn de tweedimensionale (2D) koper oxide vlakken welke verantwoordelijk worden geacht voor het genereren van de extreem hoge kritische temperaturen (tot ca. 150 Kelvin) die in deze materialen worden waargenomen. De fysische processen in deze koper oxide vlakken zijn veel intensiever bestudeerd dan de eigenschappen loodrecht op deze vlakken. Omdat *bulk* (3D) supergeleiding wordt waargenomen in deze materialen is goede kennis van de dynamica loodrecht op de koper oxide vlakken nodig om de supergeleidende toestand in de koper oxides grondig te begrijpen. Onlangs is ontdekt dat zich beneden de kritische temperatuur een scherpe laag frequente plasma *edge* ontwikkelt in infrarode reflectie spectra, wanneer het invallende licht loodrecht gepolariseerd is ten opzichte van de koper oxide vlakken. In hoofdstuk 1 hebben we de "uit-vlaks" ver infrarode respons van de hoge temperatuur supergeleider $La_{1.85}Sr_{0.15}CuO_4$ onderzocht en aangetoond dat het plasmon kan worden verklaard met behulp van een Josephson gekoppeld lagen model. We hebben een kleine afhankelijkheid gevonden van de vorm van de plasma edge als funktie van een aangelegd magnetisch veld maar de plasma frequentie ω_{ps} zelf is, in tegenstelling tot enkele theoretische voorspellingen, veldonafhankelijk. Ook vinden we geen absorptieverande-

ring bij ω_{ps}. We hebben een eenvoudig model ontwikkeld dat de diëlektrische respons van type II supergeleiders in de vortex toestand beschrijft bij frequenties die klein zijn ten opzichte van de *gap* frequentie. Het belangrijkste ingrediënt van dit model is dat de stroom die de Lorentzkracht veroorzaakt niet alleen wordt gevormd door de stroom van vrije ladingsdragers maar ook door de polarisatiestroom. Dit verhindert een noemenswaardige invloed van vortex beweging in de buurt van de plasmafrequentie, in overeenstemming met de experimentele resultaten.

In hoofdstuk 2 hebben we ver infrarode reflectiemetingen gepresenteerd aan de meest onderzochte hoge temperatuur supergeleider, $YBa_2Cu_3O_7$, bij lage temperaturen en magnetische velden tot 15.5 Tesla. In dit experiment was de lichtpolarisatie parallel aan de *ab* vlakken. Onze metingen aan dunne lagen van $YBa_2Cu_3O_7$ laten in de supergeleidende toestand een duidelijke reflectierand zien die zich tot een duidelijke knik ontwikkelt als de temperatuur wordt verlaagd tot 1.2 K. Vele onderzoekers hebben beweerd dat deze structuur veroorzaakt wordt door een ongewoon grote supergeleidende *gap* ($\hbar\omega_g \approx 8k_BT_c$). We hebben nagenoeg geen invloed gezien van het aangelegde magnetische veld op de infrarode reflectie van $YBa_2Cu_3O_7$. In het bijzonder hebben we geen veld geïnduceerde verschuiving van de 400 cm^{-1} rand zoals men bij een simpele *gap* structuur zou verwachten als gevolg van paarbrekende effecten en Zeemansplitsing. Deze bevinding ondersteunt niet-elektronische verklaringen van deze structuur zoals het *charged phonon* mechanisme. De afwezigheid van een duidelijke veldafhankelijkheid is consistent met *clean-limit* elektrodynamica en een zeer anisotrope *gap* in de *ab* vlakken.

In hoofdstuk 3 laten we zien dat het mogelijk is om via reflectiemetingen aan een uniaxiaal medium gedaan bij een eindige invalshoek met zowel *s*- als *p*-gepolariseerd licht de diëlektrische funktie te bepalen parallel aan en loodrecht op de optisch as. Wanneer deze techniek wordt toegepast op gelaagde systemen met het oppervlak parallel aan de lagen, kan de verlies funktie loodrecht op de lagen nauwkeurig worden bepaald. De techniek is vooral nuttig voor kristallen waarvan alleen dunne lagen of zeer dunne éénkristallen bestaan. De hoge temperatuur supergeleiders behoren in het algemeen tot deze categorie hoewel grotere éénkristallen langzaamaan beschikbaar komen. De techniek kan ook gebruikt worden als een aanvullende benadering bij het bestuderen van de *c*-as respons van de koper oxide supergeleiders omdat het in epitaxiale films bijvoorbeeld gemakke-

lijker is om een homogene zuurstof verdeling in het monster te verkrijgen dan in een éénkristal. Als voorbeeld hebben we zowel boven als beneden T_c gepolariseerde reflectiemetingen gedaan bij een invalshoek van 45° aan dunne *c*-as georiënteerde dunne lagen van de hoge temperatuur supergeleider $Tl_2Ba_2Ca_2Cu_3O_{10}$. We kunnen duidelijk de longitudinale optische *c*-as fononen waarnemen. Uit het gedrag van de diëlektrische verlies funktie kunnen we een bovengrens van 200 cm^{-1} afleiden voor het "uit-vlaks" plasmon.

In hoofdstuk 4 hebben we het ver infrarood excitatiespectrum onderzocht van het *charge transfer* zout $(TMTSF)_2ClO_4$. Dit materiaal is een bekend lid van de quasi-1D familie van Bechgaard zouten. $(TMTSF)_2ClO_4$ heeft als funktie van een magnetisch veld een complex fasediagram. De nadruk in ons werk is gelegd op de details in the excitatiespectrum die samenhangen met een bijzondere vorm van antiferromagnetische ordening die geïnduceerd wordt door de aanwezigheid van het magnetische veld (de zogenaamde veldgeïnduceerde-spindichtheidsgolven). We hebben een groot deel van het fasediagram van dit *charge transfer* zout onderzocht (magnetische veld tot 16 T, energie tussen 1.5 en 45 cm^{-1} (0.2 en 6.0 meV, respectievelijk) en temperatuur tussen 0.3 en 7 K). We hebben gevonden dat de optisch waargenomen faseovergangen als funktie van de temperatuur en magnetisch veld nauwkeurig het fasediagram volgen zoals dat is bepaald met thermodynamische metingen. De experimenten hebben aangetoond dat de reeks van fase-overgangen optisch waargenomen kan worden. De spectroscopische gegevens wijzen erop dat de *gap* in de veldgeïnduceerde-spindichtheidsgolftoestand onafhankelijk is van het magnetische veld en de temperatuur. Dit in tegenstelling tot de voorspellingen van het "standaard model". Ons resultaat is wel consistent met een dichtheid van ladingsdragers die in de gekondenseerde toestand stapsgewijs toeneemt bij een fase-overgang naar een subfase met een lagere index. Bovendien hebben we voor het eerst aanwijzingen gevonden voor een "gepinde" collectieve excitatie in het microgolfgebied en voor een versterkte koppeling tussen het 31 cm^{-1} fonon en het elektronische systeem als gevolg van de spindichtheidsgolfvorming.

Ten slotte is hoofdstuk 5 gewijd aan ver infrarode reflectiemetingen aan de zeldzame aard nikkel oxides $LaNiO_3$, $PrNiO_3$ en $NdNiO_3$ tussen 30 en 5000 cm^{-1} bij temperaturen van 15 K tot kamertemperatuur. Het is bekend dat de meeste leden van de familie $RNiO_3$ (R = La, Pr, Nd, Sm, Eu) een metaal-isolator overgang vertonen bij T_{MI}. Onlangs is voorgesteld dat

deze metaal-isolator overgang gerelateerd is aan het openen (sluiten) van de *charge transfer gap* doordat de elektronische bandbreedte kleiner (groter) wordt bij dalende (stijgende) temperatuur. In de isolerende toestand wordt de infrarode reflectie van $NdNiO_3$ and $PrNiO_3$ voornamelijk bepaald door fononen. We zien een dramatische verandering van de spectra van bijna isolerend naar metallisch in een smal temperatuurvenster rond T_{MI} in overeenstemming met een sluitende energie-*gap*. In het metallische regime zijn de fononstructuren volledig afgeschermd. $LaNiO_3$ vertoond metallisch gedrag bij alle temperaturen in overeenstemming met eerdere resultaten van bijvoorbeeld dc transport studies. Onze resultaten zijn kwalitatief in overeenstemming met het bovengenoemde mechanisme voor de metaal-isolator overgang. Als wordt verondersteld dat de geleiding boven T_{MI} Drude-achtig is, wijzen de meetgegevens op een nogal zware massa van de geleidingselektronen.

List of publications

Proximity-based Josephson junctions:

- Microwave response of $YBa_2Cu_3O_{7-\delta}$-Ag-Al-Pb superconducting proximity junctions,
  M.A.M. Gijs, D. Scholten, Th. van Rooy, and A.M. Gerrits,
  Phys. Rev. B **41**, 11627 (1990).

- $YBa_2Cu_3O_{7-\delta}$-Ag-Al/Al_2O_3/Pb tunnel junctions based on the superconducting proximity effect,
  M.A.M. Gijs, D. Scholten, Th. van Rooy, and A.M. Gerrits,
  Appl. Phys. Lett. **57**, 2600 (1990).

- $YBa_2Cu_3O_{7-\delta}$-Ag-Al/Al_2O_3/Pb superconducting tunnel junctions,
  M.A.M. Gijs, D. Scholten, Th. van Rooy, A.M. Gerrits, and M.F.H. Schuurmans,
  Proc. Conf. Solid State Device and Materials, Sendai, 1191 (1990).

- $YBa_2Cu_3O_{7-\delta}$-Ag/Al-Pb superconducting proximity junctions: microwave investigation,
  M.A.M. Gijs, D. Scholten, Th. van Rooy, and A.M. Gerrits,
  Physica B **165**, 1633 (1990).

- Superconducting proximity effect in thin film $YBa_2Cu_3O_{7-\delta}$-Ag/Al-Pb structures,
  M.A.M. Gijs, D. Scholten, Th. van Rooy, A.M. Gerrits, and M.F.H. Schuurmans,
  Proc. SPIE Conf.: Advances in Semicond., San Diego (March 1990).

- Proximity effect based $YBa_2Cu_3O_{7-\delta}$-Ag-Al – Al_2O_3 – Pb Josephson and tunnel junctions,
M.A.M. Gijs, A.M. Gerrits, D. Scholten, and Th. van Rooy,
Supercond. Sci. Technol. **4**, S133 (1991).

- Submicron $YBa_2Cu_3O_{7-\delta}$-Ag-$YBa_2Cu_3O_{7-\delta}$ superconducting proximity junctions,
M.A.M. Gijs, J.B. Giesbers, F.C.M.J.M. van Delft, C.E. Timmering, A.M. Gerrits, and A. Slob,
Appl. Phys. Lett. **59**, 1233 (1991).

- Anomalous resistance behaviour in $YBa_2Cu_3O_{7-\delta}$-Ag-Pb proximity junction structures,
M.A.M. Gijs, R.M. Wolf, Th. van Rooy, A.M. Gerrits, and M.E. Bijlsma,
Solid State Commun. **80**, 727 (1991).

Organic conductors:

- Far-infrared spectroscopy of the field-induced spin-density-wave gap in
$(TMTSF)_2ClO_4$,
T.J.B.M. Janssen, A.S. Perel, A.M. Gerrits, W. Kang, J.S. Brooks, A. Wittlin, J.A.A.J. Perenboom, and P.J.M. van Bentum,
Phys. Rev. B **46**, 8663 (1992).

- The FI-SDW formation in $(TMTSF)_2ClO_4$ investigated in the infrared,
A.M. Gerrits, T.J.B.M. Janssen, J.S. Brooks, A. Wittlin, J.A.A.J. Perenboom, and P.J.M. van Bentum,
J. Phys. (Paris) IV, C2, 299 (1993).

- FIR spectroscopy of the FI-SDW excitation spectrum in a quasi-1D organic conductor,
A.M. Gerrits, T.J.B.M. Janssen, A.S. Perel, J.S. Brooks, A. Wittlin, J.A.A.J. Perenboom, and P.J.M. van Bentum,
Proc. ICSM-94, Seoul (1994), to be published in Synth. Met.

High temperature superconductors:

- c-axis infrared response of $Tl_2Ba_2Ca_2Cu_3O_10$ studied by oblique-incidence polarized reflectivity measurements,
  J.H. Kim, B.J. Feenstra, H.S. Somal, W.Y. Lee, A.M. Gerrits, A. Wittlin, and D. van der Marel,
  Phys. Rev. B **49**, 13065 (1994).

- Josephson plasma oscillations in $La_{1.85}Sr_{0.15}CuO_4$,
  A.M. Gerrits, A. Wittlin, V.H.M. Duijn, A.A. Menovsky, J.J.M. Franse, and P.J.M van Bentum,
  Physica C **235-240**, 1117 (1994).

- Far infrared reflectance of $YBa_2Cu_3O_{7-\delta}$ at high magnetic fields,
  A.M. Gerrits, T.J.B.M. Janssen, A. Wittlin, N.Y. Chen, and P.J.M van Bentum,
  Physica C **235-240**, 1115 (1994).

- Far infrared ellipsometry of electrons and phonons in $La_{1.87}Sr_{0.13}CuO_4$,
  R. Henn, J. Kircher, M. Cardona, A.M. Gerrits, A. Wittlin, V.H.M. Duijn, and A.A. Menovsky,
  Physica C **235-240**, 1195 (1994).

- Josephson plasma edge in $La_{1.85}Sr_{0.15}CuO_4$,
  P.J.M. van Bentum, A.M. Gerrits, M.E.J. Boonman, A. Wittlin, V.H.M. Duijn, and A.A. Menovsky,
  Physica B, in press (1995).

- Magnetic field dependence of the *c*-axis plasma edge in $La_{1.85}Sr_{0.15}CuO_4$,
  A.M. Gerrits, M.E.J. Boonman, A. Wittlin, P.J.M. van Bentum, V.H.M. Duijn, and A.A. Menovsky
  Phys. Rev. B, in press (1995).

- Out-of-plane dielectric response of Josephson coupled layered superconductors,
  A.M. Gerrits, and P.J.M. van Bentum,
  (submitted to Phys. Rev. B).

- Strong damping of the c-axis plasmon in high-T_c cuprate superconductors,
  Jae H. Kim, H.S. Somal, M.T. Czyzyk, D. van der Marel, A. Wittlin, A.M. Gerrits, V.H.M. Duijn, N.T. Hien, and A.A. Menovsky,
  Physica C, in press (1995).

Rare earth nickelates:

- Far-infrared studies of the metal-insulator transition in rare earth nickelates,
  A. Wittlin, A.M. Gerrits, X. Granados, J.L. Garcia-Muñoz, and J. Fontcuberta,
  (submitted to Phys. Rev. B).

- Far-infrared studies of the metal-insulator transition in $PrNiO_3$ and $NdNiO_3$,
  A. Wittlin, A.M. Gerrits, X. Granados, J.L. Garcia-Muñoz, and J. Fontcuberta,
  Physica C **235-240**, 1289 (1994).

Other fields:

- Limits on deviations from Onsager-Casimir symmetry in the resistance of $YBa_2Cu_3O_{7-\delta}$,
  M.A.M. Gijs, A.M. Gerrits, and C.W.J. Beenakker,
  Phys. Rev. B **42** 10789 (1990).

- Optical properties of incommensurately modulated calaverite,
  P.H.M. van Loosdrecht, A.M. Gerrits, K. Balzuweit, W. König, A. Wittlin, and P.J.M. van Bentum.
  J. Phys.: Condens. Matter **5**, 3977 (1993).

- Detection of a combination of defect activated phonon modes in AlAs/GaAs superlattice structure by Fourier Transform Spectroscopy,
  N.V. Joshi, W. van der Vleuten, J.H. Wolter, and A.M. Gerrits,
  Infrared Phys. Technol. **35**, 41 (1994).

- Absorption studies of the sulphur donor in GaSb,
  P. Kaczor, A.M. Gerrits, L. Dobaczewski, Z. Kalinski, and A. Wittlin,
  Acta Physica Polonica A **87**, 399 (1995).

Invited lectures

- *FIR spectroscopy of the FI-SDW excitation spectrum in a quasi-1D organic conductor*, held at the International Conference on Science and Technology of Synthetic Metals, July 24-29, 1994, Seoul, Korea.

Curriculum vitae

Ton Gerrits
born 23 April 1968 in Boxmeer

1980-1986	VWO-β at the Boschveldcollege, Venray.
1986-1990	Physics at the University of Utrecht.
1990	Nine months detachment at the Philips Research Laboratories (PRL) at Eindhoven. Graduate research subject: $YBa_2Cu_3O_7$ Josephson junctions based on the superconducting proximity effect and anyon superconductivity.
1990-1995	PhD research at the University of Nijmegen in the group Experimental Solid State Physics 2 of Prof. Dr. H. van Kempen and the High Field Magnet Laboratory. Thesis: *"Far-infrared studies of some strongly correlated electron systems"*.

ISBN 90-9008284-0